

Master's thesis

2023

Master's thesis

Stian Y. Sannerud

NTNU
Norwegian University of
Science and Technology
Faculty of Engineering
Department of Structural Engineering

Stian Y. Sannerud

Rheology and printability of matrix: effect of filler from manufactured sand vs copolymer

TKT4950 Structural Engineering, Master's Thesis

June 2023



Norwegian University of
Science and Technology

Rheology and printability of matrix: effect of filler from manufactured sand vs copolymer

TKT4950 Structural Engineering, Master's Thesis

Stian Y. Sannerud

TKT4950 Structural Engineering, Master's Thesis

Submission date: June 2023

Supervisor: Stefan Jacobsen

Co-supervisor: Negin Haghghat

Norwegian University of Science and Technology
Department of Structural Engineering



MASTER THESIS 2023

SUBJECT AREA: Structural Engineering	DATE: 11.06.2023	NO. OF PAGES: 99 (Incl. Appendixes)
--	----------------------------	---

TITLE:

(English)

Rheology and printability of matrix: effect of filler from manufactured sand vs. copolymer

(Norwegian)

Reologi og printbarhet av matriks: effekt av fyllstoff fra produsert sand vs. kopolymer

BY:

Stian Ytterstad Sannerud



SUMMARY:

This study investigates the impact different amounts of filler and superplasticizer have on filler-modified cement pastes rheology and printability. There are four methods that were used to investigate the effect of fillers in cement paste: measuring air content with through weighing, measuring workability and yield stress equivalent with mini-slump, measuring maximum particle packing by centrifugation, and measuring printability by 3D printing. These tests were researched on test series of 200 ml – 400 ml filler-modified cement paste.

In all 40 individual mixes were tested, and compared to each other to check if the tests are a reliable way of measuring rheology parameters and printability of cement paste. All the test gave satisfying results, except for the air content test, which gave unreliable results.

The other tests gave clear indications of pattern and distinguishable differences when in increasing filler content or superplasticizer content. Increasing filler increased the yield stress, seen from the decrease in mini-slump flow value. Increasing superplasticizer decreased the yield stress, seen from the increase in mini-slump flow value. Increasing filler also increased the relative concentration of solids, which can then be used to control mini-slump flow value/yield stress, and superplasticizer had the same opposite effect.

The printer used in this study, Enigne SR from Hyrel 3D, is a reliable way of testing printability of cement paste as the results can easily be compared, because the result showed that it has the same printing speed for all mixes.

RESPONSIBLE TEACHER/SUPERVISOR: **Stefan Jacobsen, Professor at the Department of Structural Engineering at NTNU**

OTHER PROFESSIONAL CONTACTS: **Ph.D. candidate Negin Haghight**

CARRIED OUT AT: **The Department of Structural Engineering at NTNU**

Preface

This thesis represents the culmination of the Master's degree program in Civil Engineering offered by NTNU, specifically within the framework of the course TKT4950 Structural Engineering, Master's Thesis. The research and composition of this work were conducted during the spring semester of 2023.

This master's thesis is about the laboratory work I performed in the spring of 2023 with Negin Haghghat, a PhD Candidate at the Department of Structural Engineering. The work is part of her ongoing project at NTNU about 3D printing of filler-modified cement paste.

This study investigates the effect of filler in cement paste with different laboratory tests, which was conducted together with Negin Haghghat. The tests are inspired from previous studies done by Skare [17], Sihaklang [15] and Cepuritis [2].

I hope that this project report will prove to be valuable, offering potentially beneficial insights for Negin Haghghat's project, and those interested in exploring the same field of study.

Stian Y. Sannerud

Stian Ytterstad Sannerud

Trondheim, 11.06.2023

Abstract

This study investigates the impact different amounts of filler and superplasticizer have on filler-modified cement pastes rheology and printability. There are four methods that were used to investigate the effect of fillers in cement paste: measuring air content with through weighing, measuring workability and yield stress equivalent with mini-slump, measuring maximum particle packing by centrifugation, and measuring printability by 3D printing. These tests were researched on test series of 200 ml – 400 ml filler-modified cement paste.

In all 40 individual mixes were tested, and compared to each other to check if the tests are a reliable way of measuring rheology parameters and printability of cement paste. All the test gave satisfying results, except for the air content test, which gave unreliable results.

The other tests gave clear indications of pattern and distinguishable differences when in increasing filler content or superplasticizer content. Increasing filler increased the yield stress, seen from the decrease in mini-slump flow value. Increasing superplasticizer decreased the yield stress, seen from the increase in mini-slump flow value. Increasing filler also increased the relative concentration of solids, which can then be used to control mini-slump flow value/yield stress, and superplasticizer had the same opposite effect.

The printer used in this study, Enigne SR from Hyrel 3D, is a reliable way of testing printability of cement paste as the results can easily be compared, because the result showed that it has the same printing speed for all mixes.

Summary

Denne studien undersøker hvordan ulike mengder fyllstoff og superplastifiseringsmiddel påvirker reologi og printbarhet til sementpasta som er modifisert med fyllstoff. Fire metoder ble brukt for å undersøke effekten av fyllstoff i sementpastaen: måling av luftinnhold ved veiing, måling av arbeidsevne og flytegrense ved hjelp av mini-synkmål, måling av maksimal partikkelpakking ved sentrifugering, og måling av printbarhet ved 3D-printing. Disse testene ble utført på testserier av 200 ml - 400 ml fyllstoffmodifisert sementpasta.

Totalt ble 40 individuelle blandinger testet og sammenlignet med hverandre for å sjekke om testene er en pålitelig måte å måle reologiske parametere og printbarhet i sementpasta. Alle testene ga tilfredsstillende resultater, bortsett fra luftinnholdstesten, som ga upålitelige resultater.

De andre testene ga tydelige indikasjoner på mønstre og tydelige forskjeller når det gjelder økende mengde fyllstoff eller superplastifiseringsmiddel. Økende mengde fyllstoff økte flytegrense, noe som kunne sees gjennom en nedgang i verdien for mini-synkmål flytverdi. Økende mengde superplastifiseringsmiddel reduserte flytegrense, noe som kunne sees gjennom en økning i verdien for mini-synkmål flytverdi. Økende mengde fyllstoff økte også den relative konsentrasjonen av faste partikler, som deretter kunne brukes til å kontrollere mini-synkmål flytverdi/flytegrense, mens superplastifiseringsmiddel hadde den motsatte effekten.

3D-printeren som ble brukt i denne studien, Enigne SR fra Hyrel 3D, er en pålitelig måte å teste printbarheten til sementpastaen på, ettersom resultatene enkelt kan sammenlignes, ettersom resultatene viste at den hadde samme utskriftshastighet for alle blandinger.

Table of contents

Preface	I
Abstract	II
Sammendrag	III
List of Figures	V
List of Tables	VII
Acronyms, Initialisms and Term	VIII
1 Introduction	1
1.1 Background	1
1.2 3D-printing	1
1.2.1 Extrudability	2
1.2.2 Buildability	3
1.2.3 G-code	4
1.3 Scope	5
2 Materials, Parameters and Methods	6
2.1 Materials	6
2.1.1 Industrial cement	6
2.1.2 Fly ash	7
2.1.3 Silica fume	7
2.1.4 Manufactured sand	8
2.1.5 Superplasticizer	9
2.2 Parameters	10
2.2.1 Particle-matrix model	10
2.2.2 Maximum packing and excess fluid	10
2.2.3 Liquid thickness	11
2.3 Methods	13
2.3.1 Mix proportioning and procedure	13
2.3.2 Density and air content measurements	16
2.3.3 Mini slump test	18
2.3.4 Centrifuge	20
2.3.5 3D printer	22
3 Results and discussion	32
3.1 Results and discussion of fresh density and air void measurements	32

3.2	Results of mini-slump test	36
3.3	Results of centrifugation test	41
3.4	Results of 3D printing tests	46
3.4.1	Results of flow measurement test	46
3.4.2	Results of printability test	52
4	Conclusions	55
	References	56
	Apendix A: Matrix proportioning	58
	Apendix B: Results Density and Air	64
	Apendix C: Results Mini slump	67
	Apendix D: Results Centrifugation	69
	Apendix E: Results Print Flow	71
	Apendix F: Pictures of results	78
	Apendix G: Silica fume datasheet	79
	Apendix H: Dynamon SR-N datasheet	84

List of Figures

1.1	Schematic of a 3D printing setup: 0. System command; 1. Robot controller; 2. Printing controller; 3. Robotic arm; 4. Printhead; 5. Accelerating agent; 6. Peristaltic pump for accelerating agent; 7. Peristaltic pump for premix; 8. Premix mixer; 9. 3D printed object. [6]	1
1.2	Publications on 3DPC between 1997 and 2017 [20]	2
1.3	Illustration of working principle of screw extruder (left) and ram extruder (right) [8]	3
1.4	Different failure patterns for buildability of 3DPC [8].	4
2.1	Particle size distribution of Industrisement compared to STD FA cement	6
2.2	Particle size distribution for fillers T5 and T8	9
2.3	Illustration of falcon tubes before and after centrifugation	11
2.4	Equipment for mixing filler-modified cement paste: metal bowl for dry particles, beakers for water and SP, with pipettes and a the hand-blender	15
2.5	Cylinder for density and air content measurements and a piece of plexiglass	16
2.6	Measurements of the weight of cylinder with and without water	16
2.7	Measurements of the weight of cylinder with and without cement paste	17
2.8	Equipment for mini-slump test: mini-slump cone, plexiglass, compacting rod, steel bar, rulers	19
2.9	Examples of mini-slump test on mix G2T815W4	19
2.10	Centrifugation machine	20
2.11	Centrifugation equipment: Two falcon tubes, a syringe, filters (size $0.45 \mu m$) and a cup	20
2.12	Pictures of falcon tubes before and after centrifugation	21
2.13	3D printer Engine SR from Hyrel 3D with print head SDS 150 connected	22
2.14	Equipment for 3D printing	23
2.15	Stand and balance needed to measure mass flow	24
2.16	Printer before, during and at the end of printability test	25
2.17	Landing page of Repetrel	26
2.18	Control tab in Repetrel	27
2.19	Adding Gcode in Repetrel	27
2.20	G-code for mass flow test in Repetrel	28
2.21	Control tab when printing in Repetrel	28
2.22	G-code for printability test in Repetrel	29
3.1	Calculated average air content of mixes with $w/b=0,4$ plotted against fi/b	34
3.2	Calculated average air content of mixes with $w/b=0,4$ plotted against fi/b	34
3.3	Mini-slump flow value of mixes using filler T5 plotted against fi/b	38
3.4	Mini-slump flow value of mixes using filler T8 plotted against fi/b	38
3.5	Examples of mini-slump flow value using T8 from Group 2	39
3.6	Mini-slump value for mixes with $w/b = 0.4$ plotted against fi/b	40

3.7	Examples of mini slump test using T8 from Group 2	40
3.8	ϕ/ϕ_{max} for mixes using filler T5 plotted against mini-slump-flow value	43
3.9	ϕ/ϕ_{max} for mixes using filler T8 plotted against mini-slump-flow value	43
3.10	ϕ/ϕ_{max} for mixes plotted against mini-slump-flow value, differentiating between mixes using SP=0,75% and SP=1,0%	44
3.11	Relationship between liquid thickness (LT1 and LT2) and mini-slump flow value	45
3.12	Volumetric flow of G2T5W4 as a function of time	48
3.13	Updated plot for volumetric flow of G2T5W4 as a function of time	49
3.14	Volumetric flow of G2T5W6 as a function of time	49
3.15	Volumetric flow of G3T5W4 as a function of time	50
3.16	Volumetric flow of G3T5W6 as a function of time	50
3.17	Slope of volumetric flow for all mixes plotted against mini-slump flow value	51
3.18	Printability test on G3T51.15W6	52
3.19	Pictures from printability test	53
3.20	Example of wave during printability	53
3.21	Hardened printability specimens, from top to bottom: G3T515W4, G3T544W4, G3T585W4	54
3.22	Cut hardened printability test specimens with edge detection performed	54

List of Tables

2.1	Mineralogical composition of the different crushed filler	8
2.2	Physical properties of different fillers	8
2.3	Physical properties for fillers T5 and T8 used in this study	9
2.4	Mix proportioning for group 1	13
2.5	Mix proportioning for group 2	14
2.6	Mix proportioning for group 3	14
3.1	Density and air measurements of group 1	32
3.2	Density measurements of group 2	33
3.3	Density measurements of group 3	33
3.4	Air content measurements of G1T515W4	35
3.5	Mini-slump value and flow value for group 1	36
3.6	Mini-slump value and flow value for group 2	37
3.7	Mini-slump value and flow value for group 3	37
3.8	Measurements and results of centrifugation test for group 1	41
3.9	Measurements and results of centrifugation test for group 2	42
3.10	Measurements and results of centrifugation test for group 3	42
3.11	Measured mass flow measurements for G2T5W4	46
3.12	Calculated volumetric flow values for G2T5W4	47
3.13	Values for slope and variance of linear functions for volumetric flow	51
3.14	Relevant data on G3T5W4 for printability test	52
4.1	Material parameters used in the calculation of mix proportioning	58

List of symbols

ϕ : solid fraction.

ϕ_{max} : maximum packing.

ϕ/ϕ_{max} : relative concentration of solids.

w/c : water-to-cement ratio (in mass-ratio).

w/b : water-to-binder ratio (in mass-ratio).

FA/b : fly ash-to-binder ratio (in mass-ratio).

fi/b : filler-to-binder ratio (in mass-ratio).

s/b : silica-to-binder ratio (in mass-ratio).

w/p : water-to-powder ratio (in mass-ratio).

Acronyms, Initialisms and Terms

NTNU: Norwegian University of Science and Technology.

3DPC: 3D Printed Concrete

CAD: Computer Aided Design.

FA: Fly Ash.

SP: Superplasticizer.

SSA: Specific Surface Area.

PSD: Particle Size Distribution.

LT: Liquid Thickness.

RPM: Rounds Per Minute.

EF: Excess Fluid.

VFF: Void Filling Fluid.

powder: (cement + filler).

1. Introduction

1.1 Background

Concrete is the most widely used construction material in the world, with an annual production of over 4 billion tons worldwide [7], which is equal to around 7-8% of the world's greenhouse gas emissions [18]. The production of cement alone contributes to 90% of these emissions. Despite its crucial role in providing transportation, housing, and commerce infrastructure, the concrete industry faces significant sustainability challenges, primarily due to the high carbon footprint associated with cement production. Another problem the construction industry is facing is the depletion of natural construction sand with high quality, which has caused the use of manufactured sand as a replacement [19].

Three-dimensional printing concrete (3DPC), also called additive manufacturing, has in recent years attracted more attention as a big factor in the progress of the industrialization of the construction industry [8]. 3DPC offers numerous benefits including accelerated construction speed, reduced labor, and raw material requirements, and enhanced design flexibility by eliminating the need for traditional formworks [24]. 3DPC paired with filler-modified cement paste, with lower cement content, can therefore give many benefits, especially when it comes to sustainability.

1.2 3D-printing

3D printed concrete (3DPC) is an emerging construction technique using additive manufacturing, meaning the material deposition is done layer by layer. Without any formwork or vibration process, self-compacting concrete is extruded layer by layer through a nozzle, onto a designed/coded route. Figure 1.1 shows an example schematic of a 3D printing setup.

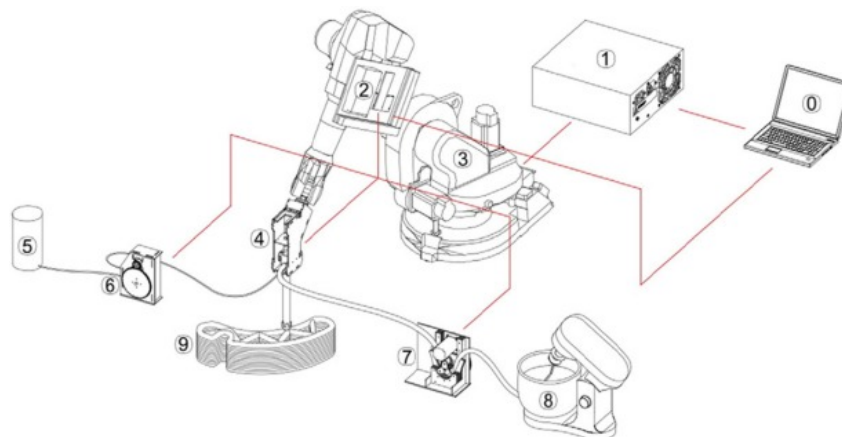


Figure 1.1: Schematic of a 3D printing setup: 0. System command; 1. Robot controller; 2. Printing controller; 3. Robotic arm; 4. Printhead; 5. Accelerating agent; 6. Peristaltic pump for accelerating agent; 7. Peristaltic pump for premix; 8. Premix mixer; 9. 3D printed object. [6]

Already in the early 1990s the concept of 3DPC was introduced, but up until 2016 it was still a minimal part of the field of building construction. An article by Tay et al. [20] saw an exponential trend of publications on 3DPC in the construction industry between the years 1997 and 2017 (see Figure 1.2), most of them coming from USA and UK. Research done by Huang et al. [10] described 42 individual projects that had used 3DPC in the years 2017 to 2021, where one of the requirements were that the construction made with 3DPC had to have structural significance or be an architectural work. So there is no doubt that it is an emerging technology.

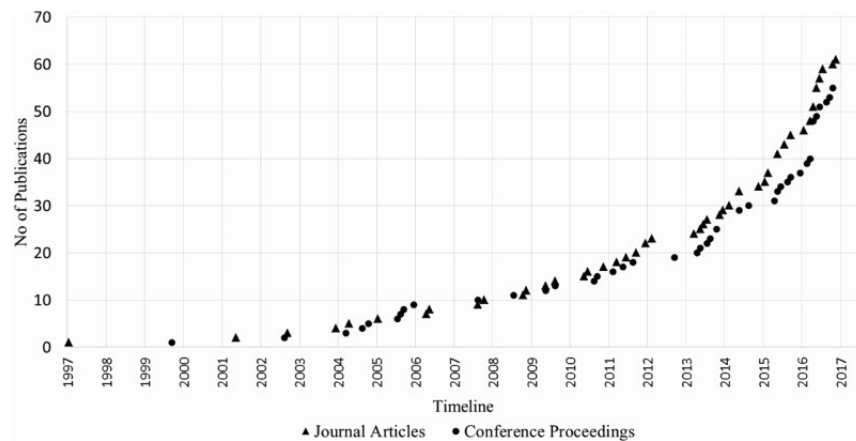


Figure 1.2: Publications on 3DPC between 1997 and 2017 [20]

According to an article on 3Printer.com [1], 3DPC, in comparison to traditional construction technology, can reduce production time by 50-70%, lower labor cost by 50-80% and save between 30-60% in construction waste.

For a successful construction of 3DPC a few key elements regarding rheological properties of the paste are the most important. The term printability has been used as a term to evaluate fresh concrete paste that is being used for 3D printing. There is no clear definition of the term printability yet, but for this thesis the term will be defined as in an article by [8]. The definition is as follows: "[...] the printability in this study is considered as the ability of fresh 3DPC to be extruded continuously and built up with acceptable deformation before setting, and it consists of extrudability and buildability [...]" (Hou et al. 2021). An article by Xiao et al. [23] also determines another key factor in printability for 3DPC, pumpability. This is more important in large-scale 3D printing of concrete because the mix has to be able to flow as a continuous paste through a pump without blockage. This thesis will not include this term because all the experiments are low-scale, and do not require a pump.

1.2.1 Extrudability

Extrudability, defined in this thesis as the ability to transport fresh concrete through a nozzle as a continuous filament, is a key factor in achieving a successful print [8]. Two extrusion methods are commonly used in 3DPC: screw extrusion and ram extrusion.

Screw extrusion involves feeding the cementitious materials into a feeding tube to the extruder barrel, where

they are pushed by a rotating screw, before being extruded from the nozzle. The rheological behavior of cementitious materials changes in the hopper of screw extruders due to the rotational screw and the thixotropy of the cementitious materials themselves. Ram extrusion involves the materials being pushed by a ram/piston inside the extruder barrel, with the shape of the extruded materials being the same as that of the extruder barrel (see Figure 1.3). The choice of method is largely dependent on the properties and requirements of the flowable cementitious materials and the application of the 3DPC. Screw extruders are suitable for cement-based materials with fine aggregates, that is homogeneous and has a high flowability. Ram extruders are suitable for concrete with larger aggregates. For this thesis a type of ram extruder is used with a syringe.

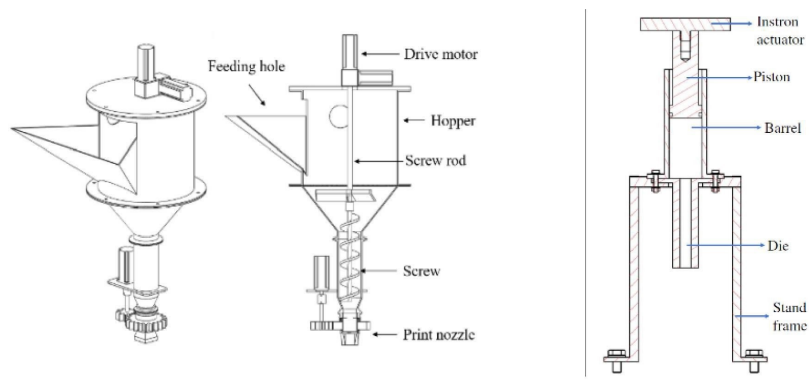


Figure 1.3: Illustration of working principle of screw extruder (left) and ram extruder (right) [8]

Achieving optimal results with 3DPC require a homogeneity and continuous extrusion while minimizing issues such as blockage, cracking, and segregation.

1.2.2 Buildability

Buildability, defined in this thesis as the ability to bear its own weight and the load from the layers above without collapsing during the printing process. This parameter is determined by two factors. Firstly, the 3DPC must maintain its shape deformation after extrusion, within a controlled range, and secondly, the 3DPC elements must be able to resist collapse as layers increase during the printing process. The layer thickness is usually set to a small value to limit the initial gravity stress to control the deformation, and the yield stress of the cementitious material must be higher than the shear stress caused by gravity for the 3DPC to maintain its shape [8]. The ability of 3DPC elements to resist collapse can be affected by a variety of factors such as the print path, layer thickness, and printing speed. Figure 1.4 show four different kinds of failures that can happen wehn 3D printing concrete, all of them related to the buildability.

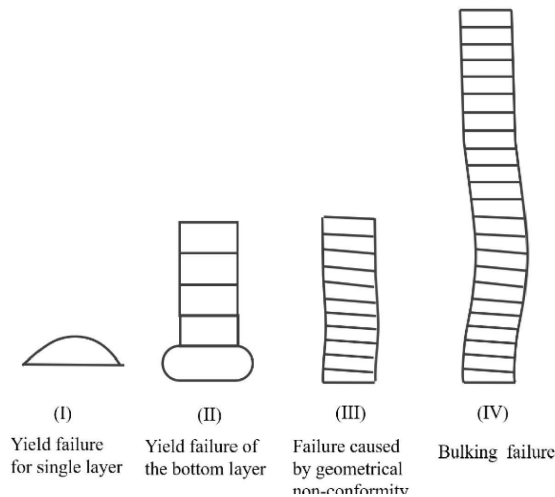


Figure 1.4: Different failure patterns for buildability of 3DPC [8].

1.2.3 G-code

G-code, short for "Geometric Code," is a language used to program CNC (Computer Numerical Control) machines, which are used in manufacturing processes such as milling, drilling, cutting, and 3D printing [9]. G-code is a series of commands that are interpreted by the CNC machine to control the movement and operation of that machine, the code tells the machine what to do and who to do it.

G-code is typically generated using CAD/CAM (Computer-Aided Design/Computer-Aided Manufacturing) software, which translates the design or model into a series of G-code commands that the CNC machine can understand and execute [21]. G-code is widely used in various industries, including aerospace, automotive, and manufacturing, to precisely control CNC machines and produce complex parts with high accuracy and repeatability.

G-code consists of a set of standardized commands, each represented by a letter followed by numbers. For example, the command "G0 X10 Y20 Z5" would instruct the CNC machine to move the tool at maximum travel speed (G0) to a point with X, Y, and Z coordinates of 10, 20, and 5 respectively, in a linear motion. Notably, "G0" solely serves to position the machine without executing any cutting or printing. In addition to movement commands, G-code also includes commands for setting different parameters such as feed rate/travel speed. An example of this can be seen using the same example as before but changed to "G1 X10 Y20 Z5 F100". Here, G1 is used to tell the machine that the feed rate/travel speed is determined by the F-parameter, in this case 100 mm/min.

Apart from the code signifiers G, X, Y, Z, and F, other letters like M, S, and T may be employed depending on the specific CNC machine and software in use. For instance, 3D printers have specialized "M" codes for controlling heating and fan speed. The commands "G" and "M" are mostly standardized for all software between G0 and G100, and M0 and M100, codes over 100 are usually dependent on the software the machine uses [12]. The code and software used for this thesis are further explained in 2.3.5

1.3 Scope

This study aims to investigate the effects of superplasticizer and filler materials, specifically T5 Limestone and T8 basalt, on the flowability and printability, rheology, of a filler-modified cement paste. To achieve this, an extensive review of existing literature on 3D printing and the rheology of filler-modified cement paste was conducted, along with an examination of the 3D printer used for cementitious material printing in this study. Subsequently, laboratory tests were conducted using various mix compositions.

The data collected from the experiments will be analyzed to identify the effects of different fillers on the properties of the matrix. The experiments conducted include:

1. Measurement of fresh density and calculation of air void content through weighing.
2. Evaluation of the workability of the paste using a mini-slump test.
3. Usage of a centrifuge to measure excess fluid and calculate maximum packing, relative concentration of solids, and liquid thickness.
4. Assessment of flow by 3D printing on a balance to evaluate printability and extrudability.
5. UPrinting of specimens using a 3D printer to visually determine buildability.

By performing these experiments and analyzing the resulting data, we aim to gain insights into how the amount of superplasticizer and different fillers affects the flow, printability, and rheological behavior of the filler-modified cement paste.

2. Materials, Parameters and Methods

2.1 Materials

The materials used in this study include industrial cement, standard fly ash and silica fume, manufactured sand, and superplasticizer, which are explained in more detail as follows.

2.1.1 Industrial cement

Industrial cement, also known as Portland cement, is a type of hydraulic cement that is widely used in construction and other industrial applications [14]. It is the most common type of cement used in the production of concrete, which is a key building material for various structures such as buildings, bridges, highways, and dams.

Industrisement has a high Blaine specific surface area which makes it a rapid-hardening Portland cement [14]. Because of the cements short setting time it has a high early age strength, which makes it good for pre-cast concrete and also 3DPC. It is also good for 3DPC because of the industry cements stability caused by its high fineness. Figure 2.1 shows the particle size distribution of Industrisement and STD FA cement.

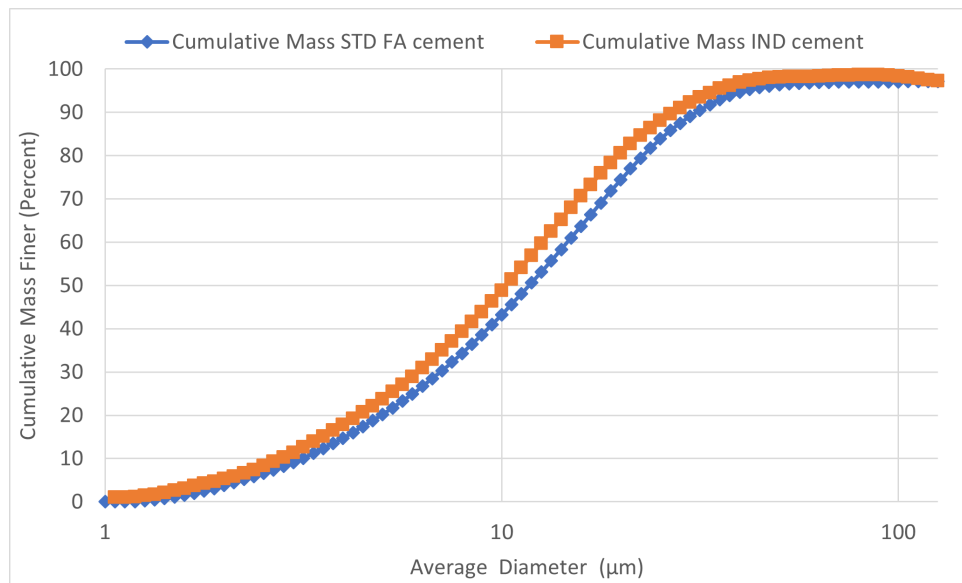


Figure 2.1: Particle size distribution of Industrisement compared to STD FA cement

Because of the high greenhouse emissions from the making of Portland cement, pozzolanic materials such as fly ash and silica fume can be used as a replacement for cement in a concrete mix. These are more economic and sustainable as they are industrial by-products.

2.1.2 Fly ash

Fly ash is a fine powdery material that is a byproduct of burning coal in thermal power plants. It is also known as coal ash or pulverized fuel ash (PFA). Fly ash consists of small, spherical particles that has a particle size close to Portland cement (10-20 μm). When mixed with water and calcium hydroxide, which is produced during the hydration of cement, fly ash reacts chemically to form additional cementitious compounds, such as calcium silicate hydrate (C-S-H) and calcium aluminate hydrate (C-A-H), which contribute to the strength and durability of concrete [14].

The use of fly ash in concrete can have several benefits, including improving the workability and cohesiveness of concrete mixtures, reducing the heat of hydration, reducing the amount of cement required, and improving the long-term performance and durability of concrete structures.

2.1.3 Silica fume

Silica fume, also known as microsilica, is a byproduct of the production of silicon metal and ferro-silicon alloys [14]. It is a fine-grained material, consisting of small particles with an average particle size of around 0.1 to 0.2 μm , which is about 100 times smaller than the average particle size of cement.

Silica fume is a supplementary cementitious material, similar to fly ash, and is used as a pozzolanic admixture in concrete. It is typically added to concrete in small quantities, usually ranging from 5% to 10% by weight of cement, although higher dosages can also be used for specific applications.

Silica fume is known for its high reactivity due to its small particle size and amorphous nature, which allows it to fill the spaces between cement particles and improve the overall packing density of the concrete mixture. When mixed with water and calcium hydroxide, which is produced during the hydration of cement, silica fume reacts chemically to form additional cementitious compounds, such as calcium silicate hydrate (C-S-H), which contributes to the strength, durability, and impermeability of concrete. This study will use a silica fume from Elkem called Elkem Microsilica (see datasheet in Appendix F).

Silica fume and fly ash have very similar effect on a cement mix, the main differences are the extent and time of reaction, because of the different particle sizes. Research done by Skare et al. [19] found that the use of silica fume could negatively effect the prediction accuracy when measuring rheology parameters. Three different reasons were speculated for being the cause of this, firstly the high specific surface area of silica fume. Secondly the ball bearing effect because of the round shapes that silica fume particles has, or thirdly because of the reduction of energy which is needed to disperse the particles.

2.1.4 Manufactured sand

The use of manufactured sand has increased because of the depletion of natural sand that can be used for concrete [14]. The difference between natural sand and manufactured sand is that natural sand is directly sieved from a gravel pit. Crushed or manufactured sand is produced in a quarry by crushing bedrock material and using technology like a vertical shaft impact crusher and air-classification to shape and classify them. Below is a list of the composition of four different type of fillers.

Table 2.1: Mineralogical composition of the different crushed filler

Type	T3	T4	T5	T8
Rock name	Quartzite	Anorthosite	Limestone	Basalt
Rock type	Metamorphic	Igneous (intrusive)	Sedimentary	Igneous (extrusive)
Mineralogical composition, mass%				
Quartz	90.0	6.5	2.3	8.9
Carbonate minerals	3.6	10.6	97.7	8.3
Epidote minerals	-	24.4	-	7.6
Feldspar minerals	3.9	33.1	-	26.5
Sheet silicates	1.5	20.4	-	5.2
chlorite	1.0	2.6	-	20.2
Inosilicate minerals	-	2.3	-	11.0

Table 2.2: Physical properties of different fillers

Type	T3	T4	T5	T8
Water absorption %	0.2	0.7	0.2	0.9
Mean density %	2.67	2.98	2.72	2.94

In this study only the fillers T5 and T8 will be used. The reason for choosing T5 and T8 for this study is because T5 has the lowest rate of water adsorption and T8 has the highest. The mixes made for testing will be divided into groups that either take into account the water adsorption of the fillers T5 and T8, or not take it into account, meaning the mix proportions will be different. This is further explained in 2.3.1 where the different groups are introduced. The assumption is that the different groups will show a larger difference in results when using T8 then when using T5, as the mix proportions are more similar when using T5 (see Appendix A for full mix proportions).

Particle size distributions and specific surface area of fillers

Figure 2.2 and Table 2.3 shows the particle size distribution and Physical properties of the two fillers T5 and T8 [2].

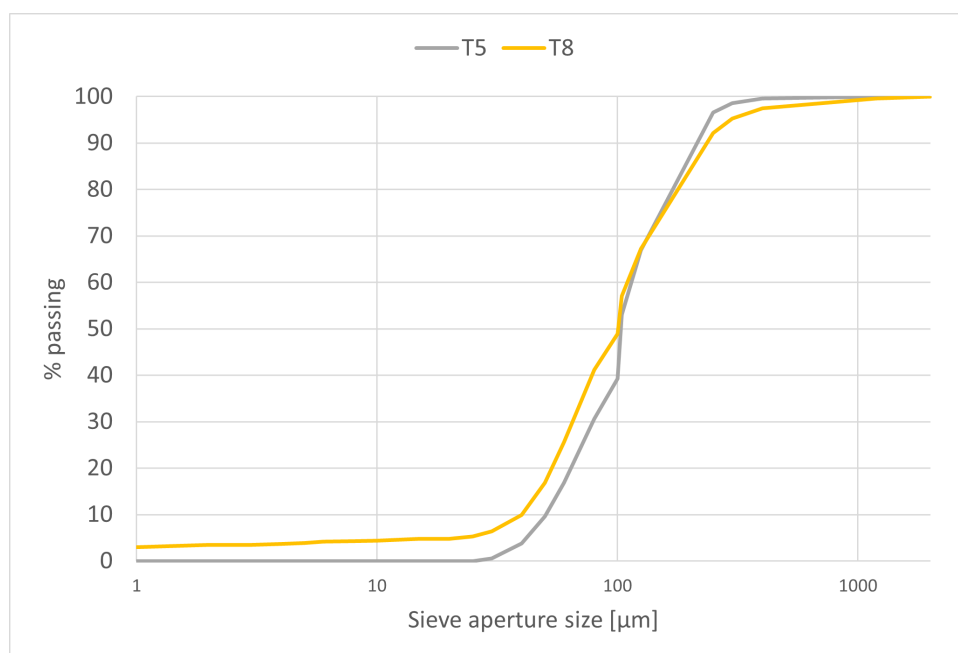


Figure 2.2: Particle size distribution for fillers T5 and T8

Table 2.3: Physical properties for fillers T5 and T8 used in this study

Type	Rock type	Quarry	Producer	Fraction	Specific surface
				[x/x μm]	BET [m^2/m^3]
T5	Limestone 1	Tromsdalen	Verdalskalk AS	63/125*	312.1
T8	Basalt	Steinskogen	Franzefoss Pukk AS	63/125*	2635.2

Rheology of filler-modified cement paste

Manufactured sand, the filler, differs from natural sand regarding microfines ($\leq 75 \mu\text{m}$) content, particle shape, surface texture, and gradation. The weight fraction of microfines in manufactured sand is much larger than in natural sand because of the manufacturing processes [25]. This significantly increases the specific surface areas (SSA) [5], which have big impacts on the rheology of the cement paste. Previous research done by Westerholm et al. [22] and Zhu et al. [25] has shown that increasing the microfines concentration, from manufactured sand, in a paste leads to higher yield stress and reduced fluidity, meaning lower flowability.

2.1.5 Superplasticizer

Superplasticizers (SP), also known as high-range water reducers, are chemical admixtures used in concrete to significantly reduce the amount of water required to achieve a desired workability or flowability

without sacrificing the strength or other performance properties of the concrete [14]. SPs are typically added to the concrete mix during batching or mixing, and they can greatly improve the workability and flowability of concrete, making it easier to place, compact, and finish.

Superplasticizers work by dispersing flocculated cement particles and other solid materials in the concrete mixture, reducing the friction between them and allowing for greater fluidity without increasing the water content. This results in a concrete mixture that can be placed and compacted with minimal effort, while still maintaining its desired strength and durability upon curing. SPs are therefore commonly used in various types of concrete applications, such as in high-strength concrete, self-compacting concrete, pumped concrete, precast concrete, and ready-mix concrete.

Superplasticizers used in Norway can be classified into two main types: sulfonate-based and polycarboxylate-based, where polycarboxylate-based SPs are the most commonly used in Norway. This study will be using a SP from Mapei called Dynamon SR-N (see datasheet in Appendix G).

2.2 Parameters

2.2.1 Particle-matrix model

The particle-matrix method, which is the dominant method for mix proportioning in Norway, follows a two-phase approach. The particle phase is defined as the particles in a concrete mix that are bigger than 0.125 mm, and the matrix phase are all the particles that are smaller than 0.125 mm. Since the mixes in this study only have particles in the matrix phase it is called a filler-modified cement paste. When crushed sand is used, the proportion of particles smaller than 125 microns significantly influences the flow behavior. Factors such as SP-dosage, water-to-binder ratio (w/b), and solid content are well-known to affect the rheology of the paste [14].

2.2.2 Maximum packing and excess fluid

The maximum packing (ϕ_{max}) of a cement paste can be described by the equation below, where a volume of 1 is considered. ϕ is the sum of volume fractions of the solid particles in the mix (cement, silica fume, fly-ash and filler), and EF is the excess fluid of the paste.

$$\phi_{max} = \frac{\phi}{1 - EF - air} \quad (2.1)$$

In order to measure ϕ_{max} a centrifuge is used to extract the EF from a fresh cement paste, as illustrated in 2.3. After centrifuging is separated into EF and $\phi + VFF$, where VFF is void filling fluid in the paste. The volume fraction of solids (ϕ) is tabulated in Appendix XX, and calculated from the mix proportioning found in 2.3.1.

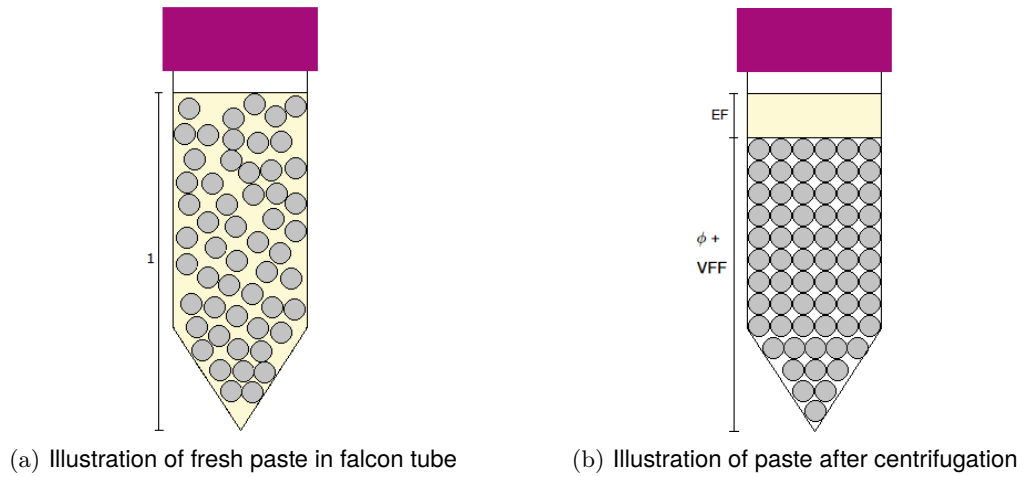


Figure 2.3: Illustration of falcon tubes before and after centrifugation

The total volume of the paste in a falcon tube test can then be determined by the equation below. The equation has also included air into the equation, which is normally negligible, but as a air content measurement will be done a part of this thesis it is accounted for.

$$1 = VFF + EF + \phi + air \quad (2.2)$$

Knowing EF, ϕ and air content makes it possible to find the maximum packing (ϕ_{max}) using equation 2.1, and then the equation for relative concentration of solids can be calculated using the equation below.

$$\frac{\phi}{\phi_{max}} = 1 - EF \quad (2.3)$$

The function ϕ/ϕ_{max} can be used to describe the relative viscosity of a suspension [19], a cement paste in this case . The purpose of measuring the relative concentration of solids, is to find its relationship with the mini-slump flow value of the mixes. Because the mini-slump value is directly correlated with the yield stress of cement paste, and ϕ/ϕ_{max} with the viscosity, they can be used to help find the effect of fillers in the paste.

2.2.3 Liquid thickness

Another parameter to describe the rheology of cement paste is liquid thickness (LT) was developed for a project at NTNU called the MiKS project [3]. The parameter describes that the solid particles in the paste have a water film coating that prevent the solid particles having direct contact. So the voids between solid particles are filled up with both VFF and LT, where LT is a defined as the thickness of the coating around the solid particles. There are two equations for calculating LT, the first one (LT1) says that VFF and EF are both a part of the liquid thickness of a paste, the second one (LT2) excludes VFF, both are listed below [19].

$$LT1 = \frac{1 - \phi}{SSA} = \frac{VFF + EF}{SSA} \quad (2.4)$$

$$LT2 = \frac{1 - \phi - VFF}{SSA} = \frac{EF}{SSA} \quad (2.5)$$

Research done by Skare [19] found that were successful in using LT for modelling rheology in suspensions.

2.3 Methods

2.3.1 Mix proportioning and procedure

In this project, three different groups of mix proportioning are selected to study the rheology of manufactured sand at different w/b ratios and SP dosages. Each group varies in admixture dosage, w/b ratio, fi/b ratio, and filler types.

In group 1, we consider the water adsorption of the filler. This means that the fillers are assumed to be in a dry condition, and a portion of the water added to the paste is adsorbed by the fillers. Within this group, we maintain a constant admixture dosage for two different water-to-binder ratios: 0.4 and 0.6. The variation lies in the filler-to-binder ratio for both types of fillers.

Table 2.4: Mix proportioning for group 1

Group	NO	Filler type	w/c	w/b	fi/b	FA/b	s/b	SP/c
1	G1T515W4	T5	0.5	0.4	0.15	0.2	0.04	0.75
1	G1T544W4	T5	0.5	0.4	0.44	0.2	0.04	0.75
1	G1T585W4	T5	0.5	0.4	0.85	0.2	0.04	0.75
1	G1T51.15W4	T5	0.5	0.4	1.15	0.2	0.04	0.75
1	G1T815W4	T8	0.5	0.4	0.15	0.2	0.04	0.75
1	G1T844W4	T8	0.5	0.4	0.44	0.2	0.04	0.75
1	G1T885W4	T8	0.5	0.4	0.85	0.2	0.04	0.75
1	G1T81.15W4	T8	0.5	0.4	1.15	0.2	0.04	0.75
1	G1T515W6	T5	0.8	0.6	0.15	0.2	0.04	0.75
1	G1T544W6	T5	0.8	0.6	0.44	0.2	0.04	0.75
1	G1T585W6	T5	0.8	0.6	0.85	0.2	0.04	0.75
1	G1T51.15W6	T5	0.8	0.6	1.15	0.2	0.04	0.75
1	G1T815W6	T8	0.8	0.6	0.15	0.2	0.04	0.75
1	G1T844W6	T8	0.8	0.6	0.44	0.2	0.04	0.75
1	G1T885W6	T8	0.8	0.6	0.85	0.2	0.04	0.75
1	G1T81.15W6	T8	0.8	0.6	1.15	0.2	0.04	0.75

In group 2, fillers are assumed to be in SSD condition (Saturated Surface Dry). In SSD conditions, the surfaces of the fillers are dry, but the inter-particle voids are saturated with water. In this condition, the fillers do not affect the free water added to the paste. Other variables remain similar to group 1. Consequently, the water-to-binder ratio in the second group is higher compared to the first group, depending on the amount of water adsorption by the fillers.

Table 2.5: Mix proportioning for group 2

Group	NO	Filler type	<i>w/c</i>	<i>w/b</i>	<i>fi/b</i>	<i>FA/b</i>	<i>s/b</i>	<i>SP/c</i>
2	G2T515W4	T5	0.5	0.4	0.15	0.2	0.04	0.75
2	G2T544W4	T5	0.5	0.4	0.44	0.2	0.04	0.75
2	G2T585W4	T5	0.5	0.4	0.85	0.2	0.04	0.75
2	G2T51.15W4	T5	0.5	0.4	1.15	0.2	0.04	0.75
2	G2T815W4	T8	0.5	0.4	0.15	0.2	0.04	0.75
2	G2T844W4	T8	0.5	0.4	0.44	0.2	0.04	0.75
2	G2T885W4	T8	0.5	0.4	0.85	0.2	0.04	0.75
2	G2T81.15W4	T8	0.5	0.4	1.15	0.2	0.04	0.75
2	G2T515W6	T5	0.8	0.6	0.15	0.2	0.04	0.75
2	G2T544W6	T5	0.8	0.6	0.44	0.2	0.04	0.75
2	G2T585W6	T5	0.8	0.6	0.85	0.2	0.04	0.75
2	G2T51.15W6	T5	0.8	0.6	1.15	0.2	0.04	0.75
2	G2T815W6	T8	0.8	0.6	0.15	0.2	0.04	0.75
2	G2T844W6	T8	0.8	0.6	0.44	0.2	0.04	0.75
2	G2T885W6	T8	0.8	0.6	0.85	0.2	0.04	0.75
2	G2T81.15W6	T8	0.8	0.6	1.15	0.2	0.04	0.75

In group 3, fillers are assumed to be in SSD conditions, similar to group 2. The superplasticizer-to-cement ratio is increased in the third group. Group 3 is specifically conducted for T5, with varying *fi/b* ratios for two different water-to-binder ratios: 0.4 and 0.6. The tables presented below offer a comprehensive overview of the mix proportioning.

Table 2.6: Mix proportioning for group 3

Group	NO	Filler type	<i>w/c</i>	<i>w/b</i>	<i>fi/b</i>	<i>FA/b</i>	<i>s/b</i>	<i>SP/c</i>
3	G3T515W4	T5	0.5	0.4	0.15	0.2	0.04	1
3	G3T544W4	T5	0.5	0.4	0.44	0.2	0.04	1
3	G3T585W4	T5	0.5	0.4	0.85	0.2	0.04	1
3	G3T51.15W4	T5	0.5	0.4	1.15	0.2	0.04	1
3	G3T515W6	T5	0.8	0.6	0.15	0.2	0.04	1
3	G3T544W6	T5	0.8	0.6	0.44	0.2	0.04	1
3	G3T585W6	T5	0.8	0.6	0.85	0.2	0.04	1
3	G3T51.15W6	T5	0.8	0.6	1.15	0.2	0.04	1

Figure 2.4 shows the equipment used for the mixing procedure. The hand-blender used is a Bosch Ergo-Mixx Style 800 W (model no. MS6CM4160).



Figure 2.4: Equipment for mixing filler-modified cement paste: metal bowl for dry particles, beakers for water and SP, with pipettes and a the hand-blender

A previous study from Sihaklang [17] designed a mixing procedure inspired by Ng et al. [15] and COIN Project [4]. As this study uses roughly the same amount of matrix for the tests, between 0.1 and 0.5L, the same mixing procedure is used. The procedure is described below.

- 1. Pre-mix dry:** All fillers and cement were premixed by hand in a metal bowl for 10 seconds.
- 2. Pre-mix wet:** Water and superplasticizer were pre-mixed together in the cylindrical plastic container.
- 3. Wet mixing:** Water and admixture from step 2 are added to the metal bowl with the dry powder.
- 4. Hand blender mixing:** Mixing with the hand blender using its highest speed for 30 seconds.
- 5. Rest:** Let the mix rest for 5 minutes
- 6. Hand blender mixing:** Mixing at high speed again for 1 minute, to avoid false set.
- 7. Finished:** The mix could then be tested.

2.3.2 Density and air content measurements

To measure the density and air content in the cement pastes a small, hollow cylinder was made (see Figure 2.5).

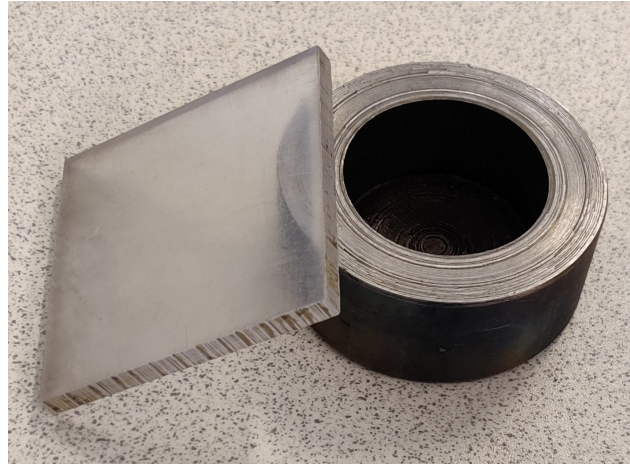


Figure 2.5: Cylinder for density and air content measurements and a piece of plexiglass

The volume of the cylinder was found by comparing the weight of the cylinder when it was empty and filled with water. The piece of plexiglass was used as a lid to prevent any air bubbles when the cylinder was filled with water (see Figure 2.6). This measurement was done before the tests on the cement paste started on the day, and the cylinder had an average volume of 39,27 cm³.



(a) Weight of cylinder and plexiglass



(b) Weight of cylinder filled with water

Figure 2.6: Measurements of the weight of cylinder with and without water

$$V_{cylinder} = \frac{W_{filled} - W_{empty}}{\rho_{water}} \quad (2.6)$$

To be able to calculate the fresh density of the cement paste, the weight of the empty cylinder was compared to the cylinder filled with cement paste (see Figure 2.7). For the soft cement pastes the mix was easily poured into the cylinder, but the stiffer mixes had to be packed by the spoon or by gently hitting the bottom of the cylinder against the table. The cylinder was filled with too much cement paste and then the plexiglass was used to scrape off excess, getting the cement paste plane with the cylinder. Paper towels were also used to remove any residue cement from the sides and top of the cylinder.

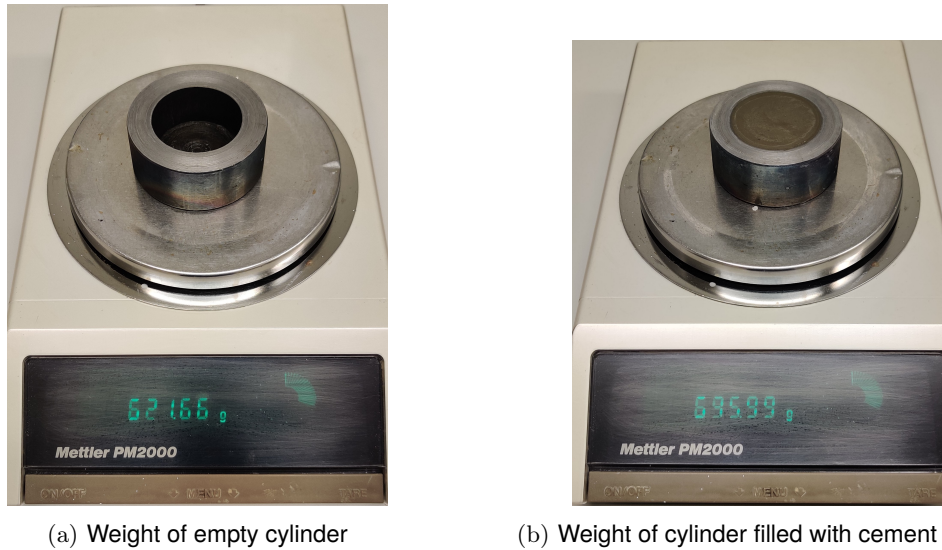


Figure 2.7: Measurements of the weight of cylinder with and without cement paste

The fresh density of the cement paste is:

$$\rho_{cement} = \frac{W_{filled} - W_{empty}}{V_{cylinder}} \quad (2.7)$$

To find the air content in the fresh cement paste, the measured density was compared to the theoretical density. The theoretical density is calculated from the density of the different materials, and the amount for the different mixes (see Appendix A). The air content is then calculated like this:

$$Air[\%] = \left(1 - \frac{\rho_{measured}}{\rho_{theoretical}}\right) * 100\% \quad (2.8)$$

2.3.3 Mini slump test

The slump test is a widely used evaluation test for assessing the workability and consistency of concrete, both in the field and laboratory settings. It provides a quick and convenient measure of the concrete's flow properties. The test involves filling a standardized slump cone with fresh concrete, compacting it, and then lifting the cone vertically. The height of the concrete slump, measured from the top of the cone to the displaced concrete surface, is reported as the slump value [16].

In addition to the traditional slump value, another parameter known as the slump flow value can be determined. The slump flow is the diameter measured as the concrete spreads after 25 drops. The slump value and slump flow are related to the static yield stress and dynamic yield stress of the concrete, respectively. The dynamic yield stress tends to vary inversely with the slump value. For 3DPC, which is a formless construction material, it is preferred to have a very low to zero slump, indicating a highly stiff and non-flowing concrete mix.

To evaluate the slump of smaller-scale cement paste or mini-cone measurements, a modified version of the slump cone test can be used [2]. This test involves using a truncated mini-cone with specific dimensions and a smooth plexiglass plate as the base (see Figure 2.8). The truncated mini-cone used has a top diameter = 39 mm, a bottom diameter = 89 mm, and a height = 70 mm. The mini-cone and the plexiglass were dampened to have less friction. The mini-cone is filled with fresh cement paste, if the paste was stiff this was done in three equal layers where each layer was compacted with 25 strokes using a compacting rod. Then the paste at the top is made level with the cone using a steel bar. The cone is then lifted, resulting in a slump specimen that is measured.

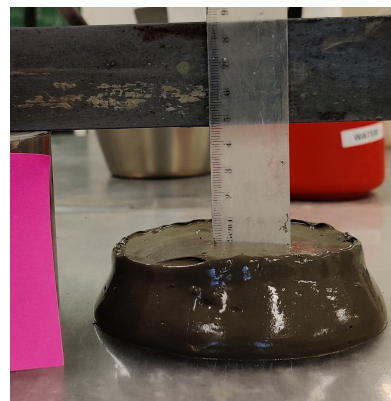


Figure 2.8: Equipment for mini-slump test: mini-slump cone, plexiglass, compacting rod, steel bar, rulers

When the flow has stopped the height and the diameter is measured. The height is measured as the difference between the top of the cone and the top of the paste, as shown in Figure 2.9b. This measurement is called the mini-slump value. The diameter of the slump specimen is measured in two orthogonal directions (see Figure 2.9a) and the average of these two measurements is called the mini-slump flow value.



(a) Measuring mini-slump flow value for G2T815W4



(b) Measuring mini-slump value for G2T815W4

Figure 2.9: Examples of mini-slump test on mix G2T815W4

2.3.4 Centrifuge

In order to measure the maximum packing density of each mixture, a centrifugation process was employed. The centrifugation machine used for this project was the Heraeus Megafuge 8 Centrifuge from Thermo Scientific (see Figure 2.10). This centrifugation procedure was based on the method previously employed by Ng [15] in her study on the kinematic viscosity of filler pore solution.



Figure 2.10: Centrifugation machine

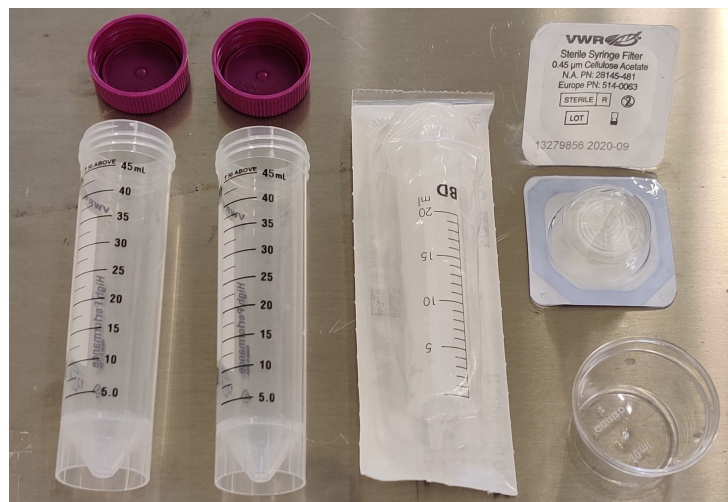
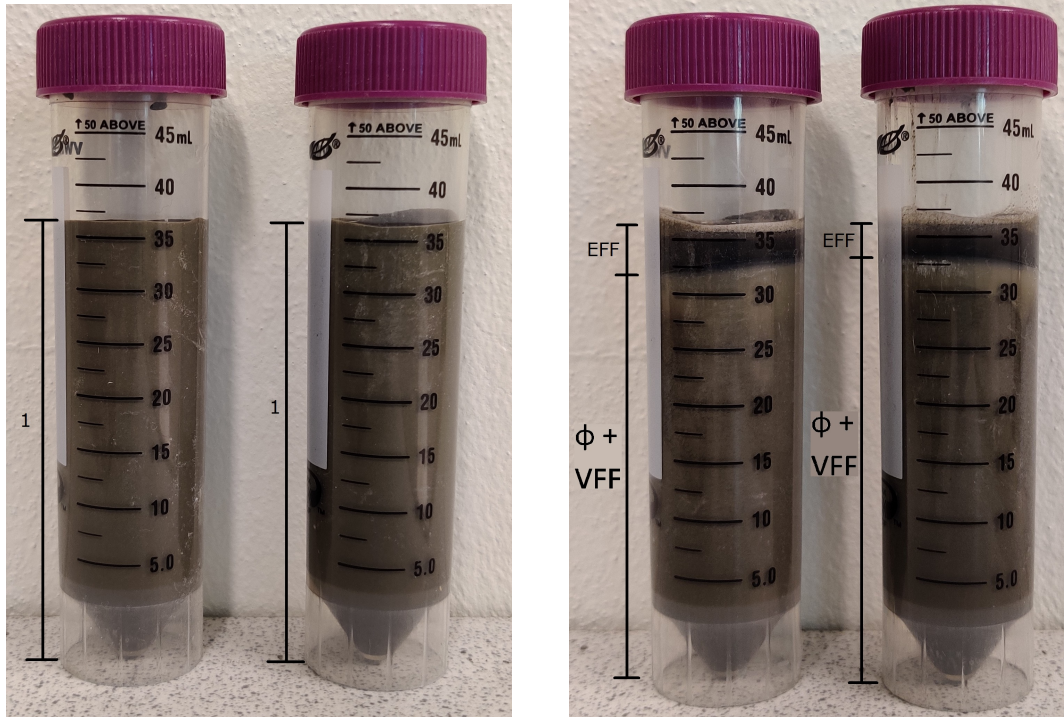


Figure 2.11: Centrifugation equipment: Two falcon tubes, a syringe, filters (size $0.45 \mu\text{m}$) and a cup

Following the completion of the mixing process, the prepared paste was transferred into a set of two falcon tubes, where it was essential to ensure that the total amount of each tube was approximately the same. This step was important because an unbalanced weight in the centrifugation machine could potentially

affect the balance and accuracy of the centrifugation process. Once the paste was transferred, the tubes were securely closed with their respective lids to prevent any leakage or contamination. These Falcon tubes had a standard volume of 45ml.

The centrifugation was carried out at a speed of 4000 RPM (rounds per minute) for a duration of 5 minutes, as specified by Ng [15]. This centrifugation process resulted in the particles being tightly packed, leading to a stiff cement paste, as seen in Figure 2.12.



(a) Falcon tube filled with paste before centrifugation (b) Falcon tube filled with paste after centrifugation

Figure 2.12: Pictures of falcon tubes before and after centrifugation

After centrifugation, the tubes were weighed individually and the EF from both tubes were poured into a small cup (see Figure 2.11). Using the syringe and two or three filters the EF was filtered and poured into a new cup, with a know weight, which was then weighed. The EF could then be calculated using the equation below, where $W_{tot,EF}$ is the weight of the EF, $W_{tot,paste}$ is the weight of the two syringes and ρ_{paste} is the theoretical density of the cement paste (see Appendix A).

$$EF\ fraction = \frac{W_{tot,EF}(g)}{W_{tot,paste}(g)} * \rho_{paste} \quad (2.9)$$

The relative concentration of solids (ϕ/ϕ_{max}) and liquid thickness (LT1, LT2) could then be calculated using the equations in 2.2.2 and 2.2.3.

2.3.5 3D printer

The printer used for this project is the Engine SR from the company Hyrel 3D, which is an American company that specializes in the development of industrial-grade 3D printing systems [11]. The Engine SR has a modular design, which allows for customization and flexibility in its configuration. It can be used to print various materials depending on the print head used, among them are cementitious materials. Figure 2.13 shows the Engine SR with a print head connected. The printer has a Windows tablet connected to it that runs Hyrel 3D's software Repetrel which is used to operate the printer.

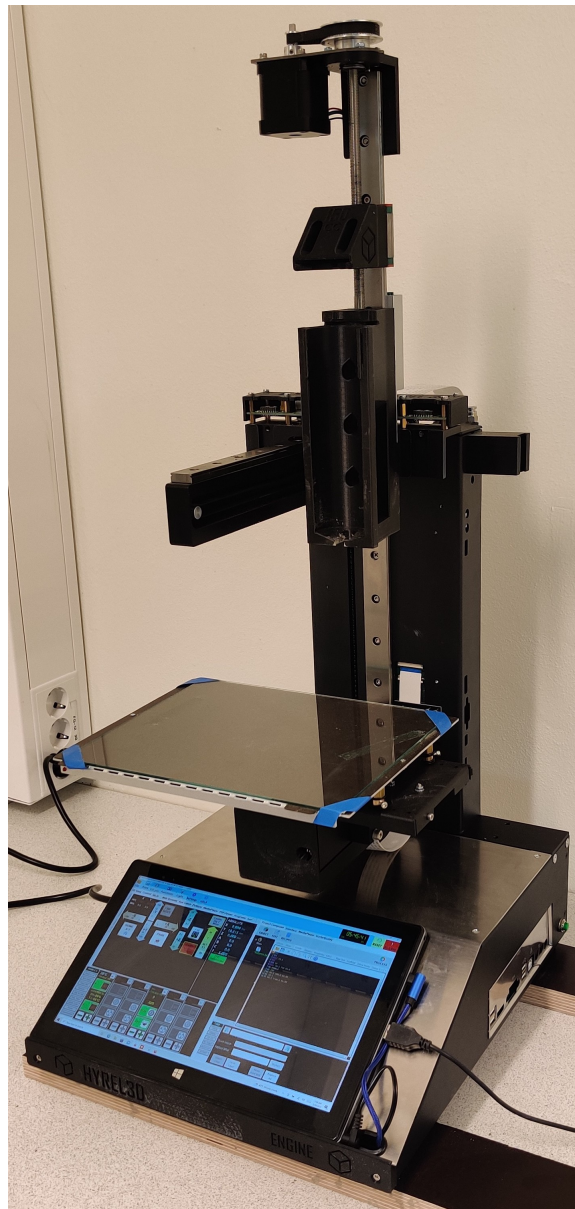


Figure 2.13: 3D printer Engine SR from Hyrel 3D with print head SDS 150 connected

Two tests were performed with the 3D printer, a mass flow measurement, and a printability test. To perform these tests the equipment shown in Figure 2.14 was used. The print head is a SDS 150, also made by Hyrel 3D, and is made for low viscosity paste to be printed at room temperature [13]. As the name suggests

this print head is made to fit a 150 ml syringe. As seen in Figure 2.13, the print head connects to the top of the printer with the pins on its circuit board located on the back of it. The print head has the motor and gears located on top of it, which rotates the drive screw to move the piston holder, which in turn moves the piston in the syringe. There is a switch on the circuit board that can be used to manually rotate the screw to push or pull the piston, without using code. The speed of the motor is decided in the G-code.

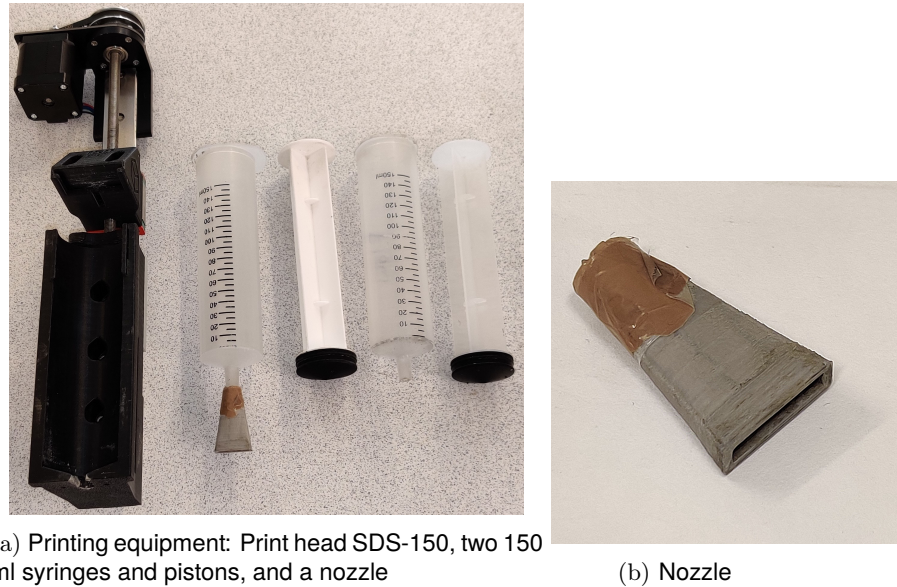


Figure 2.14: Equipment for 3D printing

The two syringes were used for the two different tests, the left syringe with the nozzle attached was used for the printability test. The nozzle is 3D printed and made to fit onto the end of the syringe and to print a rectangle shape more similar to what a wall looks like, its dimensions are 19 x 4 mm. The other syringe without the nozzle was used for the mass flow measurement.

Measuring mass flow rate

For the mass flow measurement, a balance was used to measure how much cement paste the printer printed per second. This was to see if the print head printed with the same speed with all the different mixes, or if it changed depending on the stiffness of the cement paste. The printer usually prints on a movable baseplate, which is only clamped to the back of the printer, because of this a metal stand was made to not put the heavy balance on top of the baseplate and to not have the balance accidentally move during printing (see Figure 2.15a). A metal sheet was put on top of the stand to make it easier to put the balance underneath the print head (see Figure 2.15b). The balance has two adjustable feet that were then used to make it level. When printing a couple of plexiglass pieces were put on top of the balance to make the difference between the balance and syringe lower so that the cement paste didn't drop as far. A paper towel was used to not dirty the plexiglass, so it didn't need to be cleaned between each trial.

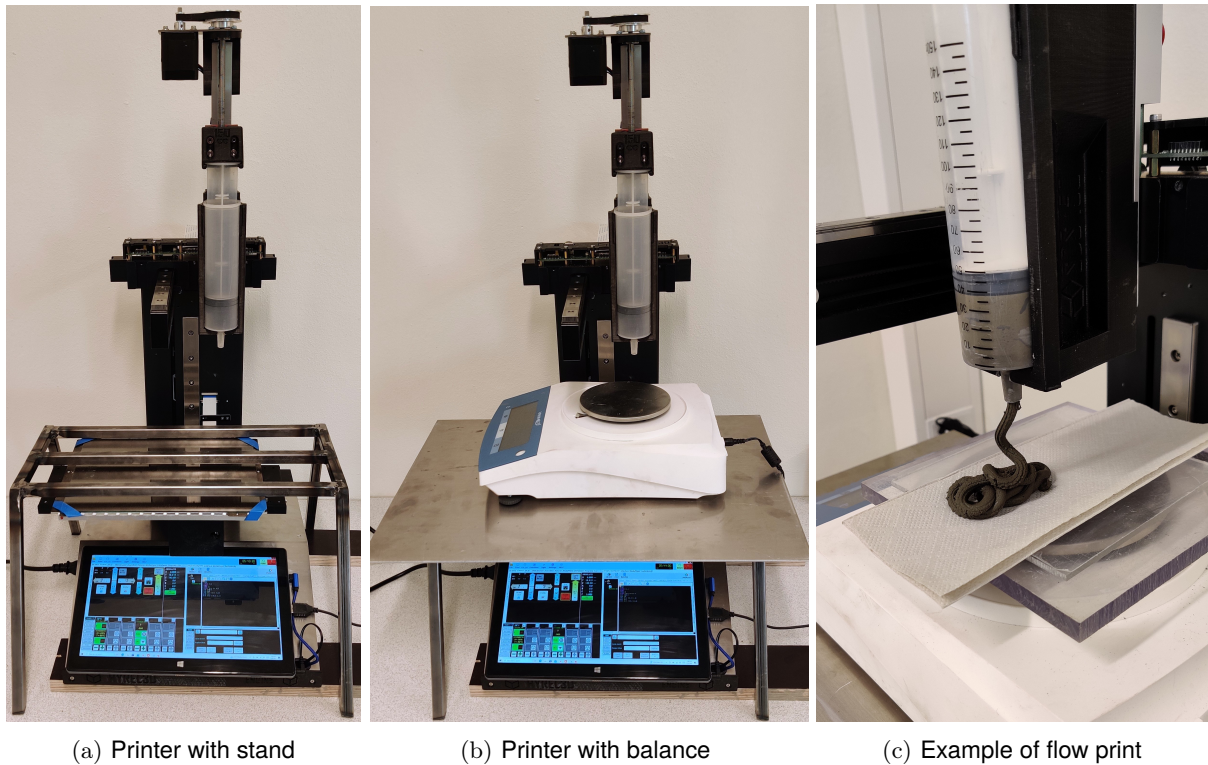


Figure 2.15: Stand and balance needed to measure mass flow

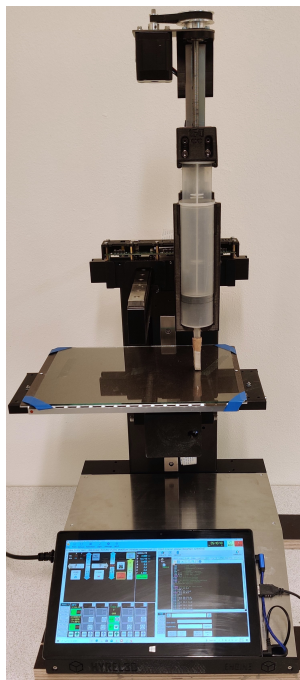
For the test around 20 to 30 ml of cement paste was filled into the syringe, then the piston was inserted into the syringe and pushed all the way so that the cement paste was at the end of the syringe tube. The syringe was then placed into the slot on the print head and the piston was hooked into place, as seen in Figure 2.15. Before starting the printing process the balance was connected to a computer where a small program was made to register the weight on the balance every second, these values were put in a simple text file. The balance was zeroed before starting the printing process.

A small code was made for this test, seen in Figure 2.20. Because of the stand, it was important to make a code that didn't move the baseplate at all, since it would hit the stand and disrupt the test. The code, therefore, made the printer print along the y-instead of the x-axis. The same printing speed as the printability test is used for this test, but only two lines were printed as it is enough data.

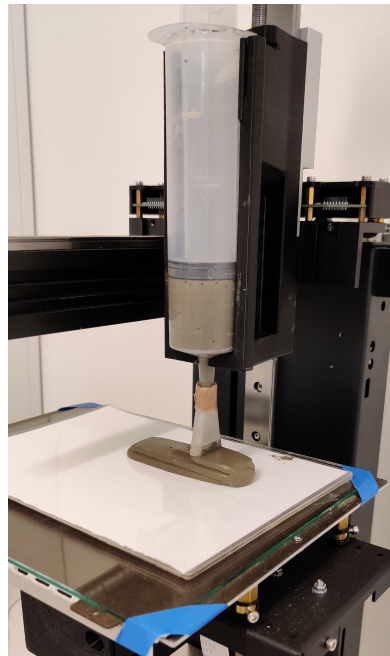
Because the mixes have various densities, the results have to be converted into volumetric flow instead of mass flow in order to compare the results to each other. The resulting list of weights/second are converted into volume/second by using the fresh density measurements. The volume is found by dividing the fresh density by 1000 to get the density converted to g/cm^3 , and then dividing the weights with this new density value.

Printability test

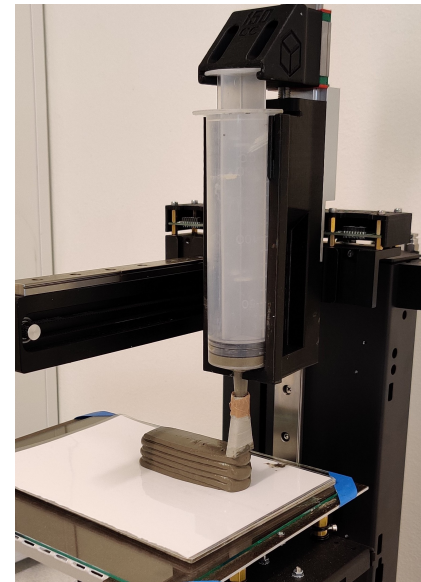
For the printability test the objective was to visually determine the extrudability and the buildability of the filler-modified cement mixes when printing it and after it is hardened. The same procedure as the mass flow measurements were followed, the only difference being that around 90 ml of the cement paste was filled into the syringe instead. After placing the syringe into the designated spot on the print head, the nozzle (Figure 2.14b) was put on the syringe. The piston was then pushed down, using the manual switch on the print head, to force the cement paste into the nozzle so that there was no delay when starting the code. A plexiglass plate was used to print on, so to avoid dirtying the baseplate. The baseplate was then moved up to the nozzle, close enough that you could barely slide a regular paper sheet between the nozzle and plexiglass plate (see Figure 2.16a).



(a) Printer in starting position for printability test



(b) During printability test



(c) End of printability test

Figure 2.16: Printer before, during and at the end of printability test

When printing the test that was gonna be hardened, a laminated paper was used so it could easily be moved to a climate room to be hardened. The G-code was then run, which printed 6 layers with a length of 80 mm.

Repetrel

Hyrel 3D has a proprietary software called Repetrel that runs its printers. Figure 2.17 shows the landing page for Repetrel.

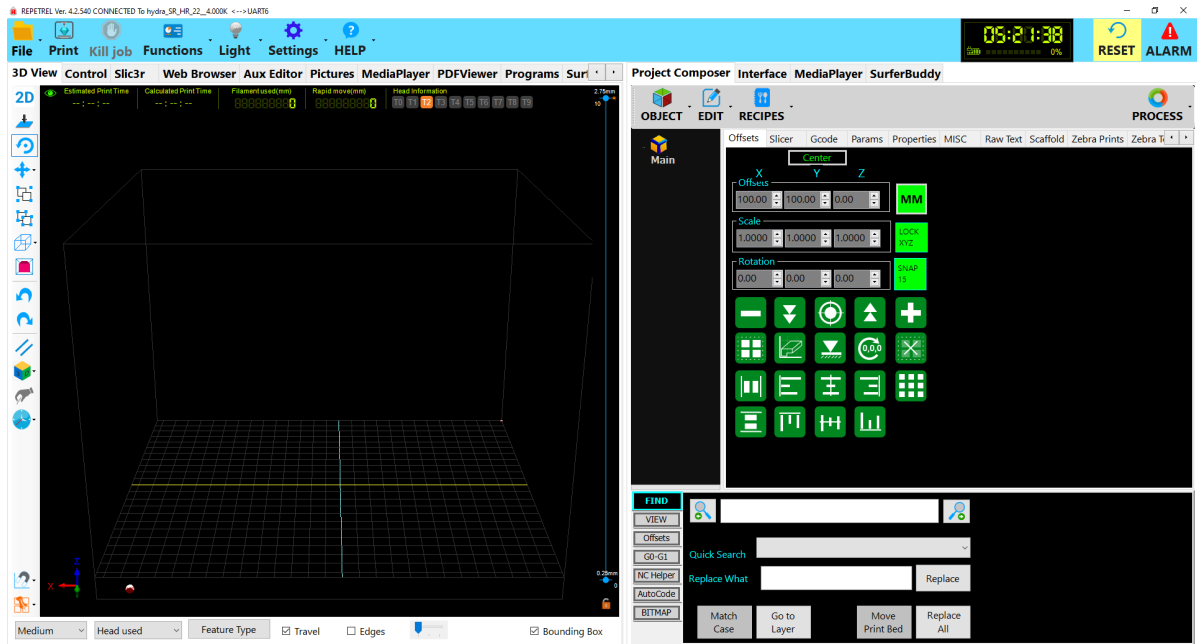


Figure 2.17: Landing page of Repetrel

The calibration for the printer's starting position is performed in the "Control" panel (see Figure 2.18). Pressing the arrows will move the print head (y-axis) or the baseplate (x- and z-axis), where the numbers are directional changes in mm. The "Home X-Y" button will move the print head and baseplate to $(x,y) = (0,0)$, and not change the z-coordinate. The "Park" button will move the print head and baseplate to a predetermined x- and y-coordinate, and again keep the same z-coordinate. The table on the right, under "Absolute", shows the current position in x, y, and z, and will give the live coordinates as it prints.

At the bottom of the "control tab" it shows the connection points of the printer and what's connected. Here it shows that the printer is connected in the third position and is the print head SDS 150.

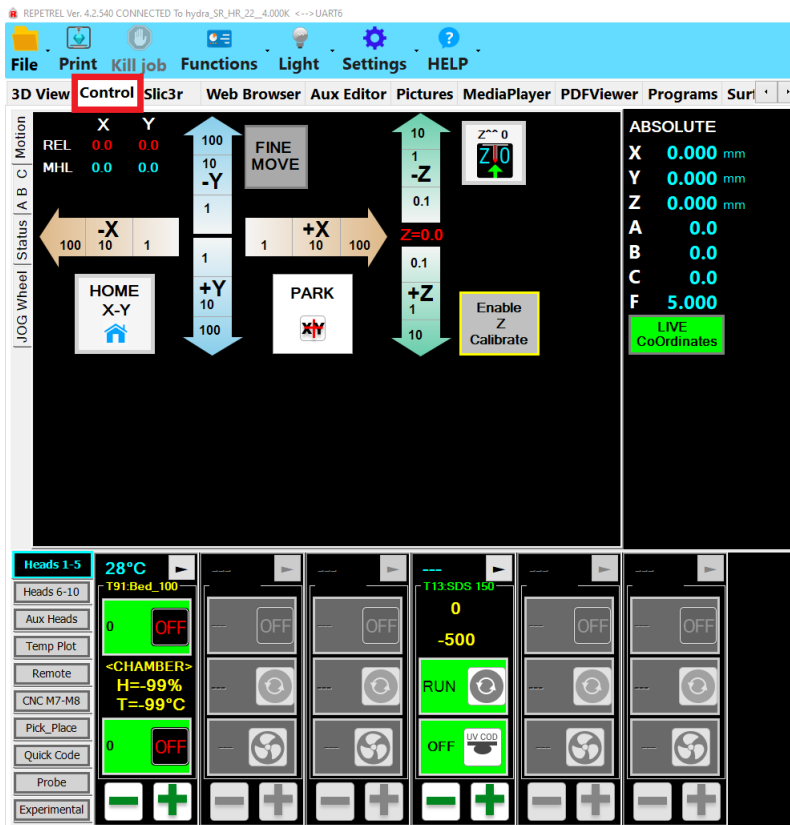


Figure 2.18: Control tab in Repetrel

The G-code file is added into the Repetrel software in the "Project Composer" tab on the right side (see Figure 2.19). As explained in 1.2.3 can G-code be generated from a CAD file, a script or made as a simple text file.

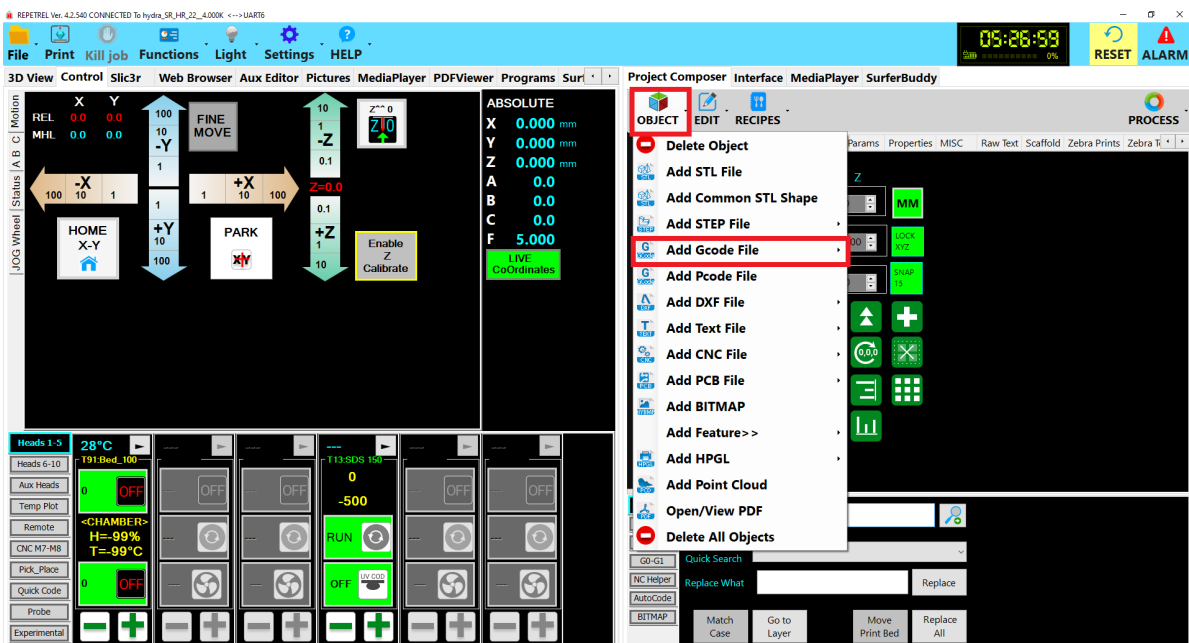


Figure 2.19: Adding Gcode in Repetrel

The G-Code file will show up by pressing the "Gcode" tab in "Project Composer" (see Figure 2.20). In this window the code can be changed, and any saved changes will also be saved in the local file on the computer. Changes made while printing will not alter the ongoing print.

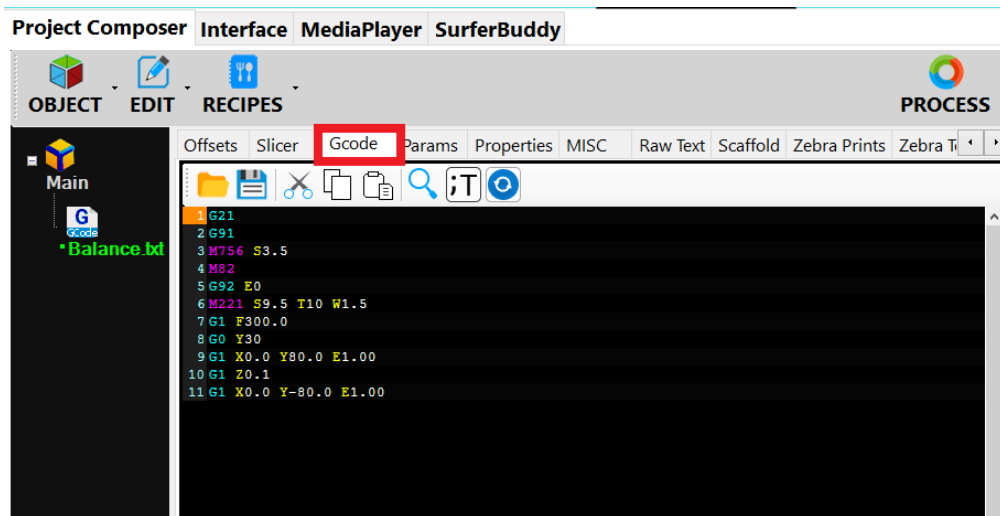


Figure 2.20: G-code for mass flow test in Repetrel

By clicking the print button (see Figure 2.21) the 3D printer will start printing the code that is added to Repetrel. If there are multiple files added, the printer will execute all of them one by one without breaks, starting with the top. While printing the height (z-axis) can be adjusted with the controls shown in Figure 2.21. Pressing the "Kill job" button, either next to the print button or in the control panel, will stop the printing job, with no changes in any direction. After the printing job is completed the "Kill job" button must be clicked in order to go back to the control panel (see Figure 2.18).

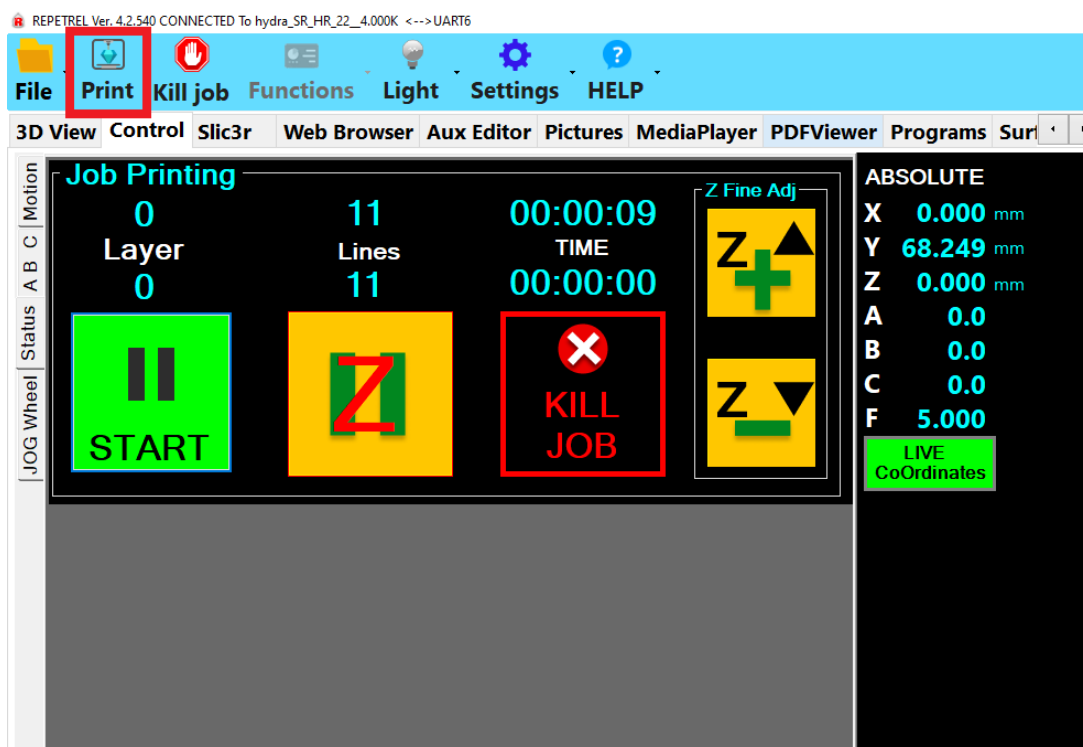
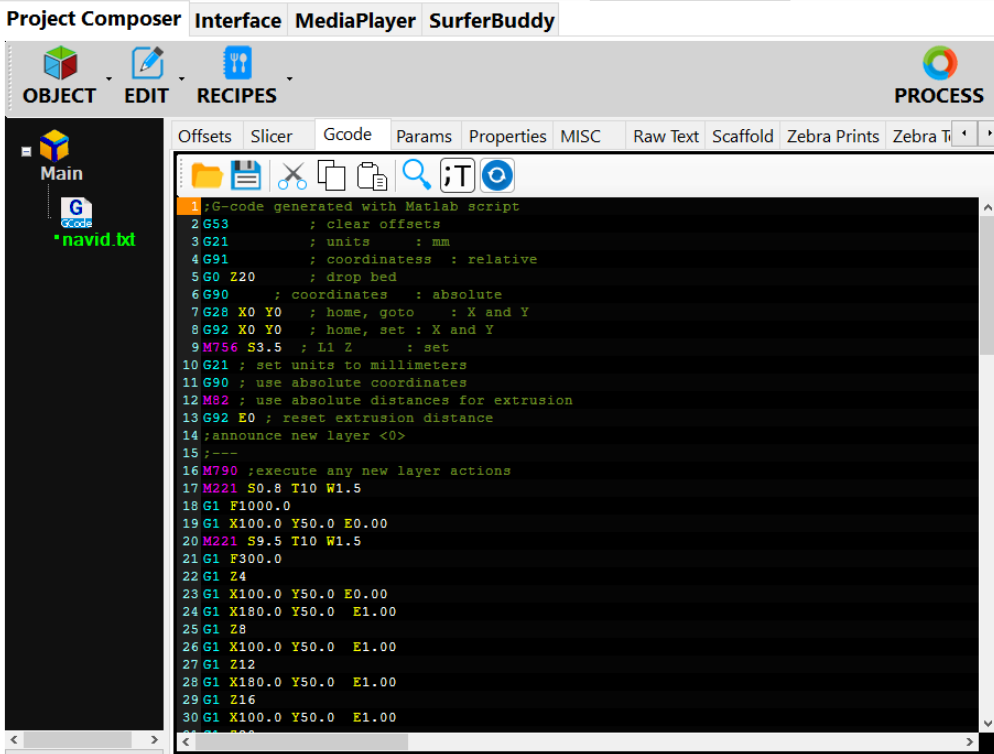


Figure 2.21: Control tab when printing in Repetrel

Coding

Two different sets of codes was used for the two different 3D printing tests, the first one for printability test was made by Navid Ranjbar from the Technical University of Denmark. The code was made from a Matlab script and is shown in Repetrel in Figure 2.22.



```
1:G-code generated with Matlab script
2 G53          ; clear offsets
3 G21          ; units      : mm
4 G91          ; coordinates : relative
5 G0 Z20      ; drop bed
6 G90          ; coordinates : absolute
7 G28 X0 Y0   ; home, goto  : X and Y
8 G92 X0 Y0   ; home, set  : X and Y
9 M756 S3.5   ; L1 Z      : set
10 G21        ; set units to millimeters
11 G90        ; use absolute coordinates
12 M82        ; use absolute distances for extrusion
13 G92 E0     ; reset extrusion distance
14 ;announce new layer <0>
15 ;---
16 M790 ;execute any new layer actions
17 M221 S0.8 T10 W1.5
18 G1 F1000.0
19 G1 X100.0 Y50.0 E0.00
20 M221 S9.5 T10 W1.5
21 G1 F300.0
22 G1 Z4
23 G1 X100.0 Y50.0 E0.00
24 G1 X180.0 Y50.0 E1.00
25 G1 Z8
26 G1 X100.0 Y50.0 E1.00
27 G1 Z12
28 G1 X180.0 Y50.0 E1.00
29 G1 Z16
30 G1 X100.0 Y50.0 E1.00
```

Figure 2.22: G-code for printability test in Repetrel

AS seen in Figure 2.22, Ranjbar has explained with a few words what each part of the code does, the explanations for each command and more can be found at Hyrel 3Ds wiki page [12]. The important commands are the first ones, listed below.

G53: clears any offsets in the coordinates that might have been set in another code previously.

G21: sets the units for the following to mm

G91: makes a stipulation that the next commands that involves any positioning, are relative to the starting position of the printer. The next command "G0 Z20" adheres to this and lowers the baseplate 20 mm from its current position. It's then important to make sure the baseplate has enough height to drop.

G90: makes a new stipulation that overrides "G91", and makes any commands involving positioning will be calculated from the origin point $(x,y)=(0,0)$, in other words absolute positioning.

G28 X0 Y0: this is a send to home command that positions the print head and baseplate in the origin point $(0,0)$, for the baseplate that's all the way to the left, and for the print head it's all the way back away from the front.

G92 X0 Y0: G92 is used to set offsets in the coordinates, but here it only sets the current position to the

same coordinates.

M756 S3.5: this is the first command that's made for this software. Because Repetrel does calculations for flow rate internally, the values for the calculations can be changed in the G-code, the flow calculation is further explained later. This command sets the desired thickness for the layer of print, here it is set to 3,5 mm.

M82: sets a stipulation that extrusion positioning is going to be calculated from the origin point, in other words absolute calculations.

G92 E0: resets the offset of extrusion position to 0.

M790: has no parameters, just declares a new layer, which can trigger new layer actions, but in this case there are none.

M221 S9.5 T10 W1.5: this command is used to set the flow rate. "S" sets the flow multiplier, so the flow rate is multiplied by 9.5. "W" sets the width of the cross section of the volume to fill, here 1.5 mm. "T" informs the printer about which print head to use, more useful if there are multiple.

G1 F300: this sets the feed rate/travel speed to 300 mm/min. It is important to note that this changes both the travel speed of the print head/baseplate, and also the print speed.

G1 X100.0 Y50.0 E0.00: moves the print head and baseplate into coordinates (100,50). "E0.00" turns off extrusion, "E1.00" turns on the extrusion.

The rest of the code is just positioning and setting feed rate, which is explained already explained in 1.2.3. The code prints 6 layers, each 80 mm long, and drops the baseplate 4 mm for every layer. The flow rate is calculated in the software from the commands that has been used, "M221" and "F". This flow rate was decided by trial and error method by Ranjbar, until a suitable 3D print was printed.

The code for the second 3D printer experiment, the flow rate test, was made for this thesis based on the code made by Ranjbar. The code is showed in Figure 2.19. The code was made with only the necessary commands to make two lines of print. The main difference is that this code uses relative positioning instead of absolute, this is because of the stand made for the balance was blocking the baseplate. So before printing with this code the print head and baseplate had to be manually moved into the desired position using the control panel in Repetrel (see Figure 2.18). The other difference is that the print is done along the y-axis instead of the x-axis. The same speed is used as in the code used for the printability test.

Flow rate

According to the Hyrel 3D wiki, the flow rate is calculated based on five values [12]:

1. **Path width [mm]:** specified by the "W" in the "M221" command.
2. **Layer thickness [mm]:** specified by "S" in the "M756" command.
3. **Print speed [mm/min]:** specified by "F" in the "G1" command.
4. **Pulses per microliter [pulses/ μl = pulses/ m^3]:** specified by the data for the print head, unless manually overridden by using a "P" command behind the "M221" command.
5. **Material Flow Rate Multiplier:** specified by "S" in the "M221" command.

Multiplying these values together gives the flow rate in pulses/min. Using the print head motor data, a calculation can be made to find how many pulses are required to make the screw do one revolution (pulses/revolution). The next step is to divide the flow rate (pulses/min) by pulses/rev. to get rev./min or rev./sec.

Then the volume one revolution of the screw would extrude is calculated, using the pitch of the screw (to figure out linear travel) and the area of the syringe. Then the flow rate in $\mu\text{l}/\text{sec}$ could be calculated.

An attempted on doing these calculations were done, using the data on the motor from the Hyrel 3D wiki, as well as the data in G-code, and assuming a linear travel of 1 mm per revolution for the screw. The calculations gave a result of 0.30 rev./sec., which is 3.34 sec./rev. But with a simple test of timing the revolutions when printing using a stopwatch, the speed was closer to 1.9 sec./rev. So it could not be used to compare with the volumetric flow from the mass flow measurements.

3. Results and discussion

3.1 Results and discussion of fresh density and air void measurements

The tables below (3.1, 3.2 and 3.3) show the result from the fresh density measurements and air content, as described in 2.3.2, for each of the groups described in 2.3.1. For groups 1 and 2 these measurements were first done twice for each mix, with the reason to check the consistency of the results and if the results were unreasonable in comparison to the theoretical density. The results of these two repetitions gave differences for some of the mixes that were too big to be satisfied with. A few of the tests also gave unreasonable results where the measured density was higher than the theoretical density, meaning the air content was below 0,0. The tests were therefore repeated one or two more times to check if the tests were a reliable way of measuring fresh density and air content (see full results in Appendix B). The third and fourth repetitions were only used on the mixes with T5 because of a limited supply of T8. The measured fresh density and air content in the tables below are an average of the results from two to four repetitions.

Table 3.1: Density and air measurements of group 1

Group	NO	Theoretical density [kg/m ³]	Average measured density [kg/m ³]	Average air content [%]
1	G1T515W4	1932,04	1927,01	0,3
1	G1T544W4	2025,00	2007,54	0,9
1	G1T585W4	2124,65	2109,09	0,7
1	G1T51.15W4	2181,37	2112,10	3,2
1	G1T815W4	1947,03	1903,53	2,2
1	G1T844W4	2066,22	2028,53	1,8
1	G1T885W4	2197,36	2117,11	3,7
1	G1T81.15W4	2273,60	2139,25	5,9
1	G1T515W6	1746,50	1702,28	2,5
1	G1T544W6	1840,47	1808,03	1,8
1	G1T585W6	1946,31	1922,71	1,2
1	G1T51.15W6	2009,05	1983,19	1,3
1	G1T815W6	1757,34	1699,06	3,3
1	G1T844W6	1871,09	1802,73	3,7
1	G1T885W6	2002,05	1929,83	3,6
1	G1T81.15W6	2081,16	2026,62	2,6

Table 3.2: Density measurements of group 2

Group	NO	Theoretical density [kg/m ³]	Average measured density [kg/m ³]	Average air content [%]
2	G2T515W4	1931,60	1900,21	1,6
2	G2T544W4	2023,82	2010,35	0,7
2	G2T585W4	2122,61	2096,46	1,2
2	G2T51.15W4	2178,81	2101,38	3,6
2	G2T815W4	1941,56	1906,09	1,8
2	G2T844W4	2051,06	2028,38	1,1
2	G2T885W4	2170,39	2133,48	1,7
2	G2T81.15W4	2239,23	2174,37	2,9
2	G2T515W6	1746,19	1692,55	3,1
2	G2T544W6	1839,60	1796,84	2,3
2	G2T585W6	1944,74	1909,55	1,8
2	G2T51.15W6	2007,03	1971,30	1,8
2	G2T815W6	1753,39	1676,94	4,4
2	G2T844W6	1859,85	1780,64	4,3
2	G2T885W6	1981,44	1926,11	2,8
2	G2T81.15W6	2054,39	2022,04	1,6

The mixes in group 3 were the last to be tested and were only tested once, as there was limited time. Also more repetitions on group 3 weren't necessary as the results from group 3 were reasonable enough, and the multiple repetitions of these tests on group 1 and 2 have also given enough valuable information.

Table 3.3: Density measurements of group 3

Group	NO	Theoretical density [kg/m ³]	Average measured density [kg/m ³]	Average air content [%]
3	G3T515W4	1929,79	1909,30	1,1
3	G3T544W4	2022,07	1995,67	1,3
3	G3T585W4	2120,96	2085,61	1,7
3	G3T51.15W4	2177,23	2107,01	3,2
3	G3T515W6	1745,03	1703,44	2,4
3	G3T544W6	1838,42	1815,03	1,3
3	G3T585W6	1943,56	1927,13	0,8
3	G3T51.15W6	2005,89	1982,42	1,2

As seen in the tables the fresh density is lower than the theoretical density, which is expected as the mixes will have some amount of air inside. The tables also show that the measured fresh density is around 1-5% lower than the theoretical density for each mix, which was the predicted result. The measured fresh densities also show little difference between the results for group 1 and 2.

Figures 3.1 and 3.2 show the calculation of the average air content plotted against fi/b ratio. The results

are separated into two plots, one for $w/b=0,4$ and one for $w/b=0,6$. This is because of the small pattern they show that with $w/b=0,4$ the air content increases with an increase of filler, and the mixes with $w/b=0,6$ have a decrease in air content with higher filler amount.

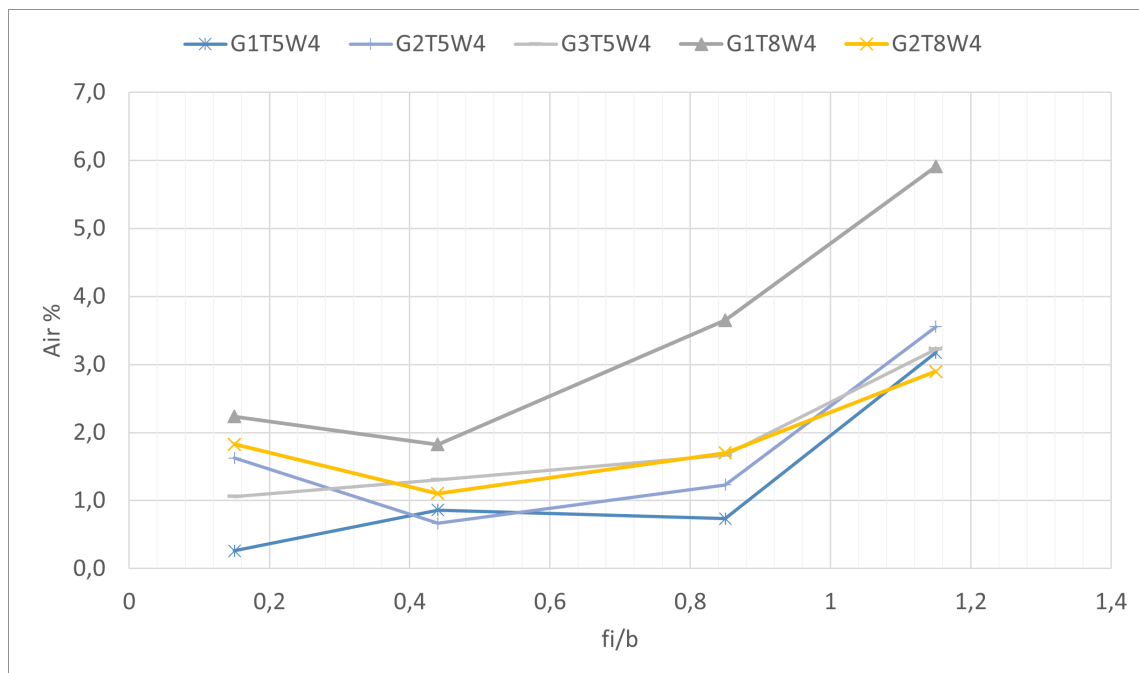


Figure 3.1: Calculated average air content of mixes with $w/b=0,4$ plotted against fi/b

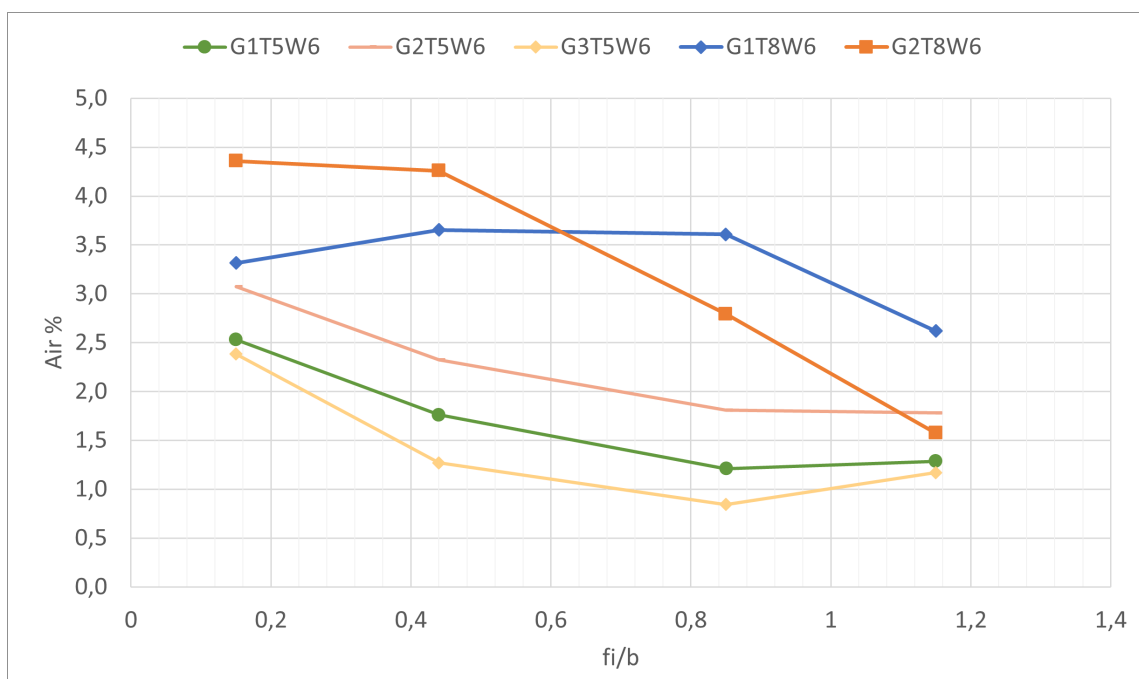


Figure 3.2: Calculated average air content of mixes with $w/b=0,6$ plotted against fi/b

When looking at the results for the repetitions done for each mix, there is big inconsistencies between the measured air content. Table 3.4 shows an example of four results from the repeated tests on the the mix G1T515W4, and as seen the results show too big of a difference between them to be deemed as a valid test for finding air content.

Table 3.4: Air content measurements of G1T515W4

Group	NO	Air %, test 1	Air %, test 2	Air %, test 3	Air %, test 4	Air %, average
1	G1T515W4	1,9	-2,6	0,3	1,3	1,1

As the air content is calculated from the fresh density measurement (see 2.3.2) we can draw the conclusion that measuring air content using this method is unreliable. The precision of the different steps in the test has too big of an impact when the test amount is so small. One of the observed possibility of error in this test was getting the exact same amount of paste into the cylinder in each test. The soft mixes ($w/b = 0,6$) were very liquid and would stick to the plexiglass when trying to scrape of excess, just like water, and would therefore scrape off too much. The method for those mixes were then changed to a visual approach where the cement paste was filled into the cylinder until it was plane with the cylinder when looking straight at it. The stiffer mixes ($w/b = 0,4$) were, as described in 2.3.2, gently hit down on the table to compact it. This causes air bubbles to rise to the surface of the cement paste and be released from the paste. As there is no way to consistently hitting the cylinder with the same exact force using only hands, there would automatically be some small differences in the air content depending on how much the cement paste compacts and how much air is released.

3.2 Results of mini-slump test

The mini-slump test was performed two times on the mixes in group 1 and 2, and once on group 3. The mini-slump value and flow value was calculated as an average of of the two tests in group 1 and 2. The mini-slump value was only measured on the stiffer mixes ($w/b = 0,4$), as it is not relevant when the cement paste is too fluid (see Figure 3.5a). The tables below (3.5, 3.6 and 3.7) show the results of the mini-slump test for the mixes in each group.

Table 3.5: Mini-slump value and flow value for group 1

Group	NO	Mini-slump value [mm]	Mini-slump flow value [mm]
1	G1T515W4	36,0	102,0
1	G1T544W4	34,5	96,5
1	G1T585W4	25,0	94,5
1	G1T51.15W4	12,5	91,8
1	G1T815W4	43,5	106,8
1	G1T844W4	40,0	99,5
1	G1T885W4	22,0	94,5
1	G1T81.15W4	11,5	92,8
1	G1T515W6	-	296,0
1	G1T544W6	-	293,0
1	G1T585W6	-	228,8
1	G1T51.15W6	-	164,0
1	G1T815W6	-	312,5
1	G1T844W6	-	265,0
1	G1T885W6	-	215,5
1	G1T81.15W6	-	166,5

Table 3.6: Mini-slump value and flow value for group 2

Group	NO	Mini-slump value [mm]	Mini-slump flow value [mm]
2	G2T515W4	44,0	115,8
2	G2T544W4	40,0	99,5
2	G2T585W4	22,0	93,3
2	G2T51.15W4	10,5	93,0
2	G2T815W4	46,5	114,0
2	G2T844W4	40,0	99,0
2	G2T885W4	22,5	91,8
2	G2T81.15W4	12,0	91,5
2	G2T515W6	-	305,0
2	G2T544W6	-	283,5
2	G2T585W6	-	221,8
2	G2T51.15W6	-	193,8
2	G2T815W6	-	322,3
2	G2T844W6	-	280,3
2	G2T885W6	-	236,3
2	G2T81.15W6	-	169,0

Table 3.7: Mini-slump value and flow value for group 3

Group	NO	Mini-slump value [mm]	Mini-slump flow value [mm]
3	G3T515W4	51,0	134,0
3	G3T544W4	47,0	110,5
3	G3T585W4	33,0	94,5
3	G3T51.15W4	18,0	95,0
3	G3T515W6	-	338,0
3	G3T544W6	-	331,5
3	G3T585W6	-	280,5
3	G3T51.15W6	-	227,0

The results of the mini-slump flow value are visualized with line graphs in the figures below, again using SSA filler as the values for the x-axis for the same reasons given before. Figure 3.3 shows that the mixes in group 1 and 2 when using T5 has little difference between them, in comparison to Figure 3.4 where we can see a more clear difference between group 1 and 2, looking at the mixes with $w/b = 0,6$ on both graphs. This results was predicted as T8 has a higher water adsorption rate, and therefore the differences in group 1 and 2 is higher than the mixes using T5. Group 3 has a higher mini-slump flow value because of the added SP, which makes the cement paste more flowable.

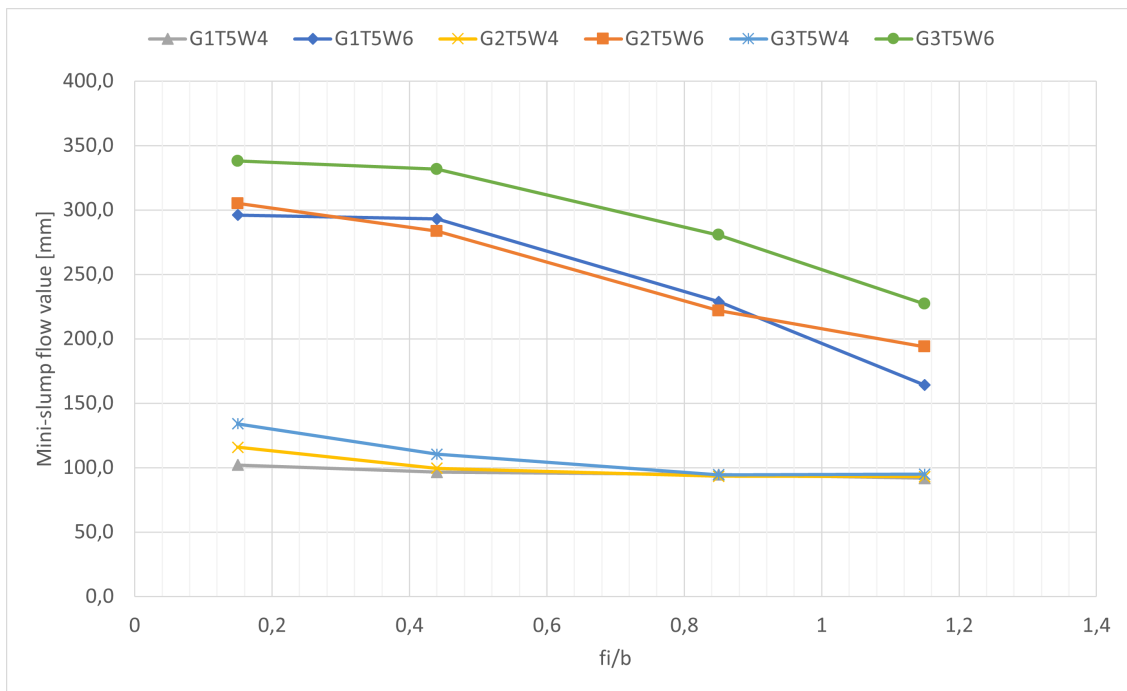
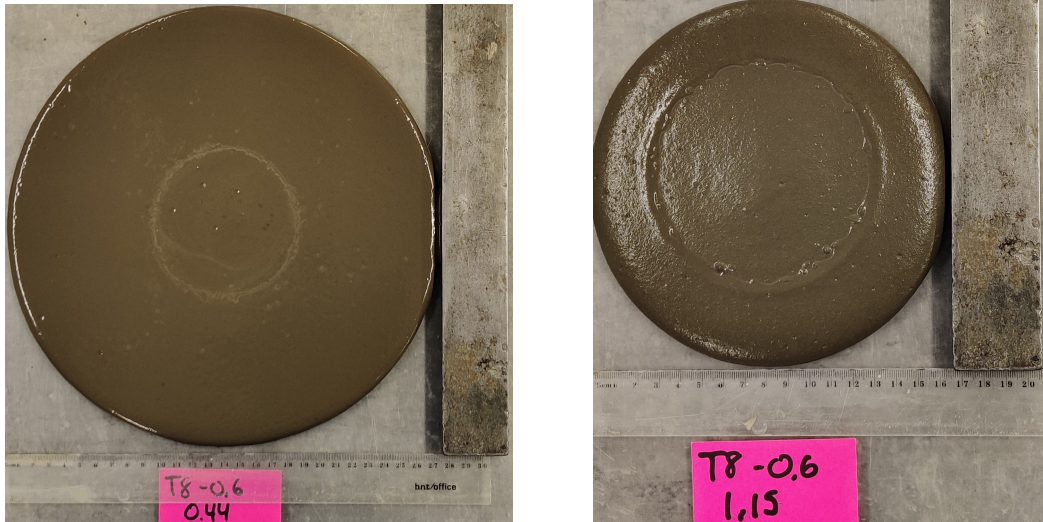


Figure 3.3: Mini-slump flow value of mixes using filler T5 plotted against f_i/b



Figure 3.4: Mini-slump flow value of mixes using filler T8 plotted against f_i/b

The tables and graphs show that the softer cement pastes ($w/b = 0,6$) have a significantly higher mini-slump flow value than the stiffer mixes ($w/b = 0,4$). They have a mini-slump flow value between 160 and 340 mm. Figure 3.5 shows two examples of the softer mixes. To be able to have a printable cement paste a stiff paste is needed, as described in section 2.3.3, and as shown in Figure 3.5, the mixes with $w/b = 0,6$ are too soft to be printable.



(a) Mini-slump flow value for G2T815W6 = 276 mm (b) Mini-slump flow value for G2T81.15W6 = 166 mm

Figure 3.5: Examples of mini-slump flow value using T8 from Group 2

As there is such a small difference in the mini-slump flow values of the mixes with $w/b = 0,4$, the mini-slump value is instead used to compare them and determine their printability. Figure 3.6 shows a line graph diagram with all of the mixes with $w/b = 0,4$. Here the measured fresh density is used for the x-axis, instead of SSA filler, to be able to more easily compare the results for mixes using both T5 and T8. The line graphs again show a small difference between the mixes from group 1 and 2, but the differences are so small so it can be assumed that it comes from the precision of the mini-slump test. G1T5W4 was also the first mix to be tested, which also may contribute to the difference in results, being unfamiliar with the testing method. All the mixes shows the same pattern of having a small difference between mixes with $f_i/b = 0,15$ and $f_i/b = 0,44$, then a bigger jump between $f_i/b = 0,44$ and $f_i/b = 0,85$, and $f_i/b = 0,85$ and $f_i/b = 1,15$. These results, as well as the visual analysis of the slump specimen, will be important to determine the buildability of the mix, as described in 1.2.2.

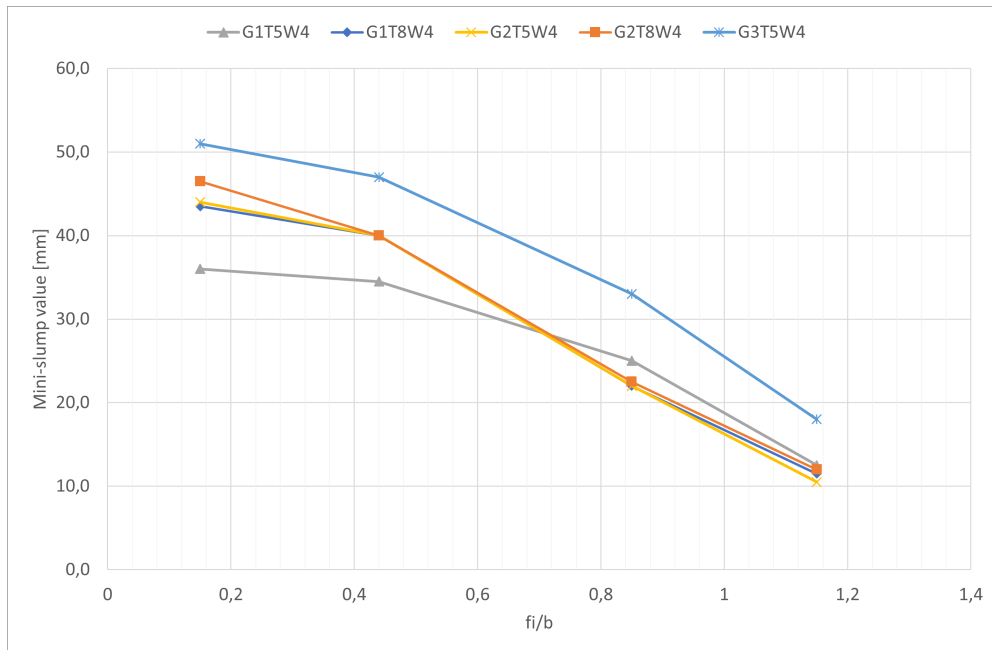
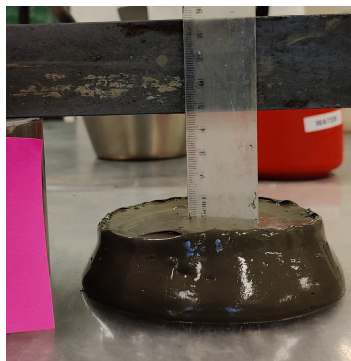
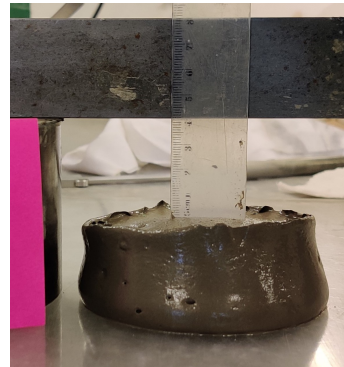


Figure 3.6: Mini-slump value for mixes with $w/b = 0.4$ plotted against f_i/b

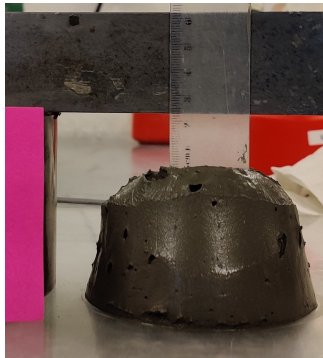
Figure 3.7 shows tests done on mixes using T8 from group 2 with $w/b = 0.4$. These slump specimens show a more desired look to what a printable cement paste looks like, in comparison to Figure 3.5. As mentioned previously in 2.3.3 3D printing of concrete is formless which means that the paste has to have high buildability, as explained in 1.2.2. By looking at these slump specimens it is easy to see that mixes G2T885W4 and G2T81.15W4 are more likely to be able to hold its form after being printed.



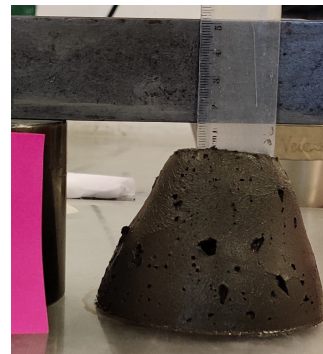
(a) Mini-slump value for G2T815W4 = 46,5 mm



(b) Mini-slump value for G2T844W4 = 40,0 mm



(c) Mini-slump value for G2T885W4 = 22,5 mm



(d) Mini-slump value for G2T81.15W4 = 12 mm

Figure 3.7: Examples of mini slump test using T8 from Group 2

3.3 Results of centrifugation test

Because the air content measurements was unreliable, the air content in equation 2.1 is neglected when calculating the maximum packing, changing it to the equation below.

$$\phi_{max} = \frac{\phi}{1 - EF} \quad (3.1)$$

The results from the measurements are tabulated in the tables 3.8, 3.9 and 3.10. The test was only done once per mix due to time constraint.

Table 3.8: Measurements and results of centrifugation test for group 1

NO	EF [g]	Falcon tubes weight [g]	EF fraction	ϕ_{max}	ϕ/ϕ_{max}	LT1 [μm]	LT2 [μm]
G1T515W4	6,10	153,30	0,08	0,54	0,92	0,169	0,052
G1T544W4	4,70	174,80	0,05	0,59	0,95	0,186	0,041
G1T585W4	2,90	168,30	0,04	0,65	0,96	0,203	0,032
G1T51.15W4	2,10	161,90	0,03	0,68	0,97	0,213	0,027
G1T815W4	4,60	133,40	0,07	0,53	0,93	0,167	0,045
G1T844W4	3,90	164,30	0,05	0,58	0,95	0,180	0,036
G1T885W4	3,20	187,70	0,04	0,64	0,96	0,190	0,030
G1T81.15W4	2,10	199,30	0,02	0,66	0,98	0,193	0,020
G1T515W6	9,20	105,40	0,15	0,47	0,85	0,203	0,129
G1T544W6	10,20	131,50	0,14	0,53	0,86	0,229	0,132
G1T585W6	4,80	138,60	0,07	0,56	0,93	0,257	0,069
G1T51.15W6	4,00	124,20	0,06	0,60	0,94	0,273	0,072
G1T815W6	12,20	126,10	0,17	0,48	0,83	0,201	0,142
G1T844W6	9,10	126,00	0,14	0,52	0,86	0,220	0,120
G1T885W6	5,40	109,50	0,10	0,57	0,90	0,238	0,094
G1T81.15W6	3,80	106,70	0,07	0,60	1,00	0,247	0,074

Table 3.9: Measurements and results of centrifugation test for group 2

NO	EF [g]	Falcon tubes weight [g]	EF fraction	ϕ_{max}	ϕ/ϕ_{max}	LT1 [μm]	LT2 [μm]
G2T515W4	6,80	168,60	0,08	0,54	0,92	0,169	0,053
G2T544W4	4,30	165,60	0,05	0,59	0,95	0,186	0,040
G2T585W4	2,90	182,80	0,03	0,64	0,97	0,203	0,029
G2T51.15W4	2,70	186,40	0,03	0,68	0,97	0,213	0,030
G2T815W4	6,10	163,20	0,07	0,54	0,93	0,167	0,049
G2T844W4	4,90	181,40	0,06	0,59	0,94	0,180	0,040
G2T885W4	2,90	171,30	0,04	0,64	0,96	0,190	0,029
G2T81.15W4	2,40	159,90	0,03	0,67	0,97	0,193	0,029
G2T515W6	12,90	143,90	0,16	0,47	0,84	0,203	0,133
G2T544W6	9,50	146,40	0,12	0,52	0,88	0,229	0,110
G2T585W6	5,80	128,80	0,09	0,57	0,91	0,257	0,090
G2T51.15W6	4,70	160,10	0,06	0,60	0,94	0,273	0,065
G2T815W6	13,40	135,60	0,17	0,48	0,83	0,201	0,145
G2T844W6	10,50	136,40	0,14	0,53	0,86	0,220	0,127
G2T885W6	7,30	146,80	0,10	0,57	0,90	0,238	0,094
G2T81.15W6	5,50	170,00	0,07	0,59	0,93	0,247	0,066

Table 3.10: Measurements and results of centrifugation test for group 3

NO	EF [g]	Falcon tubes weight [g]	EF fraction	ϕ_{max}	ϕ/ϕ_{max}	LT1 [μm]	LT2 [μm]
G3T515W4	4,90	155,50	0,06	0,53	0,94	0,169	0,041
G3T544W4	3,30	172,60	0,04	0,58	0,96	0,186	0,029
G3T585W4	2,20	197,50	0,02	0,64	0,98	0,203	0,020
G3T51.15W4	2,10	174,00	0,03	0,68	0,97	0,213	0,025
G3T515W6	11,10	137,60	0,14	0,47	0,86	0,203	0,119
G3T544W6	8,10	148,60	0,10	0,51	0,90	0,229	0,092
G3T585W6	5,10	159,70	0,06	0,56	0,94	0,257	0,064
G3T51.15W6	4,20	159,10	0,05	0,59	0,95	0,273	0,059

Figures 3.8 and 3.9 shows the relationship between the relative concentration of solids (ϕ/ϕ_{max}) and mini-slump flow value, which is directly correlated to yield stress, for mixes using T5 and T8 respectively. The plots show similar patterns of increasing ϕ/ϕ_{max} leads to a decrease in mini-slump flow value, especially for the mixes with w/b = 0,6. There is also a small noticeable difference between groups 1 and 2, where group 2 has a slightly higher mini-slump flow value for the same ϕ/ϕ_{max} . This was predicted as group 2 has a slightly higher water content, but it was predicted a bigger difference for T8 then for T5. So these differences might come from the accuracy of the testing methods.

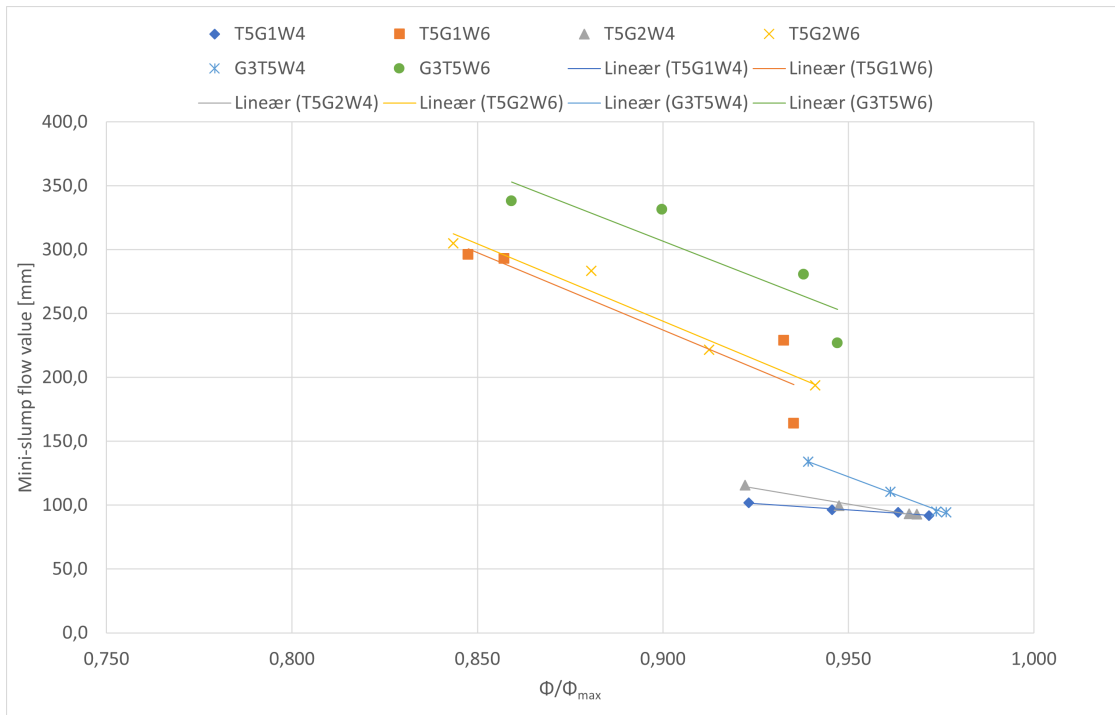


Figure 3.8: ϕ/ϕ_{max} for mixes using filler T5 plotted against mini-slump-flow value

As seen on Figure 3.8 there is a huge difference for the mixes with SP = 1%, where it shows a much higher mini-slump flow value for the same ϕ/ϕ_{max} , when compared to the mixes in group 1 and 2. This means that it is possible to control mini-slump flow value with both SP and ϕ/ϕ_{max} .

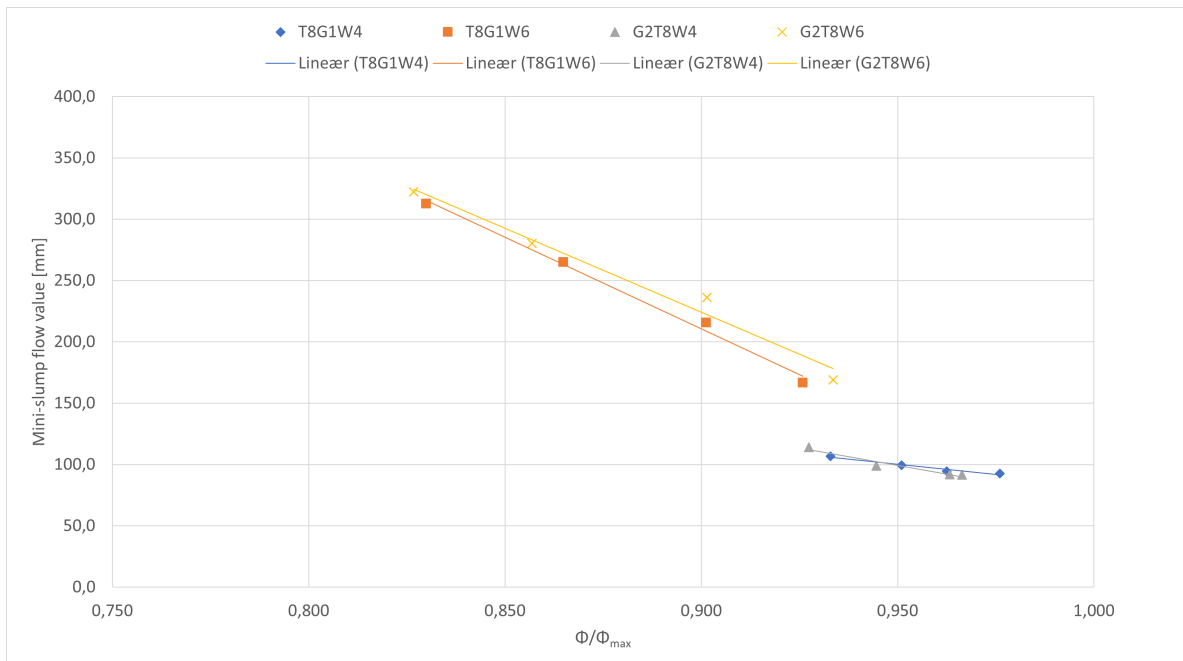


Figure 3.9: ϕ/ϕ_{max} for mixes using filler T8 plotted against mini-slump-flow value

Figure 3.10 shows the same relationships as in the previous figures, but this they are separated based on SP content, group 1 and 2 together (SP=0.75%) and group 3 alone (SP=1.0%). This is to further illustrate the differences that occurs with different SP content. A relatively accurate ($R^2=0.83$) exponential trendline can be drawn for SP=0.75%, and even though the trendline for SP=1.0% is not as accurate, the disparity is very clear. The relationship between mini-slump flow value and ϕ/ϕ_{max} shows that with decreasing ϕ/ϕ_{max} , the yield stress also decreases, possibly exponentially.

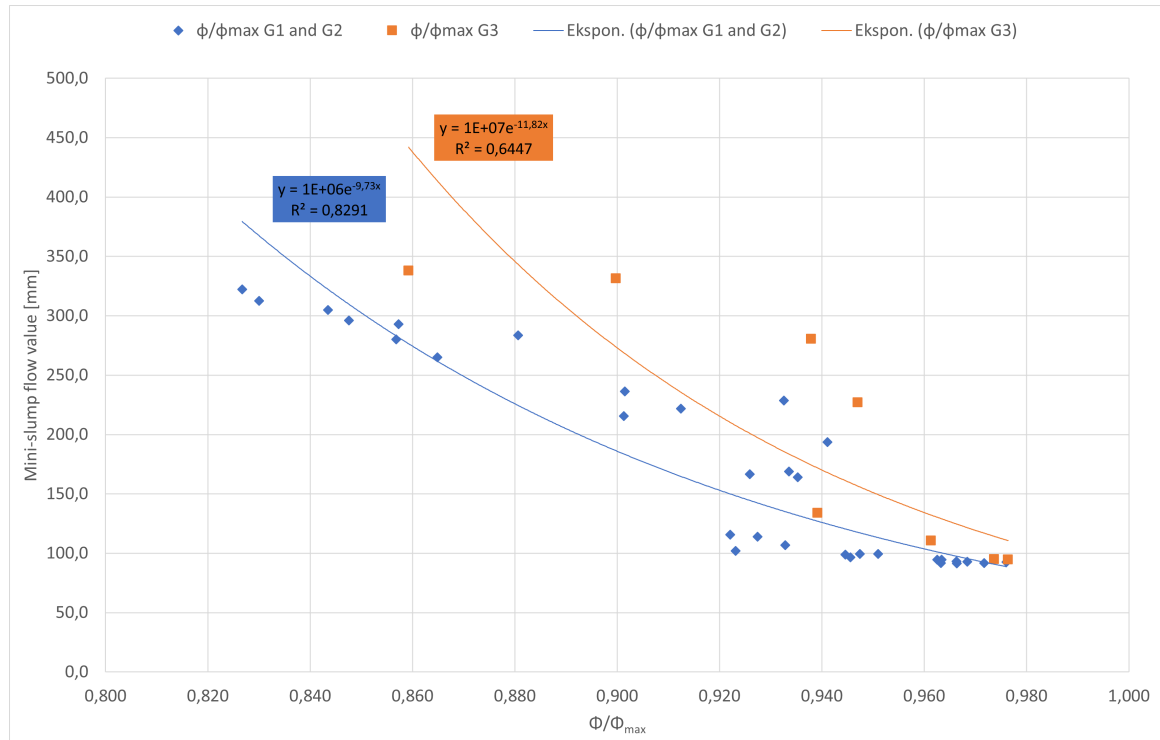


Figure 3.10: ϕ/ϕ_{max} for mixes plotted against mini-slump-flow value, differentiating between mixes using SP=0,75% and SP=1,0%

Figure 3.11 shows the relationship between both liquid thicknesses (LT1 and LT2) and mini-slump flow value, for both sets of plots a power trendline is used to represent them, because it had the highest R^2 value for both sets. The results of LT1 and LT2 calculations and their correlations to mini-slump flow value (yield stress) seem to show that LT2 fits much better to rheology than LT1.

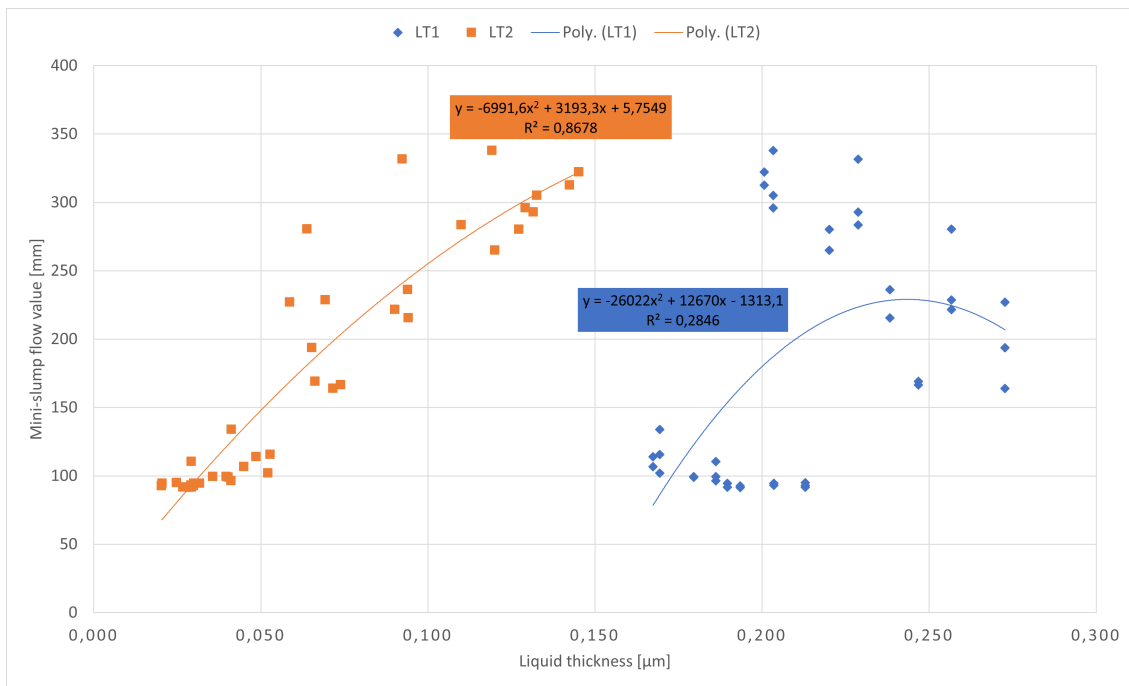


Figure 3.11: Relationship between liquid thickness (LT1 and LT2) and mini-slump flow value

3.4 Results of 3D printing tests

Because of time restraint the 3D printing tests were only done on four sets of the mixes, G2T5W4, G2T5W6, G3T5W4 and G3T5W6, again only using T5 because of the limited supply of T8.

3.4.1 Results of flow measurement test

Following the method described in 2.3.5 the mass flow measurements were first performed on the mixes G2T5W4. The tests were done once for G2T515W4 and twice for G2T544W4 and G2T585W4, table 3.11 shows the results of the tests.

Table 3.11: Measured mass flow measurements for G2T5W4

Seconds	G2T515W4	G2T544W4		G2T585W4	
	Weight [g], print 1	Weight [g], print 1	Weight [g], print 2	Weight [g], print 1	Weight [g], print 2
1	1,095	0,004	3,449	0,319	0,735
2	2,173	1,198	4,135	0,32	0,581
3	3,267	2,425	6,051	0,584	0,883
4	4,993	3,806	7,063	1,657	1,674
5	6,647	4,528	8,478	2,479	2,92
6	7,492	4,529	9,796	2,728	4,02
7	8,182	5,905	11,281	3,345	4,005
8	9,800	7,216	12,802	3,625	3,879
9	11,758	8,368	13,758	4,471	3,749
10	12,954	9,889	15,367	4,786	3,628
11	13,606	10,85	16,540	6,208	3,591
12	14,677	12,219	17,927	7,61	3,712
13	16,446	13,628	19,542	8,626	3,496
14	17,638	14,897	20,421	10,082	5,093
15	19,639	16,32	22,110	11,653	5,05
16	22,488	17,729	23,343	13,793	5,066
17	23,303	18,832	24,608	13,792	5,042
18	24,905	20,003	26,233	15,092	5,063
19	25,598	20,974	27,806	16,179	5,066
20	26,616	22,467	29,348	18,036	5,064
21	29,133	23,678	30,639	19,008	5,066
22	30,198	25,027	32,157	20,67	5,067
23	31,029	26,385	33,512	20,79	5,06
24	31,765	27,599	34,701	20,771	5,065
25	33,534	29,166	36,120		
26	35,638	30,073	37,290		
27	36,817		38,686		
28	37,430		40,011		
29	38,044		41,275		

Because these were the first tests using the 3D printer, the method was not yet familiar when doing them, that is why the tests have varying duration and results. Following the procedure in 2.3.5, the weights from table 3.11 are converted into volumes, using the fresh density measurements from 3.1. The results of these calculations are shown in table 3.12.

The reason for the different starting values after one second is because of a delay when turning on the balance before it starts registering on the connected computer. This doesn't matter for the results because it is the slope in the graphs that is the desired value, so the starting point is not significant.

Table 3.12: Calculated volumetric flow values for G2T5W4

Seconds	G2T515W4	G2T544W4		G2T585W4	
	Volume [cm ³], print 1	Volume [cm ³], print 1	Volume [cm ³], print 2	Volume [cm ³], print 1	Volume [cm ³], print 2
1	0,576	0,002	1,716	0,152	0,351
2	1,144	0,596	2,057	0,153	0,277
3	1,719	1,206	3,010	0,279	0,421
4	2,628	1,893	3,513	0,790	0,798
5	3,498	2,252	4,217	1,182	1,393
6	3,943	2,253	4,873	1,301	1,918
7	4,306	2,937	5,611	1,596	1,910
8	5,157	3,589	6,368	1,729	1,850
9	6,188	4,162	6,844	2,133	1,788
10	6,817	4,919	7,644	2,283	1,731
11	7,160	5,397	8,227	2,961	1,713
12	7,724	6,078	8,917	3,630	1,771
13	8,655	6,779	9,721	4,115	1,668
14	9,282	7,410	10,158	4,809	2,429
15	10,335	8,118	10,998	5,558	2,409
16	11,834	8,819	11,611	6,579	2,416
17	12,263	9,368	12,241	6,579	2,405
18	13,106	9,950	13,049	7,199	2,415
19	13,471	10,433	13,831	7,717	2,416
20	14,007	11,176	14,598	8,603	2,416
21	15,331	11,778	15,241	9,067	2,416
22	15,892	12,449	15,996	9,859	2,417
23	16,329	13,125	16,670	9,917	2,414
24	16,717	13,728	17,261	9,908	2,416
25	17,647	14,508	17,967		
26	18,755	14,959	18,549		
27	19,375		19,243		
28	19,698		19,903		
29	20,021		20,531		
30	20,186		21,247		
31	19,901		21,869		
32			22,380		
33			22,945		

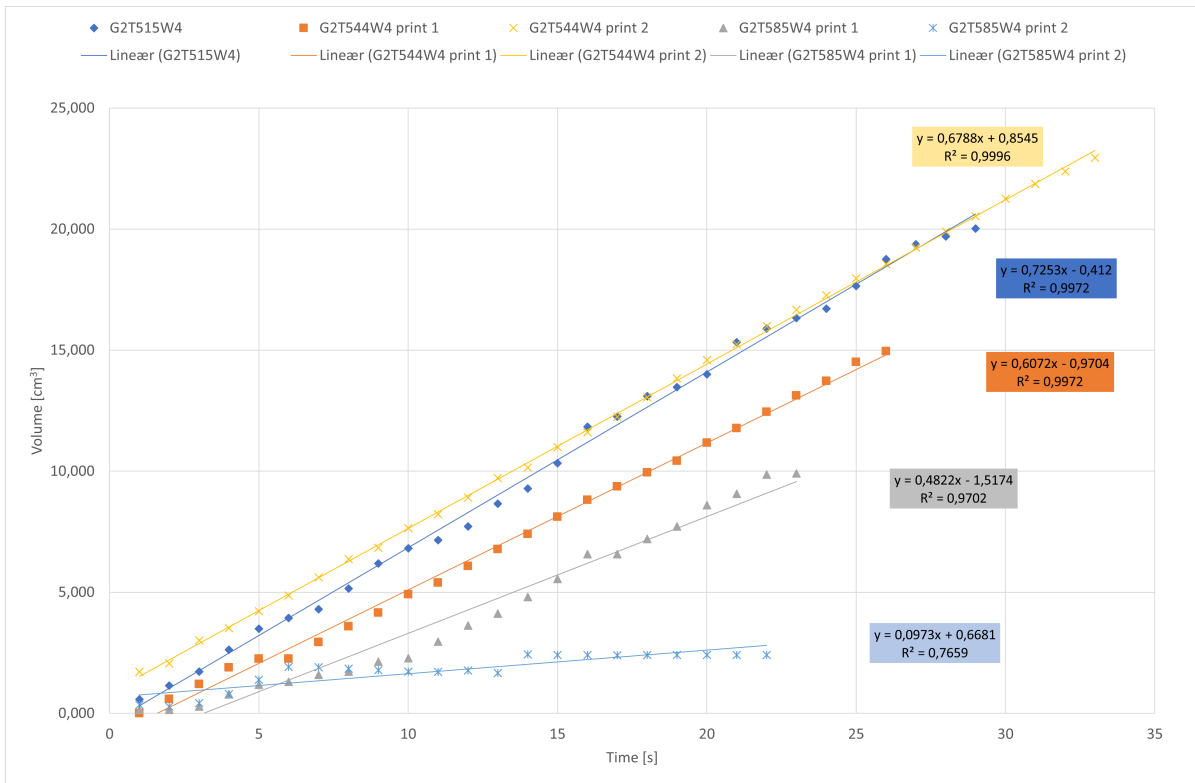


Figure 3.12: Volumetric flow of G2T5W4 as a function of time

Figure 3.12 shows the results from table 3.12 as a linear plot. This plot shows that there are to clear deviations from the others, which are the two measurements of G2T585W4. This is because the testing method was unfamiliar, as mentioned earlier, which lead to results that were anomalous. These two tests were therefore treated as an error in the method. After getting more familiar with the method later in the study, the mass flow test was repeated three times using the mix G2T585W4. The results of the test were again calculated from g/s to cm^3/s (see Appendix E for full results) before making a new linear plot for the G2T5W4 mixes (see Figure 3.13). This linear plot with updated results confirms that the irregularities in the tests that were previously done was caused by unfamiliarity.

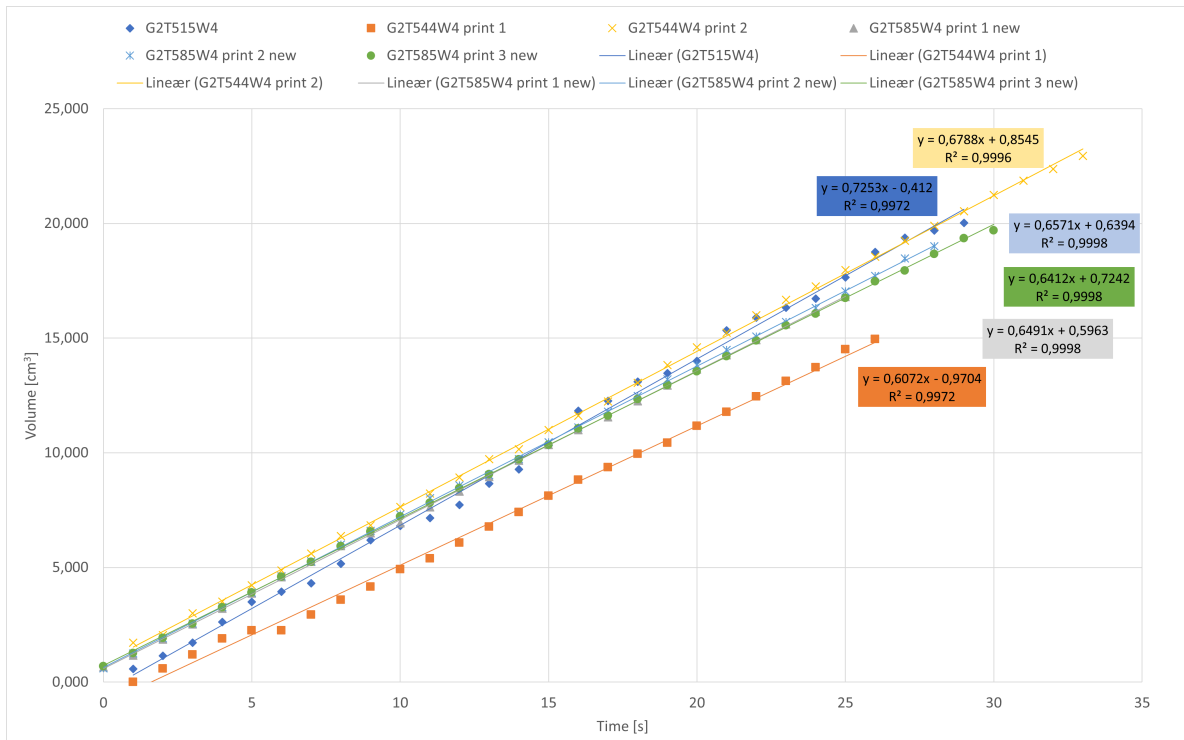


Figure 3.13: Updated plot for volumetric flow of G2T5W4 as a function of time

The tests were done on three more sets of mixes, G2T5W6, G3T5W4 and G3T5W6, with the same calculations as previously to present the graphs in Figures 3.14, 3.15 and 3.16 (see Appendix E for full results).

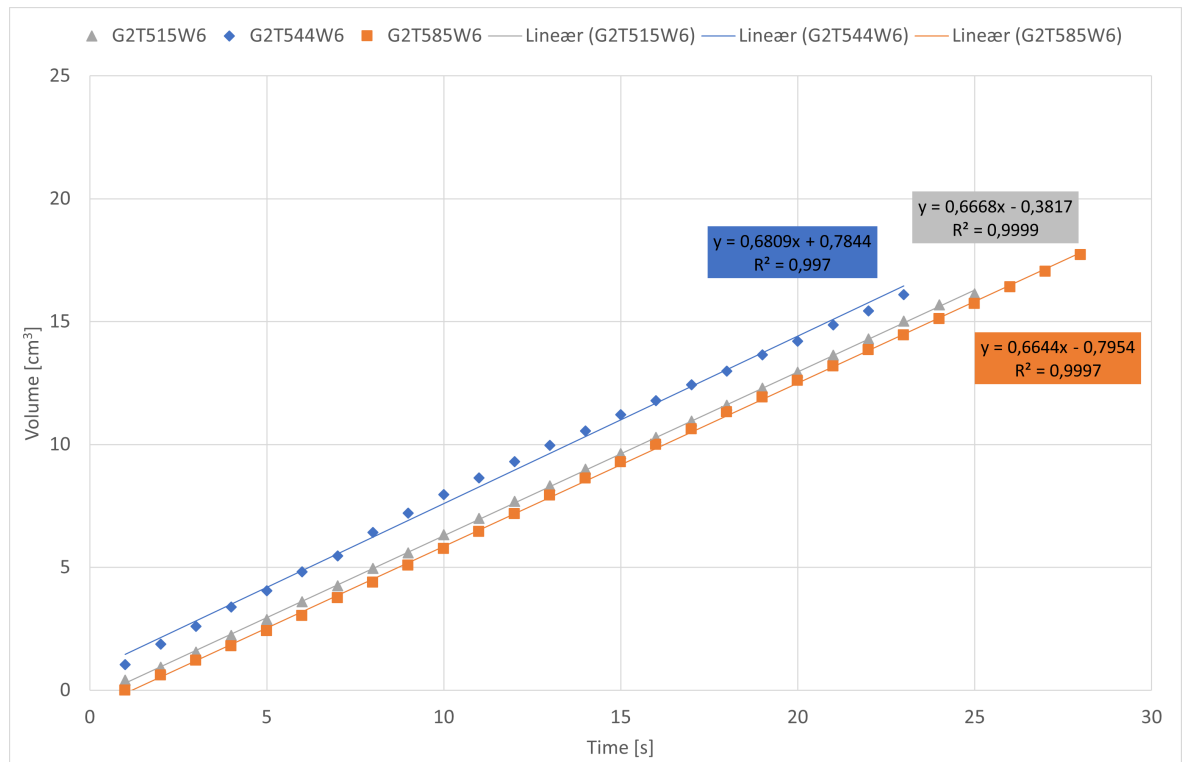


Figure 3.14: Volumetric flow of G2T5W6 as a function of time

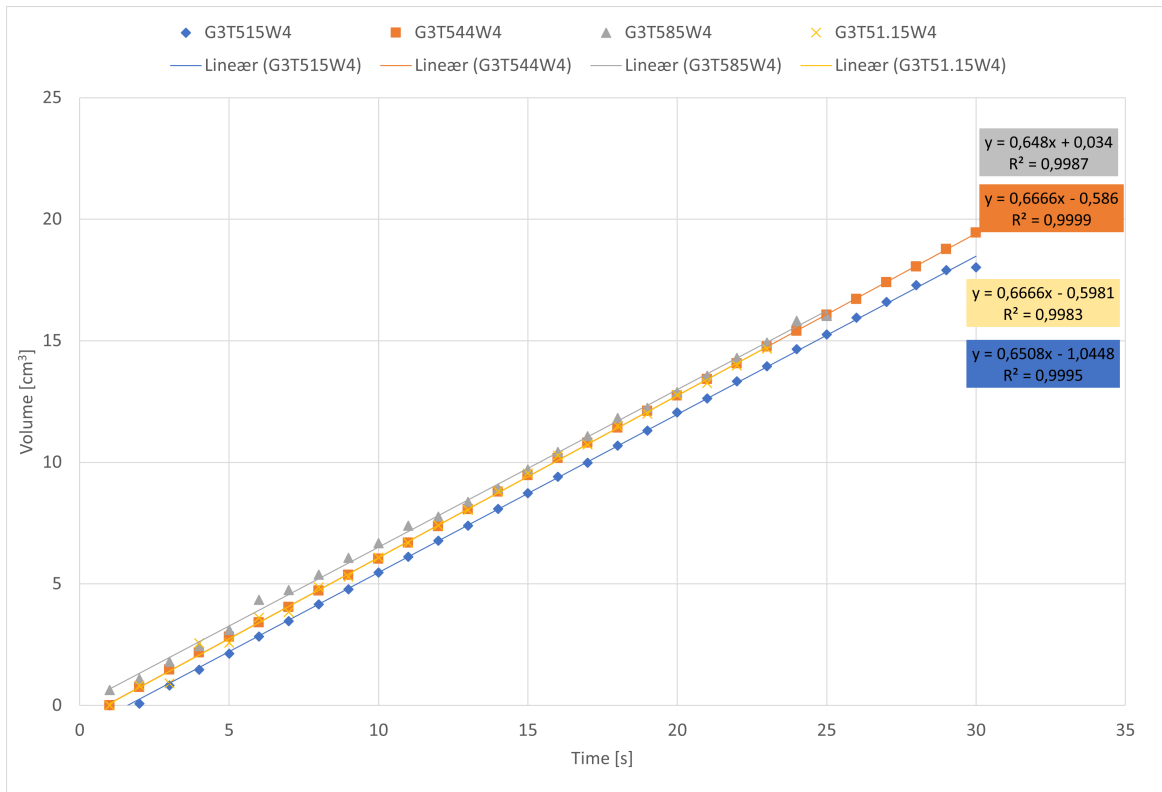


Figure 3.15: Volumetric flow of G3T5W4 as a function of time

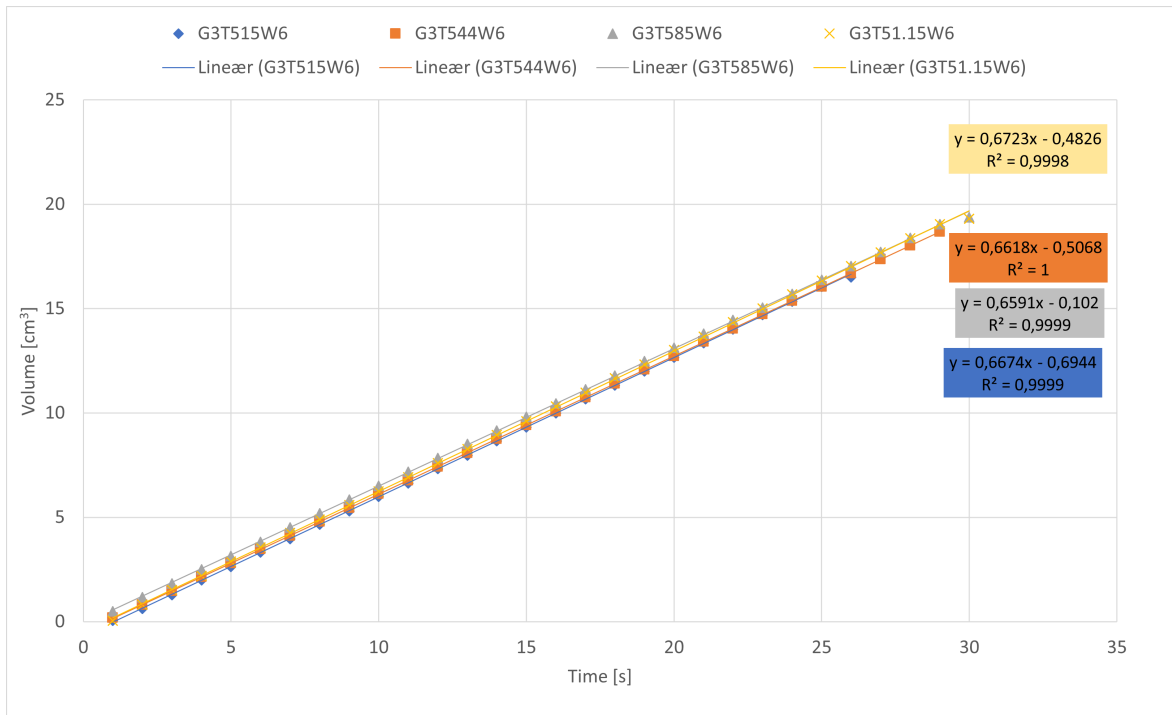


Figure 3.16: Volumetric flow of G3T5W6 as a function of time

The graphs show the trendline and its function for all of the different scatter plots ($y = ax + b$), as well as their respective R-Squared values (R^2). As mentioned earlier, the interesting values for these results are the slope values (a) and the R^2 values, as the starting point of the function doesn't matter we ignore the intercept value (b). These values are tabulated in Table 3.13.

Table 3.13: Values for slope and variance of linear functions for volumetric flow

NO	Slope (a) [cm ³ /s]	R ²
G2T515W4	0,725	0,997
G2T544W4	0,643	0,998
G2T585W4	0,649	1,000
G2T515W6	0,667	1,000
G2T544W6	0,681	0,997
G2T585W6	0,664	1,000
G3T515W4	0,651	1,000
G3T544W4	0,667	1,000
G3T585W4	0,648	0,999
G3T51.15W4	0,667	0,998
G3T515W6	0,667	1,000
G3T544W6	0,662	1,000
G3T585W6	0,659	1,000
G3T51.15W6	0,672	1,000
Average	0,666	0,999

The results from table 3.13 shows that there is a 0,1% variance on average for the flow of the printer, which means that the printer prints with a steady rate during the whole printing process. The slope value is also very constant, with all of the results being between 0,640 and 0,685, except for the first one. Which gives evidence to the presumption that the printer prints with the same speed, and forces the same volumetric amount of cement paste out of the syringe, no matter how stiff or soft the paste is. This amount is around 0,66-0,67 cm³/s. The linear plot in Figure 3.17 confirms this by showing that the trendline for the slope values for each sets of mixes has a very low slope value.

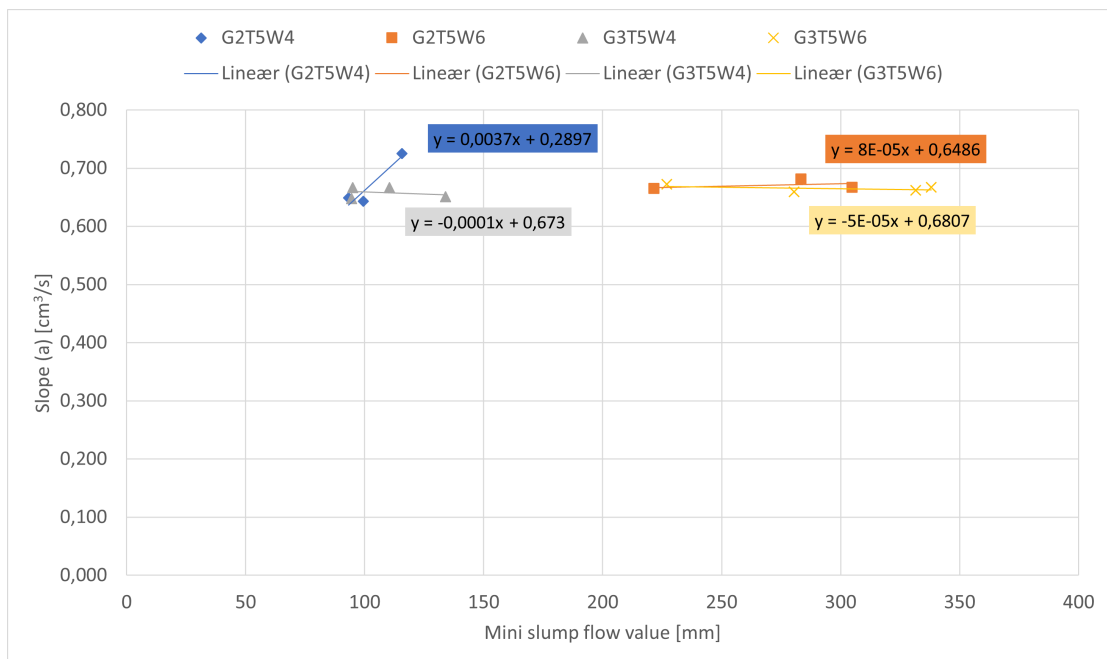


Figure 3.17: Slope of volumetric flow for all mixes plotted against mini-slump flow value

3.4.2 Results of printability test

As seen in previous results, all of the mixes with w/b = 0.6 are too liquid to have good printability, this was confirmed by doing a printability test on the mix G3T51.15W6, which has the lowest mini-slump value of that set. As seen on Figure 3.18, the mix is too soft and cannot be layered.

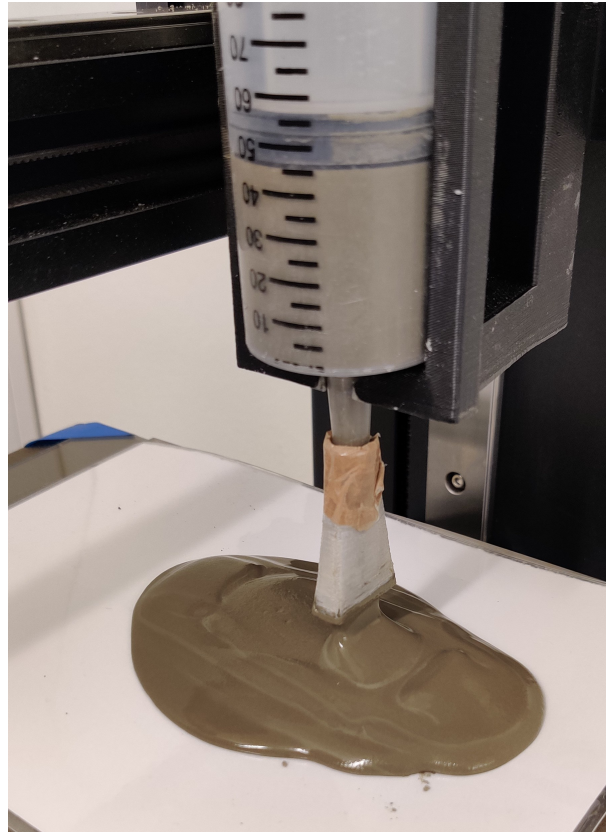


Figure 3.18: Printability test on G3T51.15W6

The printability test was therefore only performed on three mixes in the set G3T5W4, G3T51.15W4 could not be printed as it was too stiff and could not be compressed by the piston in the syringe. Relevant information for printability regarding these mixes are tabulated in Table 3.14, as well as comments about the print specimens.

Table 3.14: Relevant data on G3T5W4 for printability test

	G3T515W4	G3T544W4	G3T585W4
Slump value [mm]	51	47	33
Slump flow value [mm]	134	111	95
ϕ/ϕ_{max}	0,94	0,96	0,98
Comments about printability	Very wet, smooth surface on side edge, less separation between layers	Wet, a bit rougher surface side edges, separation between layers	Airpockets in syringe cause rough side edges, clearer separation between layers

Figure 3.19 shows the print specimens right after the printing was completed, the comments in Table 3.14 are based on these specimens. The figures show that the extrudability, as defined in 1.2.1 as the ability to be transported as a continuous filament, are good for the prints G3T515W4 and G3T544W4, because of the smooth edges. For the last specimen, G3T585W4, the edges are much rougher which was caused by the print not coming out of the nozzle continuously. It was observed during printing that this was mostly caused by airpockets in the syringe, which caused small cut-offs when printing.

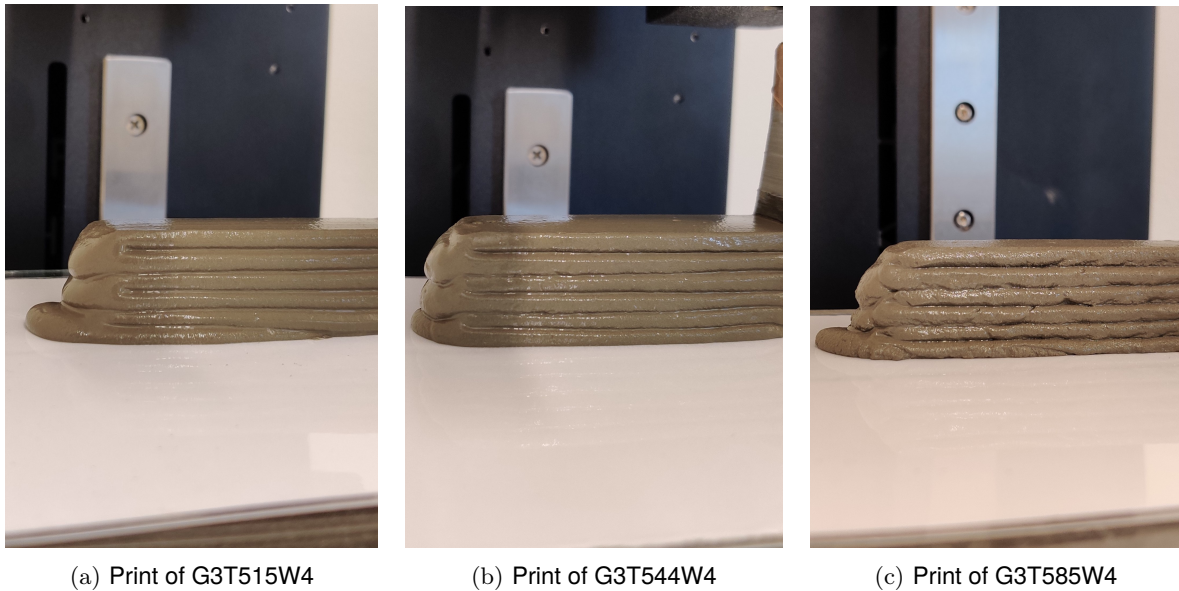


Figure 3.19: Pictures from printability test

Another observation from Figure 3.19 is the flow over the edges on the short side off the specimens. This is caused by a wave of cement paste that gets pushed over the edge when switching direction, this can be seen in Figure 3.20 to the right of the nozzle. This is believed to be the result of the nozzle not being high enough above the specimen when printing, or a cement paste that is too soft. As 3D printing of concrete usually follows a pattern that goes in a loop, and not back and forth, this is not a problematic issue.



Figure 3.20: Example of wave during printability

Figures 3.21 and 3.22 show the specimens after being hardened and cut. From these figures, a visual conclusion about buildability can be drawn. As defined in 1.2.2, buildability is the ability to bear its own weight and the layer above without collapsing. The bottom layer of print specimen G3T515W4 has flowed a lot more than the others, so it has lower buildability. Print specimen G3T544W4 have sank a bit, giving it the shape of a trapezoid (Figure 3.22c), having better buildability than G3T515W4, but could still be better. Print specimen G3T585W4 is the closest of having all the layers equally wide, which means it got the best buildability.

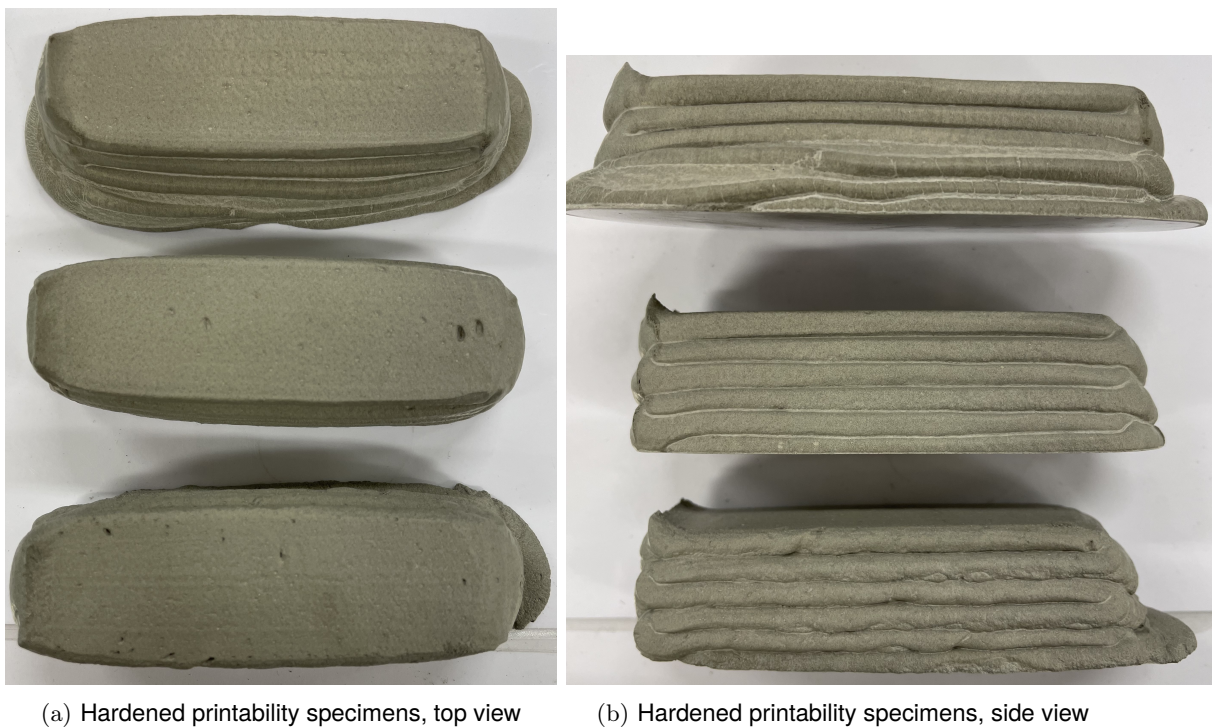


Figure 3.21: Hardened printability specimens, from top to bottom: G3T515W4, G3T544W4, G3T585W4

Another observation that can be made from Figure 3.22 is seen in the cuts, where no difference in layers can be seen, all the layers have merged together, which is desired.



(a) Hardened printability test specimens that has been cut, left to right: G3T515W4, G3T544W4, G3T585W4

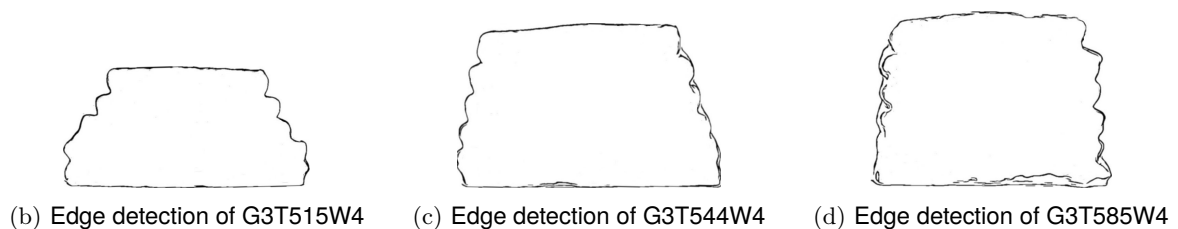


Figure 3.22: Cut hardened printability test specimens with edge detection performed

4. Conclusions

The following conclusions can be drawn from this study.

- To find the air content in filler-modified cement paste, in order to see if there is correlations between air content and rheology, a more precise method has to be used.
- Mini-slump test is a easy and reliable way of measuring the yield stress of filler-modified cement paste, which can be used as comparison.
- The water adsorption of the fillers gives no noticeable difference when using T5, and a very small one when using T8, but can also come from the accuracy in the tests.
- Increasing SP content lead to a noticeable increase in mini-slump flow value and relative concentration of solids.
- Controlling SP content and relative concentration of solids are two ways to control the yield stress of the cement paste.
- The printer used in this project prints with the same speed, no matter the flowability of the cement paste.
- The use of VMA should be tested on mixes with $w/b = 0.6$ to see if it becomes printable.

References

- [1] 3Print. *3D Concrete Printing Market to Reach \$ 56.4 Million by 2021*. Available at: <https://www.3print.com/3d-concrete-printing-market-reach-56-4-million-2021-1239664/> (Accessed: 21.04.2023). 2016.
- [2] Cepuritis, R. et al. 'Influence of crushed aggregate fines with micro-proportioned particle size distributions on rheology of cement paste'. In: *Cement and Concrete Composites* 80 (2017), 64–79.
- [3] Cepuritis, R. et al. 'Microproportioning with crushed sand'. NTNU, 2021.
- [4] Cepuritis, R. et al. *Rheology of matrix and SCC with different mineral fillers and admixtures*. (COIN Project report 41). Trondheim: Sintef. 2012.
- [5] Cepuritis, R. et al. 'Sand production with VSI crushing and air classification: Optimising fines grading for concrete production with micro-proportioning'. In: *Minerals Engineering* 78 (2015), 1–14.
- [6] Gosselin, C. et al. 'Large-scale 3D printing of ultra-high performance concrete – a new processing route for architects and builders'. In: *Materials and Design* 100 (2016), 102–109.
- [7] Heidelberg Materials. *Sementproduksjon og CO2*. Available at: <https://www.sement.heidelbergmaterials.no/no/sementproduksjon-co2> (Accessed: 17.04.2023). n.d.
- [8] Hou, S. et al. 'A review of 3D printed concrete: Performance requirements, testing measurements and mix design'. In: *Construction and Building Materials* 273 (2021), 121745.
- [9] How To Mechatronics. *G-code Explained | List of Most Important G-code Commands*. Available at: <https://howtomechatronics.com/tutorials/g-code-explained-list-of-most-important-g-code-commands/> (Accessed: 19.04.2023). n.d.
- [10] Huang, S. et al. 'The impacts of fabrication systems on 3D concrete printing building forms'. In: *Frontiers of Architectural Research* 11 (2022), 653–669.
- [11] Hyrel 3D. *ENGINE SR - STANDARD RESOLUTION*. Available at: <https://www.hyrel3d.com/portfolio/engine-sr-standard-resolution/> (Accessed: 26.05.2023). n.d.
- [12] Hyrel 3D. *Gcode*. Available at: <https://hyrel3d.com/wiki/index.php/Gcode> (Accessed: 22.05.2023). 2023.
- [13] Hyrel 3D. *SDS*. Available at: <https://hyrel3d.com/wiki/index.php/SDS> (Accessed: 26.05.2023). 2020.
- [14] Jacobsen, S. et al. *Concrete technology*. NTNU, 2023, 104–115.
- [15] Ng, S. et al. 'Design of a simple and cost-efficient mixer for matrix rheology testing'. In: *Nordic Concrete Research* 3 (2014), 15–28.
- [16] Norsk Standard. *Prøving av fersk betong Del 2: Synkmål*. Available at: <https://online.standard.no/ns-en-12350-2-2019> (Accessed: 02.03.2023). 2019.
- [17] Sihaklang, M. 'Microproportioning modelling, with measurements of the maximum particle packing in filler-modified cement paste and the viscosity of paste fluid'. NTNU, 2019.
- [18] Sintef. *Betong er en del av klimaløsningen*. Available at: <https://www.sintef.no/siste-nytt/2020/-betong-er-en-del-av-klimalosningen/> (Accessed: 17.04.2023). 2020.

- [19] Skare, E.L. et al. 'Rheology modelling of cement paste with manufactured sand and silica fume: Comparing suspension models with artificial neural network predictions'. In: *Construction and Building Materials* 317 (2022), 126114.
- [20] Tay, Y.W.D. et al. '3D printing trends in building and construction industry: a review'. In: *Virtual and Physical Prototyping* 12 (2017), 261–276.
- [21] Thomas. *An Introduction to G-Code and CNC Programming*. Available at: <https://www.thomasnet.com/articles/custom-manufacturing-fabricating/introduction-gcode/> (Accessed: 19.04.2023). n.d.
- [22] Westerholm, M. et al. 'Rheological properties of micromortars containing fines from manufactured aggregates'. In: *Materials and Structures* 40 (2007), 615–625.
- [23] Xiao, J. et al. 'Large-scale 3D printing concrete technology: Current status and future opportunities'. In: *Elsevier Cement and Concrete Composites* 122 (2021), 104–115.
- [24] Zhang, J. et al. 'A review of the current progress and application of 3D printed concrete'. In: *Composites Part A: Applied Science and Manufacturing* 125 (2019), 105533.
- [25] Zhu, J. et al. 'Effect of microfines from manufactured sand on yield stress of cement paste'. In: *Construction and Building Materials* 267 (2021), 120987.

Appendix A: Matrix proportioning

The full excel used for matrix proportioning, results, and plots can be found as an online appendix in the link below:

<https://www.dropbox.com/s/32hdjea6ul70dz1/Mix%20proportioning.xlsx?dl=0>

Table 4.1 used to calculate the matrix proportioning.

Table 4.1: Material parameters used in the calculation of mix proportioning

Material	SSA [1/mm]	Density
IND cem.	1302	3,13
Fly-ash	970	2,38
Silica fume	55000	2,2
T5 (63-125)	64,9	2,72
T8 (63-125)	460,1	2,94
Water		1

NO	w/c	w/b	FA/b	fi/b	s/b	Cement type	VMA	SP
G1T515W4	0,53	0,40	0,20	0,15	0,04	IND	0,00	0,75
G1T544W4	0,53	0,40	0,20	0,44	0,04	IND	0,00	0,75
G1T585W4	0,53	0,40	0,20	0,85	0,04	IND	0,00	0,75
G1T51.15W4	0,53	0,40	0,20	1,15	0,04	IND	0,00	0,75
G1T815W4	0,53	0,40	0,20	0,15	0,04	IND	0,00	0,75
G1T844W4	0,53	0,40	0,20	0,44	0,04	IND	0,00	0,75
G1T885W4	0,53	0,40	0,20	0,85	0,04	IND	0,00	0,75
G1T81.15W4	0,53	0,40	0,20	1,15	0,04	IND	0,00	0,75
G1T515W6	0,79	0,60	0,20	0,15	0,04	IND	0,00	0,75
G1T544W6	0,79	0,60	0,20	0,44	0,04	IND	0,00	0,75
G1T585W6	0,79	0,60	0,20	0,85	0,04	IND	0,00	0,75
G1T51.15W6	0,79	0,60	0,20	1,15	0,04	IND	0,00	0,75
G1T815W6	0,79	0,60	0,20	0,15	0,04	IND	0,00	0,75
G1T844W6	0,79	0,60	0,20	0,44	0,04	IND	0,00	0,75
G1T885W6	0,79	0,60	0,20	0,85	0,04	IND	0,00	0,75
G1T81.15W6	0,79	0,60	0,20	1,15	0,04	IND	0,00	0,75
G2T515W4	0,53	0,40	0,20	0,15	0,04	IND	0,00	0,75
G2T544W4	0,53	0,40	0,20	0,44	0,04	IND	0,00	0,75
G2T585W4	0,53	0,40	0,20	0,85	0,04	IND	0,00	0,75
G2T51.15W4	0,53	0,40	0,20	1,15	0,04	IND	0,00	0,75
G2T815W4	0,53	0,40	0,20	0,15	0,04	IND	0,00	0,75
G2T844W4	0,53	0,40	0,20	0,44	0,04	IND	0,00	0,75
G2T885W4	0,53	0,40	0,20	0,85	0,04	IND	0,00	0,75
G2T81.15W4	0,53	0,40	0,20	1,15	0,04	IND	0,00	0,75
G2T515W6	0,79	0,60	0,20	0,15	0,04	IND	0,00	0,75
G2T544W6	0,79	0,60	0,20	0,44	0,04	IND	0,00	0,75
G2T585W6	0,79	0,60	0,20	0,85	0,04	IND	0,00	0,75
G2T51.15W6	0,79	0,60	0,20	1,15	0,04	IND	0,00	0,75
G2T815W6	0,79	0,60	0,20	0,15	0,04	IND	0,00	0,75
G2T844W6	0,79	0,60	0,20	0,44	0,04	IND	0,00	0,75
G2T885W6	0,79	0,60	0,20	0,85	0,04	IND	0,00	0,75
G2T81.15W6	0,79	0,60	0,20	1,15	0,04	IND	0,00	0,75
G3T515W4	0,53	0,40	0,20	0,15	0,04	IND	0,00	1,00
G3T544W4	0,53	0,40	0,20	0,44	0,04	IND	0,00	1,00
G3T585W4	0,53	0,40	0,20	0,85	0,04	IND	0,00	1,00
G3T51.15W4	0,53	0,40	0,20	1,15	0,04	IND	0,00	1,00
G3T515W6	0,79	0,60	0,20	0,15	0,04	IND	0,00	1,00
G3T544W6	0,79	0,60	0,20	0,44	0,04	IND	0,00	1,00
G3T585W6	0,79	0,60	0,20	0,85	0,04	IND	0,00	1,00
G3T51.15W6	0,79	0,60	0,20	1,15	0,04	IND	0,00	1,00

NO	[Mass fractions of total mix]								[Mass fraction of powder]				
	Binder	IND cem.	Fly-ash	Silica fume	Filler	Water	TOTAL powder	TOTAL	IND cem.	Fly-ash	Silica fume	Filler	TOTAL
G1T515W4	0,645	0,490	0,129	0,026	0,097	0,258	0,742	1,00	0,661	0,174	0,035	0,130	1,00
G1T544W4	0,543	0,413	0,109	0,022	0,239	0,217	0,783	1,00	0,528	0,139	0,028	0,306	1,00
G1T585W4	0,444	0,338	0,089	0,018	0,378	0,178	0,822	1,00	0,411	0,108	0,022	0,459	1,00
G1T51.15W4	0,392	0,298	0,078	0,016	0,451	0,157	0,843	1,00	0,353	0,093	0,019	0,535	1,00
G1T815W4	0,645	0,490	0,129	0,026	0,097	0,258	0,742	1,00	0,661	0,174	0,035	0,130	1,00
G1T844W4	0,543	0,413	0,109	0,022	0,239	0,217	0,783	1,00	0,528	0,139	0,028	0,306	1,00
G1T885W4	0,444	0,338	0,089	0,018	0,378	0,178	0,822	1,00	0,411	0,108	0,022	0,459	1,00
G1T81.15W4	0,392	0,298	0,078	0,016	0,451	0,157	0,843	1,00	0,353	0,093	0,019	0,535	1,00
G1T515W6	0,571	0,434	0,114	0,023	0,086	0,343	0,657	1,00	0,661	0,174	0,035	0,130	1,00
G1T544W6	0,490	0,373	0,098	0,020	0,216	0,294	0,706	1,00	0,528	0,139	0,028	0,306	1,00
G1T585W6	0,408	0,310	0,082	0,016	0,347	0,245	0,755	1,00	0,411	0,108	0,022	0,459	1,00
G1T51.15W6	0,364	0,276	0,073	0,015	0,418	0,218	0,782	1,00	0,353	0,093	0,019	0,535	1,00
G1T815W6	0,571	0,434	0,114	0,023	0,086	0,343	0,657	1,00	0,661	0,174	0,035	0,130	1,00
G1T844W6	0,490	0,373	0,098	0,020	0,216	0,294	0,706	1,00	0,528	0,139	0,028	0,306	1,00
G1T885W6	0,408	0,310	0,082	0,016	0,347	0,245	0,755	1,00	0,411	0,108	0,022	0,459	1,00
G1T81.15W6	0,364	0,276	0,073	0,015	0,418	0,218	0,782	1,00	0,353	0,093	0,019	0,535	1,00
G2T515W4	0,645	0,490	0,129	0,026	0,097	0,258	0,742	1,00	0,661	0,174	0,035	0,130	1,00
G2T544W4	0,543	0,413	0,109	0,022	0,239	0,217	0,783	1,00	0,528	0,139	0,028	0,306	1,00
G2T585W4	0,444	0,338	0,089	0,018	0,378	0,178	0,822	1,00	0,411	0,108	0,022	0,459	1,00
G2T51.15W4	0,392	0,298	0,078	0,016	0,451	0,157	0,843	1,00	0,353	0,093	0,019	0,535	1,00
G2T815W4	0,645	0,490	0,129	0,026	0,097	0,258	0,742	1,00	0,661	0,174	0,035	0,130	1,00
G2T844W4	0,543	0,413	0,109	0,022	0,239	0,217	0,783	1,00	0,528	0,139	0,028	0,306	1,00
G2T885W4	0,444	0,338	0,089	0,018	0,378	0,178	0,822	1,00	0,411	0,108	0,022	0,459	1,00
G2T81.15W4	0,392	0,298	0,078	0,016	0,451	0,157	0,843	1,00	0,353	0,093	0,019	0,535	1,00
G2T515W6	0,571	0,434	0,114	0,023	0,086	0,343	0,657	1,00	0,661	0,174	0,035	0,130	1,00
G2T544W6	0,490	0,373	0,098	0,020	0,216	0,294	0,706	1,00	0,528	0,139	0,028	0,306	1,00
G2T585W6	0,408	0,310	0,082	0,016	0,347	0,245	0,755	1,00	0,411	0,108	0,022	0,459	1,00
G2T51.15W6	0,364	0,276	0,073	0,015	0,418	0,218	0,782	1,00	0,353	0,093	0,019	0,535	1,00
G2T815W6	0,571	0,434	0,114	0,023	0,086	0,343	0,657	1,00	0,661	0,174	0,035	0,130	1,00
G2T844W6	0,490	0,373	0,098	0,020	0,216	0,294	0,706	1,00	0,528	0,139	0,028	0,306	1,00
G2T885W6	0,408	0,310	0,082	0,016	0,347	0,245	0,755	1,00	0,411	0,108	0,022	0,459	1,00
G2T81.15W6	0,364	0,276	0,073	0,015	0,418	0,218	0,782	1,00	0,353	0,093	0,019	0,535	1,00
G3T515W4	0,645	0,490	0,129	0,026	0,097	0,258	0,742	1,00	0,661	0,174	0,035	0,130	1,00
G3T544W4	0,543	0,413	0,109	0,022	0,239	0,217	0,783	1,00	0,528	0,139	0,028	0,306	1,00
G3T585W4	0,444	0,338	0,089	0,018	0,378	0,178	0,822	1,00	0,411	0,108	0,022	0,459	1,00
G3T51.15W4	0,392	0,298	0,078	0,016	0,451	0,157	0,843	1,00	0,353	0,093	0,019	0,535	1,00
G3T515W6	0,571	0,434	0,114	0,023	0,086	0,343	0,657	1,00	0,661	0,174	0,035	0,130	1,00
G3T544W6	0,490	0,373	0,098	0,020	0,216	0,294	0,706	1,00	0,528	0,139	0,028	0,306	1,00
G3T585W6	0,408	0,310	0,082	0,016	0,347	0,245	0,755	1,00	0,411	0,108	0,022	0,459	1,00
G3T51.15W6	0,364	0,276	0,073	0,015	0,418	0,218	0,782	1,00	0,353	0,093	0,019	0,535	1,00

[Volume fraction of total mix]								SSA filler	SSA pulver	SSA matrixvol	
IND cem.	Fly-ash	Sliica fume	Filler	Water	TOTAL powder	TOTAL	Φ		[1/mm]	[mm2/ mm3 matriks]	water adsorption %
0,303	0,105	0,023	0,069	0,500	0,500	1,00	0,50	4,47	2950,66	1475,65	0,12
0,268	0,093	0,020	0,178	0,441	0,559	1,00	0,56	11,58	2369,50	1324,27	0,12
0,230	0,079	0,017	0,296	0,378	0,622	1,00	0,62	19,18	1858,75	1155,69	0,12
0,208	0,072	0,016	0,362	0,343	0,657	1,00	0,66	23,50	1608,44	1057,52	0,12
0,305	0,106	0,023	0,064	0,502	0,498	1,00	0,50	29,49	3002,20	1493,65	1,50
0,271	0,094	0,020	0,167	0,447	0,553	1,00	0,55	76,96	2490,25	1376,90	1,50
0,235	0,081	0,018	0,280	0,387	0,613	1,00	0,61	128,63	2040,33	1251,14	1,50
0,214	0,074	0,016	0,344	0,352	0,648	1,00	0,65	158,40	1819,83	1179,15	1,50
0,243	0,084	0,018	0,055	0,600	0,400	1,00	0,40	3,58	2950,66	1180,57	0,12
0,219	0,076	0,016	0,146	0,542	0,458	1,00	0,46	9,49	2369,50	1084,98	0,12
0,193	0,067	0,014	0,249	0,477	0,523	1,00	0,52	16,13	1858,75	971,89	0,12
0,178	0,061	0,013	0,309	0,439	0,561	1,00	0,56	20,06	1608,44	902,89	0,12
0,244	0,084	0,018	0,051	0,602	0,398	1,00	0,40	23,57	3002,20	1193,73	1,50
0,222	0,077	0,017	0,137	0,548	0,452	1,00	0,45	62,90	2490,25	1125,34	1,50
0,197	0,068	0,015	0,234	0,486	0,514	1,00	0,51	107,79	2040,33	1048,39	1,50
0,182	0,063	0,014	0,293	0,449	0,551	1,00	0,55	134,69	1819,83	1002,65	1,50
0,303	0,105	0,023	0,069	0,500	0,500	1,00	0,50	4,47	2950,66	1475,65	0,12
0,268	0,093	0,020	0,178	0,441	0,559	1,00	0,56	11,58	2369,50	1324,27	0,12
0,230	0,079	0,017	0,296	0,378	0,622	1,00	0,62	19,18	1858,75	1155,69	0,12
0,208	0,072	0,016	0,362	0,343	0,657	1,00	0,66	23,50	1608,44	1057,52	0,12
0,305	0,106	0,023	0,064	0,502	0,498	1,00	0,50	29,49	3002,20	1493,65	1,50
0,271	0,094	0,020	0,167	0,447	0,553	1,00	0,55	76,96	2490,25	1376,90	1,50
0,235	0,081	0,018	0,280	0,387	0,613	1,00	0,61	128,63	2040,33	1251,14	1,50
0,214	0,074	0,016	0,344	0,352	0,648	1,00	0,65	158,40	1819,83	1179,15	1,50
0,243	0,084	0,018	0,055	0,600	0,400	1,00	0,40	3,58	2950,66	1180,57	0,12
0,219	0,076	0,016	0,146	0,542	0,458	1,00	0,46	9,49	2369,50	1084,98	0,12
0,193	0,067	0,014	0,249	0,477	0,523	1,00	0,52	16,13	1858,75	971,89	0,12
0,178	0,061	0,013	0,309	0,439	0,561	1,00	0,56	20,06	1608,44	902,89	0,12
0,244	0,084	0,018	0,051	0,602	0,398	1,00	0,40	23,57	3002,20	1193,73	1,50
0,222	0,077	0,017	0,137	0,548	0,452	1,00	0,45	62,90	2490,25	1125,34	1,50
0,197	0,068	0,015	0,234	0,486	0,514	1,00	0,51	107,79	2040,33	1048,39	1,50
0,182	0,063	0,014	0,293	0,449	0,551	1,00	0,55	134,69	1819,83	1002,65	1,50
0,303	0,105	0,023	0,069	0,500	0,500	1,00	0,50	4,47	2950,66	1475,65	0,12
0,268	0,093	0,020	0,178	0,441	0,559	1,00	0,56	11,58	2369,50	1324,27	0,12
0,230	0,079	0,017	0,296	0,378	0,622	1,00	0,62	19,18	1858,75	1155,69	0,12
0,208	0,072	0,016	0,362	0,343	0,657	1,00	0,66	23,50	1608,44	1057,52	0,12
0,243	0,084	0,018	0,055	0,600	0,400	1,00	0,40	3,58	2950,66	1180,57	0,12
0,219	0,076	0,016	0,146	0,542	0,458	1,00	0,46	9,49	2369,50	1084,98	0,12
0,193	0,067	0,014	0,249	0,477	0,523	1,00	0,52	16,13	1858,75	971,89	0,12
0,178	0,061	0,013	0,309	0,439	0,561	1,00	0,56	20,06	1608,44	902,89	0,12

NO	Density (kg/m3)							free water of SP	water adsorption	new volume
	IND cem.	Fly-ash	Silica fume	Filler	Water	SP	TOTAL			
G1T515W4	949,79	249,95	49,99	187,46	499,89	7,12	1942,96	5,88	0,22	1,01
G1T544W4	838,12	220,56	44,11	485,23	441,12	6,29	2034,32	5,19	0,58	1,00
G1T585W4	718,66	189,12	37,82	803,76	378,24	5,39	2132,05	4,45	0,96	1,00
G1T51.15W4	650,78	171,26	34,25	984,74	342,52	4,88	2187,58	4,03	1,18	1,00
G1T815W4	954,72	251,24	50,25	188,43	502,48	7,16	1953,03	5,91	2,83	1,00
G1T844W4	849,46	223,54	44,71	491,79	447,08	6,37	2061,84	5,26	7,38	1,00
G1T885W4	734,91	193,40	38,68	821,94	386,79	5,51	2180,26	4,55	12,33	0,99
G1T81.15W4	668,91	176,03	35,21	1012,16	352,06	5,02	2248,49	4,14	15,18	0,99
G1T515W6	759,87	199,97	39,99	149,97	599,90	5,70	1754,40	4,70	0,18	1,00
G1T544W6	686,67	180,70	36,14	397,55	542,11	5,15	1847,41	4,25	0,48	1,00
G1T585W6	604,36	159,04	31,81	675,93	477,13	4,53	1952,01	3,74	0,81	1,00
G1T51.15W6	555,63	146,22	29,24	840,75	438,65	4,17	2013,93	3,44	1,01	1,00
G1T815W6	763,02	200,79	40,16	150,60	602,38	5,72	1761,67	4,72	2,26	1,00
G1T844W6	694,26	182,70	36,54	401,94	548,10	5,21	1867,84	4,30	6,03	1,00
G1T885W6	615,81	162,06	32,41	688,74	486,17	4,62	1988,99	3,81	10,33	0,99
G1T81.15W6	568,78	149,68	29,94	860,66	449,04	4,27	2061,62	3,52	12,91	0,99
G2T515W4	949,79	249,95	49,99	187,46	499,89	7,12	1942,96	5,88	0,00	1,01
G2T544W4	838,12	220,56	44,11	485,23	441,12	6,29	2034,32	5,19	0,00	1,01
G2T585W4	718,66	189,12	37,82	803,76	378,24	5,39	2132,05	4,45	0,00	1,00
G2T51.15W4	650,78	171,26	34,25	984,74	342,52	4,88	2187,58	4,03	0,00	1,00
G2T815W4	954,72	251,24	50,25	188,43	502,48	7,16	1953,03	5,91	0,00	1,01
G2T844W4	849,46	223,54	44,71	491,79	447,08	6,37	2061,84	5,26	0,00	1,01
G2T885W4	734,91	193,40	38,68	821,94	386,79	5,51	2180,26	4,55	0,00	1,00
G2T81.15W4	668,91	176,03	35,21	1012,16	352,06	5,02	2248,49	4,14	0,00	1,00
G2T515W6	759,87	199,97	39,99	149,97	599,90	5,70	1754,40	4,70	0,00	1,00
G2T544W6	686,67	180,70	36,14	397,55	542,11	5,15	1847,41	4,25	0,00	1,00
G2T585W6	604,36	159,04	31,81	675,93	477,13	4,53	1952,01	3,74	0,00	1,00
G2T51.15W6	555,63	146,22	29,24	840,75	438,65	4,17	2013,93	3,44	0,00	1,00
G2T815W6	763,02	200,79	40,16	150,60	602,38	5,72	1761,67	4,72	0,00	1,00
G2T844W6	694,26	182,70	36,54	401,94	548,10	5,21	1867,84	4,30	0,00	1,00
G2T885W6	615,81	162,06	32,41	688,74	486,17	4,62	1988,99	3,81	0,00	1,00
G2T81.15W6	568,78	149,68	29,94	860,66	449,04	4,27	2061,62	3,52	0,00	1,00
G3T515W4	949,79	249,95	49,99	187,46	499,89	9,50	1944,91	7,84	0,00	1,01
G3T544W4	838,12	220,56	44,11	485,23	441,12	8,38	2036,05	6,91	0,00	1,01
G3T585W4	718,66	189,12	37,82	803,76	378,24	7,19	2133,53	5,93	0,00	1,01
G3T51.15W4	650,78	171,26	34,25	984,74	342,52	6,51	2188,92	5,37	0,00	1,01
G3T515W6	759,87	199,97	39,99	149,97	599,90	7,60	1755,96	6,27	0,00	1,01
G3T544W6	686,67	180,70	36,14	397,55	542,11	6,87	1848,83	5,67	0,00	1,01
G3T585W6	604,36	159,04	31,81	675,93	477,13	6,04	1953,25	4,99	0,00	1,00
G3T51.15W6	555,63	146,22	29,24	840,75	438,65	5,56	2015,08	4,58	0,00	1,00

NO	Density (kg/m3)						
	IND cem.	Fly-ash	Silica fume	Filler	Water	SP	TOTAL
G1T515W4	944,46	248,54	49,71	186,41	497,08	7,08	1932,04
G1T544W4	834,28	219,55	43,91	483,00	439,09	6,26	2025,00
G1T585W4	716,16	188,46	37,69	800,97	376,93	5,37	2124,65
G1T51.15W4	648,94	170,77	34,15	981,95	341,55	4,87	2181,37
G1T815W4	951,78	250,47	50,09	187,85	500,94	7,14	1947,03
G1T844W4	851,26	224,02	44,80	492,84	448,03	6,38	2066,22
G1T885W4	740,67	194,91	38,98	828,38	389,83	5,56	2197,36
G1T81.15W4	676,38	177,99	35,60	1023,46	355,99	5,07	2273,60
G1T515W6	756,45	199,07	39,81	149,30	597,20	5,67	1746,50
G1T544W6	684,09	180,02	36,00	396,05	540,07	5,13	1840,47
G1T585W6	602,60	158,58	31,72	673,96	475,73	4,52	1946,31
G1T51.15W6	554,28	145,86	29,17	838,72	437,59	4,16	2009,05
G1T815W6	761,14	200,30	40,06	150,23	600,90	5,71	1757,34
G1T844W6	695,47	183,02	36,60	402,64	549,05	5,22	1871,09
G1T885W6	619,85	163,12	32,62	693,26	489,36	4,65	2002,05
G1T81.15W6	574,18	151,10	30,22	868,82	453,30	4,31	2081,16
G2T515W4	944,24	248,49	49,70	186,36	496,97	7,08	1931,60
G2T544W4	833,80	219,42	43,88	482,72	438,84	6,25	2023,82
G2T585W4	715,48	188,28	37,66	800,20	376,57	5,37	2122,61
G2T51.15W4	648,17	170,57	34,11	980,79	341,14	4,86	2178,81
G2T815W4	949,11	249,77	49,95	187,32	499,53	7,12	1941,56
G2T844W4	845,02	222,37	44,47	489,22	444,75	6,34	2051,06
G2T885W4	731,58	192,52	38,50	818,22	385,04	5,49	2170,39
G2T81.15W4	666,15	175,30	35,06	1007,99	350,60	5,00	2239,23
G2T515W6	756,31	199,03	39,81	149,27	597,09	5,67	1746,19
G2T544W6	683,76	179,94	35,99	395,86	539,81	5,13	1839,60
G2T585W6	602,11	158,45	31,69	673,41	475,35	4,52	1944,74
G2T51.15W6	553,72	145,72	29,14	837,87	437,15	4,15	2007,03
G2T815W6	759,43	199,85	39,97	149,89	599,55	5,70	1753,39
G2T844W6	691,29	181,92	36,38	400,22	545,76	5,18	1859,85
G2T885W6	613,47	161,44	32,29	686,12	484,32	4,60	1981,44
G2T81.15W6	566,79	149,16	29,83	857,64	447,47	4,25	2054,39
G3T515W4	942,41	248,00	49,60	186,00	496,00	9,42	1929,79
G3T544W4	832,36	219,04	43,81	481,90	438,09	8,32	2022,07
G3T585W4	714,42	188,01	37,60	799,02	376,01	7,14	2120,96
G3T51.15W4	647,31	170,34	34,07	979,48	340,69	6,47	2177,23
G3T515W6	755,13	198,72	39,74	149,04	596,16	7,55	1745,03
G3T544W6	682,80	179,68	35,94	395,31	539,05	6,83	1838,42
G3T585W6	601,36	158,25	31,65	672,58	474,76	6,01	1943,56
G3T51.15W6	553,09	145,55	29,11	836,92	436,65	5,53	2005,89

Appendix B: Results Density and Air

	Fresh density measurements					
NO	measured density 1	measured density 2	measured density 3	measured density 4	measured density 5	measured density average
G1T515W4	1894,78		1981,66	1925,61	1905,99	1927,01
G1T544W4	2008,15	2008,66	1993,63	2026,24	2001,02	2007,54
G1T585W4	2124,04	2125,10	2084,33	2124,59	2087,39	2109,09
G1T51.15W4	2071,06	2105,73	2133,50	2145,99	2104,20	2112,10
G1T815W4	1882,07	1938,34	1890,19			1903,53
G1T844W4	2032,86		2024,20			2028,53
G1T885W4	2120,33		2113,89			2117,11
G1T81.15W4	2152,38		2126,11			2139,25
G1T515W6	1692,19		1659,62	1722,04	1735,29	1702,28
G1T544W6	1813,02		1768,92	1815,03	1835,16	1808,03
G1T585W6	1905,37		1906,75	1939,87	1938,85	1922,71
G1T51.15W6	1990,58		1960,25		1998,73	1983,19
G1T815W6	1693,66		1704,46			1699,06
G1T844W6	1797,81		1807,64			1802,73
G1T885W6	1912,15		1947,52			1929,83
G1T81.15W6	2020,37		2032,87			2026,62
G2T515W4	1889,99		1896,00		1914,65	1900,21
G2T544W4	1982,68		2024,92		2023,44	2010,35
G2T585W4	2079,49		2110,27		2099,62	2096,46
G2T51.15W4	2097,83		2100,08		2106,24	2101,38
G2T815W4	1910,57		1901,61			1906,09
G2T844W4	2016,31		2040,46			2028,38
G2T885W4	2132,99		2133,96			2133,48
G2T81.15W4	2174,01		2174,73			2174,37
G2T515W6	1692,74		1659,82		1725,10	1692,55
G2T544W6	1783,95		1776,00		1830,57	1796,84
G2T585W6	1897,83		1891,21		1939,62	1909,55
G2T51.15W6	1951,85		1967,13		1994,90	1971,30
G2T815W6	1676,43		1677,45			1676,94
G2T844W6	1781,91		1779,36			1780,64
G2T885W6	1918,47		1933,76			1926,11
G2T81.15W6	2031,34		2012,74			2022,04
G3T515W4	1909,30					1909,30
G3T544W4	1995,67					1995,67
G3T585W4	2085,61					2085,61
G3T51.15W4	2107,01					2107,01
G3T515W6	1703,44					1703,44
G3T544W6	1815,03					1815,03
G3T585W6	1927,13					1927,13
G3T51.15W6	1982,42					1982,42

	Air content calculation					
NO	% air1	% air2	% air3	% air4	% air5	air average
G1T515W4	1,93		-2,57	0,33	1,35	0,3
G1T544W4	0,83	0,81	1,55	-0,06	1,18	0,9
G1T585W4	0,03	-0,02	1,90	0,00	1,75	0,7
G1T51.15W4	5,06	3,47	2,19	1,62	3,54	3,2
G1T815W4	3,34	0,45	2,92			2,2
G1T844W4	1,61		2,03			1,8
G1T885W4	3,51		3,80			3,7
G1T81.15W4	5,33		6,49			5,9
G1T515W6	3,11		4,97	1,40	0,64	2,5
G1T544W6	1,49		3,89	1,38	0,29	1,8
G1T585W6	2,10		2,03	0,33	0,38	1,2
G1T51.15W6	0,92		2,43		0,51	1,3
G1T815W6	3,62		3,01			3,3
G1T844W6	3,92		3,39			3,7
G1T885W6	4,49		2,72			3,6
G1T81.15W6	2,92		2,32			2,6
G2T515W4	2,15		1,84		0,88	1,6
G2T544W4	2,03		-0,05		0,02	0,7
G2T585W4	2,03		0,58		1,08	1,2
G2T51.15W4	3,72		3,61		3,33	3,6
G2T815W4	1,60		2,06			1,8
G2T844W4	1,69		0,52			1,1
G2T885W4	1,72		1,68			1,7
G2T81.15W4	2,91		2,88			2,9
G2T515W6	3,06		4,95		1,21	3,1
G2T544W6	3,03		3,46		0,49	2,3
G2T585W6	2,41		2,75		0,26	1,8
G2T51.15W6	2,75		1,99		0,60	1,8
G2T815W6	4,39		4,33			4,4
G2T844W6	4,19		4,33			4,3
G2T885W6	3,18		2,41			2,8
G2T81.15W6	1,12		2,03			1,6
G3T515W4	1,06					1,1
G3T544W4	1,31					1,3
G3T585W4	1,67					1,7
G3T51.15W4	3,23					3,2
G3T515W6	2,38					2,4
G3T544W6	1,27					1,3
G3T585W6	0,85					0,8
G3T51.15W6	1,17					1,2

Apendix C: Results Mini slump

NO	Mini-slump [mm]									
	mini-slump value	mini-slump flow d1	mini-slump flow d2	average mini slump flow	mini-slump value	mini-slump flow d1	mini-slump flow d2	average mini slump flow	Average mini-slump flow Total	average mini-slump value
G1T515W4	41	108	109	108,5	31	95	96	95,5	102	36
G1T544W4	32	97	97	97	37	97	95	96	96,5	34,5
G1T585W4	27	93	95	94	23	94	96	95	94,5	25
G1T51.15W4	12	91	90	90,5	13	93	93	93	91,75	12,5
G1T815W4	45	109	112	110,5	42	103	103	103	106,75	43,5
G1T844W4	38	99	98	98,5	42	101	100	100,5	99,5	40
G1T885W4	22	93	95	94	22	95	95	95	94,5	22
G1T81.15W4	11	91	95	93	12	93	92	92,5	92,75	11,5
G1T515W6	-	287	287	287	-	305	305	305	296	-
G1T544W6	-	307	307	307	-	279	279	279	293	-
G1T585W6	-	241	241	241	-	216	217	216,5	228,75	-
G1T51.15W6	550	153	153	153	-	175	175	175	164	-
G1T815W6	-	305	305	305	-	320	320	320	312,5	-
G1T844W6	-	231	231	231	-	299	299	299	265	-
G1T885W6	-	200	200	200	-	231	231	231	215,5	-
G1T81.15W6	550	160	160	160	-	173	173	173	166,5	-
G2T515W4	43	113	109	111	45	121	120	120,5	115,75	44
G2T544W4	40	100	98	99	40	100	100	100	99,5	40
G2T585W4	21	94	95	94,5	23	92	92	92	93,25	22
G2T51.15W4	10	93	92	92,5	11	93	94	93,5	93	10,5
G2T815W4	46	114	113	113,5	47	116	113	114,5	114	46,5
G2T844W4	41	99	99	99	39	98	100	99	99	40
G2T885W4	23	90	95	92,5	22	90	92	91	91,75	22,5
G2T81.15W4	12	91	91	91	12	91	93	92	91,5	12
G2T515W6	-	280	280	280	-	330	330	330	305	-
G2T544W6	-	241	241	241	-	326	326	326	283,5	-
G2T585W6	-	213	213	213	-	232	229	230,5	221,75	-
G2T51.15W6	-	210	210	210	-	176	179	177,5	193,75	-
G2T815W6	-	303	303	303	-	342	341	341,5	322,25	-
G2T844W6	-	276	276	276	-	285	284	284,5	280,25	-
G2T885W6	-	218	218	218	-	255	254	254,5	236,25	-
G2T81.15W6	-	166	166	166	-	172	172	172	169	-
G3T515W4					51	134	134	134	134	51
G3T544W4					47	111	110	110,5	110,5	47
G3T585W4					33	95	94	94,5	94,5	33
G3T51.15W4					18	94	96	95	95	18
G3T515W6						338	338	338	338	-
G3T544W6						331	332	331,5	331,5	-
G3T585W6						278	283	280,5	280,5	-
G3T51.15W6						228	226	227	227	-

Appendix D: Results Centrifugation

Centrifugation							
NO	EF (g)	Total Weight of samples/paste (g)	EF Fraction	Φ max	Φ/Φ max	LT1	LT2
G1T515W4	6,1	153,3	0,08	0,542	0,923	0,169	0,052
G1T544W4	4,7	174,8	0,05	0,591	0,945	0,186	0,041
G1T585W4	2,9	168,3	0,04	0,645	0,963	0,203	0,032
G1T51.15W4	2,1	161,9	0,03	0,677	0,972	0,213	0,027
G1T815W4	4,6	133,4	0,07	0,533	0,933	0,167	0,045
G1T844W4	3,9	164,3	0,05	0,581	0,951	0,180	0,036
G1T885W4	3,2	187,7	0,04	0,637	0,963	0,190	0,030
G1T81.15W4	2,1	199,3	0,02	0,664	0,976	0,193	0,020
G1T515W6	9,2	105,4	0,15	0,472	0,848	0,203	0,129
G1T544W6	10,2	131,5	0,14	0,534	0,857	0,229	0,132
G1T585W6	4,8	138,6	0,07	0,561	0,933	0,257	0,069
G1T51.15W6	4,0	124,2	0,06	0,600	0,935	0,273	0,072
G1T815W6	12,2	126,1	0,17	0,479	0,830	0,201	0,142
G1T844W6	9,1	126,0	0,14	0,523	0,865	0,220	0,120
G1T885W6	5,4	109,5	0,10	0,570	0,901	0,238	0,094
G1T81.15W6	3,8	106,7	0,07	0,595	1,000	0,247	0,074
G2T515W4	6,8	168,6	0,08	0,542	0,922	0,169	0,053
G2T544W4	4,3	165,6	0,05	0,590	0,947	0,186	0,040
G2T585W4	2,9	182,8	0,03	0,643	0,966	0,203	0,029
G2T51.15W4	2,7	186,4	0,03	0,679	0,968	0,213	0,030
G2T815W4	6,1	163,2	0,07	0,536	0,927	0,167	0,049
G2T844W4	4,9	181,4	0,06	0,585	0,945	0,180	0,040
G2T885W4	2,9	171,3	0,04	0,637	0,963	0,190	0,029
G2T81.15W4	2,4	159,9	0,03	0,670	0,966	0,193	0,029
G2T515W6	12,9	143,9	0,16	0,474	0,843	0,203	0,133
G2T544W6	9,5	146,4	0,12	0,520	0,881	0,229	0,110
G2T585W6	5,8	128,8	0,09	0,573	0,912	0,257	0,090
G2T51.15W6	4,7	160,1	0,06	0,596	0,941	0,273	0,065
G2T815W6	13,4	135,6	0,17	0,481	0,827	0,201	0,145
G2T844W6	10,5	136,4	0,14	0,527	0,857	0,220	0,127
G2T885W6	7,3	146,8	0,10	0,570	0,901	0,238	0,094
G2T81.15W6	5,5	170,0	0,07	0,590	0,934	0,247	0,066
G3T515W4	4,9	155,5	0,06	0,532	0,939	0,169	0,041
G3T544W4	3,3	172,6	0,04	0,581	0,961	0,186	0,029
G3T585W4	2,2	197,5	0,02	0,637	0,976	0,203	0,020
G3T51.15W4	2,1	174,0	0,03	0,675	0,974	0,213	0,025
G3T515W6	11,1	137,6	0,14	0,466	0,859	0,203	0,119
G3T544W6	8,1	148,6	0,10	0,509	0,900	0,229	0,092
G3T585W6	5,1	159,7	0,06	0,557	0,938	0,257	0,064
G3T51.15W6	4,2	159,1	0,05	0,593	0,947	0,273	0,059

Appendix E: Results Print Flow

G2T515W4	Density:	1,900
Seconds	Weight	Volume
1	1,095	0,576
2	2,173	1,144
3	3,267	1,719
4	4,993	2,628
5	6,647	3,498
6	7,492	3,943
7	8,182	4,306
8	9,800	5,157
9	11,758	6,188
10	12,954	6,817
11	13,606	7,160
12	14,677	7,724
13	16,446	8,655
14	17,638	9,282
15	19,639	10,335
16	22,488	11,834
17	23,303	12,263
18	24,905	13,106
19	25,598	13,471
20	26,616	14,007
21	29,133	15,331
22	30,198	15,892
23	31,029	16,329
24	31,765	16,717
25	33,534	17,647
26	35,638	18,755
27	36,817	19,375
28	37,430	19,698
29	38,044	20,021
30	38,358	20,186
31	37,817	19,901

G2T544W4	Density:	2,010		
Seconds	Weight 1	Weight 2	Volume 1	Volume 2
1	0,004	3,449	0,002	1,716
2	1,198	4,135	0,596	2,057
3	2,425	6,051	1,206	3,010
4	3,806	7,063	1,893	3,513
5	4,528	8,478	2,252	4,217
6	4,529	9,796	2,253	4,873
7	5,905	11,281	2,937	5,611
8	7,216	12,802	3,589	6,368
9	8,368	13,758	4,162	6,844
10	9,889	15,367	4,919	7,644
11	10,85	16,540	5,397	8,227
12	12,219	17,927	6,078	8,917
13	13,628	19,542	6,779	9,721
14	14,897	20,421	7,410	10,158
15	16,32	22,110	8,118	10,998
16	17,729	23,343	8,819	11,611
17	18,832	24,608	9,368	12,241
18	20,003	26,233	9,950	13,049
19	20,974	27,806	10,433	13,831
20	22,467	29,348	11,176	14,598
21	23,678	30,639	11,778	15,241
22	25,027	32,157	12,449	15,996
23	26,385	33,512	13,125	16,670
24	27,599	34,701	13,728	17,261
25	29,166	36,120	14,508	17,967
26	30,073	37,290	14,959	18,549
27		38,686		19,243
28		40,011		19,903
29		41,275		20,531
30		42,713		21,247
31		43,965		21,869

G2T585W4	Density:	2,096			
Seconds	Weight 1	Weight 2	Volume 1	Volume 2	
1	0,319	0,735	0,152	0,351	
2	0,32	0,581	0,153	0,277	
3	0,584	0,883	0,279	0,421	
4	1,657	1,674	0,790	0,798	
5	2,479	2,92	1,182	1,393	
6	2,728	4,02	1,301	1,918	
7	3,345	4,005	1,596	1,910	
8	3,625	3,879	1,729	1,850	
9	4,471	3,749	2,133	1,788	
10	4,786	3,628	2,283	1,731	
11	6,208	3,591	2,961	1,713	
12	7,61	3,712	3,630	1,771	
13	8,626	3,496	4,115	1,668	
14	10,082	5,093	4,809	2,429	
15	11,653	5,05	5,558	2,409	
16	13,793	5,066	6,579	2,416	
17	13,792	5,042	6,579	2,405	
18	15,092	5,063	7,199	2,415	
19	16,179	5,066	7,717	2,416	
20	18,036	5,064	8,603	2,416	
21	19,008	5,066	9,067	2,416	
22	20,67	5,067	9,859	2,417	
23	20,79	5,06	9,917	2,414	
24	20,771	5,065	9,908	2,416	

G2T585W4	Density:	2,096				
Seconds	Weight 1	Weight 2	Weight 3	Volume 1	Volume 2	Volume 3
0	1,369	1,271	1,452	0,653	0,606	0,693
1	2,445	2,61	2,643	1,166	1,245	1,261
2	3,896	4,01	4,023	1,858	1,913	1,919
3	5,298	5,374	5,337	2,527	2,563	2,546
4	6,732	6,868	6,822	3,211	3,276	3,254
5	8,098	8,175	8,186	3,863	3,899	3,905
6	9,588	9,685	9,632	4,573	4,620	4,594
7	11,003	11,032	10,984	5,248	5,262	5,239
8	12,451	12,575	12,417	5,939	5,998	5,923
9	13,62	13,832	13,743	6,497	6,598	6,555
10	14,52	15,319	15,14	6,926	7,307	7,222
11	15,994	16,815	16,391	7,629	8,021	7,818
12	17,417	17,977	17,724	8,308	8,575	8,454
13	18,756	18,908	19,003	8,947	9,019	9,064
14	20,242	20,38	20,362	9,655	9,721	9,713
15	21,679	21,923	21,691	10,341	10,457	10,346
16	23,053	23,282	23,189	10,996	11,105	11,061
17	24,229	24,724	24,356	11,557	11,793	11,618
18	25,684	26,17	25,869	12,251	12,483	12,339
19	27,11	27,672	27,153	12,931	13,199	12,952
20	28,593	28,994	28,405	13,639	13,830	13,549
21	29,902	30,38	29,786	14,263	14,491	14,208
22	31,275	31,595	31,235	14,918	15,071	14,899
23	32,715	32,916	32,61	15,605	15,701	15,555
24	33,864	34,212	33,661	16,153	16,319	16,056
25	35,223	35,728	35,108	16,801	17,042	16,746
26		37,135	36,639		17,713	17,477
27		38,726	37,601		18,472	17,935
28		39,852	39,131		19,009	18,665
29			40,568			19,351
30			41,28			19,690

G2T515W6	Density:	1,693
Seconds	Weight	Volume
1	0,694	0,410
2	1,591	0,940
3	2,631	1,554
4	3,768	2,226
5	4,868	2,876
6	6,088	3,597
7	7,190	4,248
8	8,384	4,953
9	9,464	5,592
10	10,720	6,334
11	11,824	6,986
12	13,010	7,687
13	14,082	8,320
14	15,214	8,989
15	16,297	9,629
16	17,404	10,283
17	18,527	10,946
18	19,634	11,600
19	20,795	12,286
20	21,909	12,944
21	23,079	13,636
22	24,202	14,299
23	25,409	15,012
24	26,535	15,678
25	27,297	16,128

G2T544W6	Density:	1,797
Seconds	Weight	Volume
1	1,866	1,038
2	3,378	1,880
3	4,669	2,598
4	6,090	3,389
5	7,282	4,053
6	8,652	4,815
7	9,819	5,465
8	11,539	6,422
9	12,960	7,213
10	14,318	7,968
11	15,525	8,640
12	16,722	9,306
13	17,891	9,957
14	18,970	10,557
15	20,143	11,210
16	21,172	11,783
17	22,332	12,428
18	23,343	12,991
19	24,518	13,645
20	25,528	14,207
21	26,717	14,869
22	27,730	15,433
23	28,913	16,091
24	28,894	16,080
25	29,045	16,164
26	28,975	16,126
27	28,994	16,136
28	28,902	16,085
29	28,899	16,083
30	28,842	16,052
31	28,562	15,896

G2T585W6	Density:	1,910
Seconds	Weight	Volume
1	0,003	0,002
2	1,176	0,616
3	2,330	1,220
4	3,441	1,802
5	4,606	2,412
6	5,794	3,034
7	7,160	3,750
8	8,391	4,394
9	9,713	5,087
10	10,984	5,752
11	12,322	6,453
12	13,714	7,182
13	15,137	7,927
14	16,471	8,626
15	17,741	9,291
16	19,080	9,992
17	20,299	10,630
18	21,619	11,321
19	22,768	11,923
20	24,051	12,595
21	25,163	13,177
22	26,432	13,842
23	27,577	14,442
24	28,857	15,112
25	30,043	15,733
26	31,339	16,412
27	32,524	17,032
28	33,824	17,713

G3T515W4	Density:	1,909
Seconds	Weight	Volume
1	0,004	0,002
2	0,134	0,070
3	1,572	0,823
4	2,813	1,473
5	4,050	2,121
6	5,412	2,835
7	6,607	3,460
8	7,928	4,152
9	9,129	4,781
10	10,432	5,464
11	11,669	6,112
12	12,937	6,776
13	14,101	7,385
14	15,437	8,085
15	16,657	8,724
16	17,949	9,401
17	19,054	9,980
18	20,404	10,687
19	21,581	11,303
20	23,015	12,054
21	24,101	12,623
22	25,451	13,330
23	26,642	13,954
24	27,966	14,647
25	29,133	15,258
26	30,462	15,955
27	31,682	16,594
28	33,009	17,289
29	34,189	17,907
30	34,409	18,022

G3T544W4	Density:	1,996
Seconds	Weight	Volume
1	0,002	0,001
2	1,493	0,748
3	2,930	1,468
4	4,339	2,174
5	5,616	2,814
6	6,794	3,404
7	8,067	4,042
8	9,423	4,722
9	10,692	5,358
10	12,013	6,020
11	13,333	6,681
12	14,692	7,362
13	16,093	8,064
14	17,532	8,785
15	18,871	9,456
16	20,288	10,166
17	21,563	10,805
18	22,801	11,425
19	24,173	12,113
20	25,425	12,740
21	26,764	13,411
22	28,062	14,061
23	29,443	14,753
24	30,734	15,400
25	32,048	16,059
26	33,351	16,712
27	34,727	17,401
28	36,010	18,044
29	37,444	18,763
30	38,795	19,440

G3T585W4	Density:	2,086
Seconds	Weight	Volume
1	1,311	0,629
2	2,265	1,086
3	3,763	1,804
4	5,094	2,442
5	6,476	3,105
6	9,062	4,345
7	9,883	4,739
8	11,204	5,372
9	12,644	6,063
10	13,904	6,667
11	15,405	7,386
12	16,201	7,768
13	17,443	8,364
14	18,614	8,925
15	20,231	9,700
16	21,732	10,420
17	23,099	11,075
18	24,645	11,817
19	25,535	12,243
20	26,859	12,878
21	28,294	13,566
22	29,812	14,294
23	31,131	14,927
24	33,001	15,823
25	33,402	16,015

G3T51.15W4	Density:	2,107
Seconds	Weight	Volume
1	0,005	0,002
2	1,740	0,826
3	1,911	0,907
4	5,379	2,553
5	5,415	2,570
6	7,615	3,614
7	8,105	3,847
8	10,244	4,862
9	11,146	5,290
10	12,819	6,084
11	14,103	6,693
12	15,614	7,411
13	16,952	8,046
14	18,546	8,802
15	20,125	9,551
16	21,650	10,275
17	22,604	10,728
18	24,245	11,507
19	25,265	11,991
20	26,892	12,763
21	27,927	13,254
22	29,466	13,985
23	30,893	14,662

G3T515W6	Density:	1,703
Seconds	Weight	Volume
1	0,076	0,045
2	1,050	0,616
3	2,182	1,281
4	3,377	1,982
5	4,469	2,624
6	5,649	3,316
7	6,738	3,956
8	7,921	4,650
9	9,004	5,286
10	10,198	5,987
11	11,276	6,620
12	12,466	7,318
13	13,572	7,967
14	14,748	8,658
15	15,854	9,307
16	17,011	9,986
17	18,152	10,656
18	19,291	11,325
19	20,448	12,004
20	21,558	12,656
21	22,746	13,353
22	23,848	14,000
23	25,049	14,705
24	26,140	15,345
25	27,343	16,052
26	28,118	16,507

G3T544W6	Density:	1,815
Seconds	Weight	Volume
1	0,343	0,189
2	1,454	0,801
3	2,651	1,461
4	3,901	2,149
5	5,073	2,795
6	6,309	3,476
7	7,474	4,118
8	8,710	4,799
9	9,888	5,448
10	11,103	6,117
11	12,280	6,766
12	13,480	7,427
13	14,680	8,088
14	15,882	8,750
15	17,080	9,410
16	18,282	10,073
17	19,509	10,749
18	20,696	11,403
19	21,941	12,088
20	23,094	12,724
21	24,336	13,408
22	25,496	14,047
23	26,736	14,730
24	27,903	15,373
25	29,131	16,050
26	30,307	16,698
27	31,524	17,368
28	32,702	18,017
29	33,904	18,680

G3T585W6	Density:	1,927
Seconds	Weight	Volume
1	0,938	0,487
2	2,273	1,179
3	3,529	1,831
4	4,835	2,509
5	6,078	3,154
6	7,373	3,826
7	8,697	4,513
8	9,986	5,182
9	11,278	5,852
10	12,548	6,511
11	13,840	7,182
12	15,094	7,832
13	16,394	8,507
14	17,646	9,157
15	18,912	9,814
16	20,131	10,446
17	21,453	11,132
18	22,709	11,784
19	24,038	12,473
20	25,283	13,119
21	26,590	13,798
22	27,841	14,447
23	28,996	15,046
24	30,265	15,705
25	31,552	16,373
26	32,830	17,036
27	34,126	17,708
28	35,437	18,388
29	36,700	19,044
30	37,342	19,377

G3T51.15W6	Density:	1,982
Seconds	Weight	Volume
1	0,078	0,039
2	1,613	0,814
3	3,019	1,523
4	4,344	2,191
5	5,727	2,889
6	7,043	3,553
7	8,416	4,245
8	9,716	4,901
9	11,081	5,590
10	12,394	6,252
11	13,734	6,928
12	15,065	7,599
13	16,392	8,269
14	17,737	8,947
15	19,031	9,600
16	20,459	10,320
17	21,763	10,978
18	23,120	11,663
19	24,436	12,326
20	25,797	13,013
21	27,091	13,666
22	28,452	14,352
23	29,745	15,004
24	31,103	15,689
25	32,407	16,347
26	33,758	17,029
27	35,075	17,693
28	36,426	18,375
29	37,761	19,048
30	38,267	19,303
31	38,279	19,309

Appendix F: Pictures of results

The pictures taken of the three tests can be found in the shared folder given below.

<https://www.dropbox.com/sh/2o3yan9cq6hz1sx/AAD3aGRazyfUguGqllGy57hza?dl=0>

Apendix G: Silica fume datasheet

1. Identification of the Substance and Company

Product name: **Elkem Microsilica** ®

Product application: Cementitious systems

Address/Phone No.: **Elkem ASA,
Materials**
P.O.Box 8126 Vaagsbygd
N-4675 Kristiansand, Norway
Telephone: + 47 38 01 75 00
Telefax: + 47 38 01 49 70
<http://www.materials.elkem.com>

Contact person: Arne Skagen, e-mail: arne.skagen@elkem.no

Emergency Phone No.: Not applicable

2. Composition/Information on Ingredients

Synonyms: Silica fumes, Microsilica, Silica powder, Amorphous silica, Silicon dioxide powder, condensed SiO₂-fume, Silica fume.

IUPAC-name: Silicon dioxide

CAS No.: 69012-64-2
EINECS No.: 273-761-1

Symbol: None
R-phrases: None
S-phrases: None

Microsilica may contain small amounts of crystalline quartz (<0.5%).

3. Hazards Identification

Microsilica is unlikely to cause harmful effects when handled and stored as advised. See section 7.

4. First Aid Measures

Inhalation:	Remove exposed person from dusty area. Fresh air.
Skin contact:	Wash contaminated skin with water and/or a mild detergent.
Eye contact:	Rinse eyes with water/saline solution. If discomfort persists, obtain medical attention.
Ingestion:	Not applicable.

5. Fire Fighting Measures

Microsilica is not combustible and the dust entails no danger of explosion.

Extinguishing media: Not applicable

6. Accidental Release Measures

Avoid exposure to dust of microsilica. Released material should be collected in suitable containers.

7. Handling and Storage

Handling:	Avoid dust generation. See section 8.
Storage:	Keep away from hydrofluoric acid (HF). Not to be stored at temperatures near to or below 0°C.

8. Exposure Controls/Personal Protection

A) Occupational exposure controls:

Avoid inhalation of dust. Ensure good dust ventilation during use. Wear a CE-marked respirator according to EN 149 FFP 2S/3S during dust generating operations. Use protective gloves and eye protection. Facilities for Eye flushing should be available.

Occupational Exposure Limits (HSE, EH40/2002-2003):

	CAS Number	8hr TWA		10 minute STEL	
		ppm	mg/m ³	ppm	mg/m ³
Silica, amorphous (SiO ₂)	-				
Total inhalable dust		-	6	-	-
Respirable dust		-	2.4	-	-
Silica, crystalline (SiO ₂)	-				
Respirable dust		-	0.3 ¹⁾	-	-

¹⁾ The indicated value is a Maximum Exposure Limit, MEL.

B) Environmental exposure controls:

See sections 6, 7 and 12.

Limit values ambient air (Directive 1999/30/EC):

	Averaging time	Limit value	By date
PM ₁₀ ★	24 Hrs	50 µg/m ³	1 January 2005
PM ₁₀	Calendar year	40 µg/m ³	1 January 2005

★ not to be exceeded more than 35 times a calendar year

9. Physical and Chemical Properties

Form:	Ultrafine amorphous powder (respirable dust), dust forms agglomerates
Colour:	Grey
Odour:	Odourless
Melting Point (°C):	1550-1570
Solubility (Water):	Insoluble/Slightly soluble
Solubility (Organic solvents):	Insoluble/Slightly soluble
Specific Gravity (water =1):	2.2-2.3
Bulk density (kg/m ³) approx.:	150-700
Specific surface (m ² /g):	15-30
Particle size, mean (µm):	≈ 0.15 (≈ 80 weight% of primary particles have a diameter < 5 µm).

10. Stability and reactivity

Conditions to avoid:	See below
Materials to avoid:	Hydrofluoric acid (HF).

Hazardous Decomposition Product(s):

Microsilica reacts with hydrofluoric acid (HF) forming toxic gas (SiF₄).
Heating microsilica above 1000°C can result in the formation of crystalline SiO₂-modifications as cristobalite / tridymite which may cause pulmonary fibrosis (silicosis).

11. Toxicological Information

Acute effects:

INGESTION:	Finely divided dust may cause irritation and dehydration of mucous membranes.
INHALATION:	Finely divided dust may cause irritation and dehydration of mucous membranes.
SKIN CONTACT:	Finely divided dust may cause mechanical irritation and dehydration.
EYE CONTACT:	Finely divided dust may cause mechanical irritation and dehydration.

Chronic effects:

Inhalation of microsilica dust is considered to entail minimal risk of pulmonary fibrosis (silicosis). However, chronic obstructive lung disease is suspected following long term exposure (years) for concentrations above recommended occupational exposure limits.

12. Ecological Information

Microsilica is not characterised as dangerous for the environment.

MOBILITY:	The product is not mobile under normal environmental conditions.
PERSISTENCE:	Not relevant for inorganic substances.
BIOACCUMULATION:	Not relevant.
ECOTOXICITY:	Elkem Microsilica: <i>Daphnia magna</i> : 24 h EC ₅₀ > 1002 mg.l ⁻¹ 24 h EC ₁₀₀ >1002 mg.l ⁻¹ NOEC 319 mg.l ⁻¹ Coarse microsilica has been subject to Microtox™ screening test. No acute toxicological effects could be observed in the test organisms.

13. Disposal Considerations

The material should be recovered for recycling if possible.

This material is not classified as hazardous waste according to Commission Decisions 2000/532/EC and 2001/118/EC. Prior to disposal of large quantities of this material advice should be sought from the relevant Waste Regulation Authority.

14. Transport Information

UN	-
IMDG/IMO	Not subject to classification
ADR/RID	Not subject to classification
ICAO/IATA	Not subject to classification

15. Regulatory Information

Product classification and labelling:

Symbol:	Not subject to classification
R-phrases:	None
S-phrases:	None

The text of this Data Sheet is prepared in compliance with:

- Commission Directive 2001/58/EC.
- Council Directive 67/548/EEC and its subsequent amendments.

16. Other Information

Literature references are available upon application to the manufacturer.

Elkem Microsilica[®] is a registered trademark owned by Elkem ASA.

Apendix H: Dynamon SR-N datasheet



Dynamon SR-N

Superplastiserende
tilsetningsstoff



PRODUCT DESCRIPTION

Dynamon SR-N is a high performance superplasticizing admixture based on modified acrylic polymers.

The product is part of the **Dynamon System**, based on the Mapei developed DPP technology (DPP = Designed Performance Polymers) where the properties of the admixture are tailored according to the specific performances required of the concrete.

The **Dynamon System** is developed on the basis of Mapei's own design and production of monomers.

AREAS OF APPLICATION

Dynamon SR-N is a superplasticizing admixture used to improve workability and/or reduce the amount of mixing water.

Dynamon SR-N is a **Dynamon** variant where by normal dosage (0.3 - 1.5 %) a longer pot life (less slump loss) can be achieved than with **Dynamon SX** products. The product is therefore specially suited for ready-mix concrete production, where the time from mixing to placement is relatively long, e.g. due to long transportation times or requirements for a slow rate of climb. **Dynamon SR-N** nevertheless gives high early strength at normal dosages due to its effective dispersion of the cement. All **Dynamon** products are significantly different from conventional sulphonated melamine based and sulphonated naphthalene based superplasticizers, and also from first generation acrylic based polymers in terms of their superior water-reduction. Over-dosing can cause concrete separation. We always recommend the use of trial pours using the actual parameters.

The dosage required to achieve a particular workability will be considerably lower for **Dynamon SR-N** than for previous superplasticizers. In contrast to conventional melamine or naphthalene based admixtures, **Dynamon SR-N** produces the maximum effect regardless of when it is added, but the time of addition can influence the mixing time. If at least 80 % of the mixing water is added before **Dynamon SR-N** the required mixing time will generally be shortest. It is nevertheless important to perform trials using the actual mixing equipment.

TECHNICAL PROPERTIES

Dynamon SR-N is an aqueous solution of active acrylic copolymers which effectively disperse the cement grains.

This effect can, in principle, be used in three ways:

1. To reduce the amount of mixing water, but at the same time maintain the concrete workability. Lower w/c ratio gives increased strength, reduced permeability and improved durability.
2. To increase workability compared to concrete with the same w/c ratio. The strength remains the same but ease of placement is improved.
3. To reduce both the water and the cement without altering the mechanical strength. Through this method it is possible to reduce costs (less cement), shrinkage (less water) and also the risk of temperature gradients due to the lower heat of hydration. This last effect is particularly important for concrete containing a high percentage of cement.

Dynamon SR-N

COMPATIBILITY WITH OTHER PRODUCTS

Dynamon SR-N can be combined with other Mapei admixtures, e.g. set accelerating additives such as **Mapefast SA** and set retarding admixtures, such as **Mapetard R**. The product is also compatible with air entraining admixtures for the production of frost resistant concrete, e.g. **Mapeair L** or **Mapeair 25** (the selection of air entraining admixture depends upon the other components e.g. cement type and aggregate).

DOSAGE

To achieve the desired results (strength, durability, workability, cement reduction) add **Dynamon SR-N** in dosages between 0.3 and 1.5 % of the cement weight. Increased dosages will also increase the open time (the length of time the concrete is workable).

PACKAGING

Dynamon SR-N is available in 25 liter cans, 200 liter drums, 1000 liter IBC tanks and in tank.

STORAGE

The product must be stored at temperatures between +8 and +35°C, and will retain its properties for at least one year if stored unopened in its original packaging. If the product is exposed to direct sunlight, colour variation may occur, but this will not affect the technical properties of the product.

SAFETY INSTRUCTIONS FOR PREPARATION AND INSTALLATION

Instructions for the safe use of our products can be found on the latest version of the SDS available from our website www.mapei.no

PRODUCT FOR PROFESSIONAL USE

WARNING

Although the technical details and recommendations contained in this product data sheet correspond to the best of our knowledge and experience, all the above information must, in every case, be taken as merely indicative and subject to confirmation after long-term practical application: for this reason, anyone who intends to use the product must ensure beforehand that it is suitable for the envisaged application: in every case, the user alone is fully responsible for any consequences deriving from the use of the product.

Please refer to the current version of the technical data sheet, available from our web site www.mapei.no

LEGAL NOTICE

The contents of this Technical Data Sheet ("TDS") may be copied into another project-related document, but the resulting document shall not supplement or replace requirements per the TDS in force at the time of the MAPEI product installation.

The most up-to-date TDS can be downloaded from our website www.mapei.no

ANY ALTERATION TO THE WORDING OR REQUIREMENTS CONTAINED OR DERIVED FROM THIS TDS EXCLUDES THE RESPONSIBILITY OF MAPEI.

All relevant references for the product are available upon request and from www.mapei.no

Dynamon SR-N

TECHNICAL DATA (typical values)

PRODUCT IDENTITY

Appearance:	liquid
Colour:	yellowish brown
Viscosity (Brookfield Viscometer DV-1, LV1, 100rpm at 20±2°C):	low viscosity; < 30 mPa·S
Dry solids content, %:	19.5 ± 1.0
Density, g/cm ³ :	1.05 ± 0.02
pH:	6.5 ± 1
Chloride content, %:	< 0.05
Alkali content (equiv. Na ₂ O) %:	< 2.0

CONCRETE PROPERTIES

As water reducing admixture	Reference	Dynamon SR-N
Quantity of cement kg/m ³ (CEM I-42.5R):	350	350
Admixture dosage (% by weight of cement):	0	1.1
Mass ratio (w/c ratio):	0.50	0.41
Compressive strength (N/mm ²):		
- 1 day	26	37
- 7 days	43	56
- 28 days	52	66

As superplasticising admixture	Reference	Dynamon SR-N
Quantity of cement kg/m ³ (CEM I-42.5R):	350	350
Admixture dosage (in % of cement weight):	0	1.1
Mass ratio (w/c ratio):	0.49	0.49
Air content:	2.4	1.9
Workability, mm:		
- slump, 5 min	40	200
- slump, 30 min	30	200
- slump, 60 min	20	210
- slump, 90 min	20	180
- slump flow, 5 min	200	430
- slump flow, 30 min	200	340
- slump flow, 60 min	200	330
- slump flow, 90 min	200	320

Any reproduction of texts, photos and illustrations published here is prohibited and subject to prosecution

6917-07-2017(GB)

